

Cooling System Design for 1974cc Gray Cast Iron Alloy Engine

Su Yin Win
Department of Mechanical
Engineering,
Technological University
Thanlyin, Myanmar

Thwe Thwe Htay
Department of Mechanical
Engineering,
Technological University
Thanlyin, Myanmar

Maung Maung Yi
Department of Mechanical
Engineering,
Technological University
Thanlyin, Myanmar

Abstract: The cooling system is necessary in any internal combustion engine. If no cooling system is provided, parts would melt from the heat of burning fuel and the piston would expand so much they could not move in the burning. In this paper, the design engine is made of the cast iron alloy and it can be studied on engine water cooling system. The cast iron engine head can get over heat at high temperature because the thermal conductivity of cast iron is not good. So, the design engine head is necessary of increasing the cooling efficiency and it must be also needed to increase water tube and cooling fins more than original radiator. The rate of circulation of water coolant, is determined from the quantity of heat received by the cooling system. In the radiator design calculation, design amount of heat to the coolant, heat dissipation surface areas, radiator face area and radiator design selection are described.

Keywords: water flow rate, water velocity, water jacket length, heat dissipation surface, Auto CAD, Master cam

1. INTRODUCTION

When the engine rotates the coolant pump, an impeller is driven within the housing crating low pressure at its inlet, usually located at or closed to the center of impeller. When the cooling system pressure at the inlet to the coolant pump is at its lowest ,boiling will always occur at this location first. This will vary rapidly accelerate the overheating condition as the pump impeller will be acting on vapor. Coolant pumps are main reason that engine coolants should have some lubricating properties because they are vulnerable to abrasion damage when the coolant dissolved solids levels are high.[7]

2. CALCULATION OF WATER FLOW RATE AND WATER VELOCITY

The simplest and most familiar closed cooling system is used in the automobile field. In this system, the coolant circulates through the until it reaches the operating temperature at which point the thermostat at opens and coolant passes through the radiator carries away the excess heat, which prevents engine overheating. It is designed with force circulating of the water and with one or two regulation system controlling of the temperature of the water and the air.[2] To calculate the heat which is lost to the cooling system after first calculating the heat input, 35% of the available heat of the fuel is disposed to the cooling system [1]. Fuel consumption per hour is 13.06 kg / hr.

$$Q_{cool} = 35\% Q_{total} \quad (1)$$

$$Q_{total} = C.V \times m^{\circ}_f \quad (2)$$

The design amount of heat is increased by 10%.

$$Q_{des} = 56.66 \text{ kW}$$

The rate of circulation of water is determined the quality of heat received by cooling system.

$$v_w = Q_{des} / (C_w \times \Delta t_w \times \rho_w) \quad (3)$$

where,

C_w = Specific heat of water = 4.19 kJ/kg °C

Δt_w = Drop in water temperature in radiator
≥ 7 to 8 °C [3]

ρ_w = Density of coolant = 998 kg / m³

V_w = 7.214 m³ / hr

The required water velocity is calculated from

$$v_w = V_w / (A_{oj} \times n) \quad (4)$$

v_w = water velocity, m/s

A_{oj} = Area of water jacket inlet pipe, m²

n = Number of cylinder

$v_w = 2.8 \text{ m / s}$

2.1 Amount of water passed through the engine

The quality of water that must be circulated depend upon the initial temperature and the atmospheric conditions, either directly as in marine engine ,or indirectly if recooling system is used and the water is circulated over and over again. In order to avoid excessive heat stresses, the temperature different between the incoming and out going must not excess 20°C in small and medium size engine and less down to 10°C large engine. The heat rejected to the cooling medium through the cylinder walls and head, the piston and its ring when an engine is cooled by water can be found following equation 4[2].

$$Q_{cool} = m^{\circ}_w \times C_w (t_{out} - t_{in}) \quad (5)$$

m°_w =Amount of water passed through the engine kg/s

C_w =Specific heat of water J/kg

t_{out} = Temperature of water flowing outlet of the engine °C

t_{in} = Temperature of water flowing into the engine °C

$m^{\circ}_w = 1.8182 \text{ kg/s}$

The amount of heat rejected to the cooling system is circulated by using equation (5) and the result is shown figure (1) to (4).

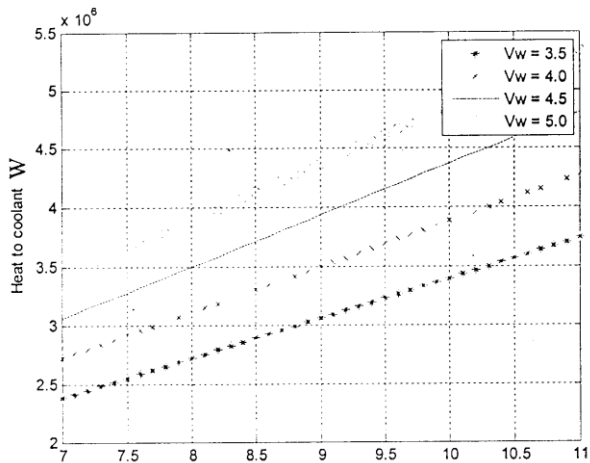


Figure 1.Amount of Heat Reject to The cooling System

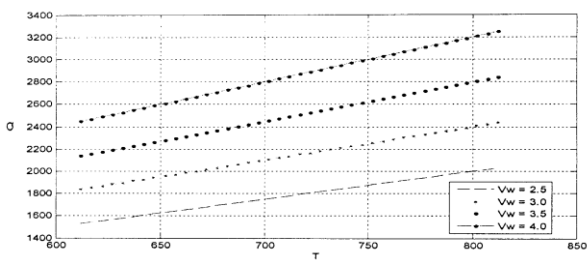


Figure 2.Heat Flux at the Exhaust Channel with Various Water velocity

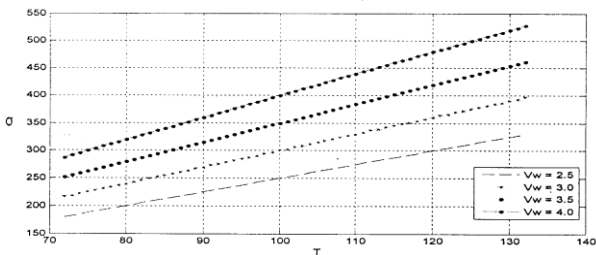


Figure 3.Heat Flux at the Cylinder wall near the Cylinder with Various Water velocity

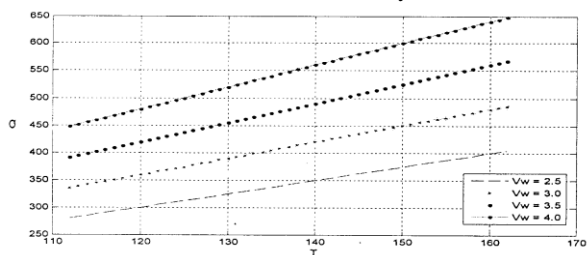


Figure 4.Heat Flux at the Cylinder Head with Various Water velocity

2.2 Determination of water jacket

An adequate cooling system must be designed to keep the engine at a temperature that lubrication is not destroyed. In this way, engine parts will not have been heated to such a degree that expansion has not caused clearances to be materially reduced. It is necessary that the water jacket to be sufficient size with an adequate supply of coolant.[10]The amount of heat absorbed by the engine head varies with the load form (11 to 19) % of the total head supplied with fuel.[4]

For one cylinder

$$Q_H' = (11 \text{ to } 19) \text{ of } Q_t \quad (6)$$

$$Q_H' = 19\% Q_t$$

For one cylinder,

$$Q_H'' = 723 \text{ kW}$$

The water jacket in most present day engine are cast as integral part of the cylinder block and cylinder head, and provide water passages around the cylinders and valves for the circulation of water. The water passages must allow an unrestricted flow of water around the cylinder and valves. As the coolant passes the hot metal part, some of the heat transfers to the lower temperature coolant. This cools the metal parts and heat the coolant. The circulation then carried the heat to the radiator. [8] The average length of the water jacket is determined by

$$L_{wj} = Q_H'' / [\alpha_1 (T_{wc} - T_{coolant}) \pi D_{wj}] \quad (7)$$

α_1 = The heat exchange between metal wall and water
 $= 4340 \text{ W/m}^2 \text{ } ^\circ\text{C}$

T_{wc} = Engine head average wall temperature at the coolant side
 $^\circ\text{C} = 190 \text{ } ^\circ\text{C}$

$T_{coolant}$ = Temperature of coolant
 $^\circ\text{C} = 86 \text{ to } 91$

D_{wj} = Average diameter of water jacket
 $= 15 \text{ mm}$

$L_{wj} = 348.5 \text{ mm}$

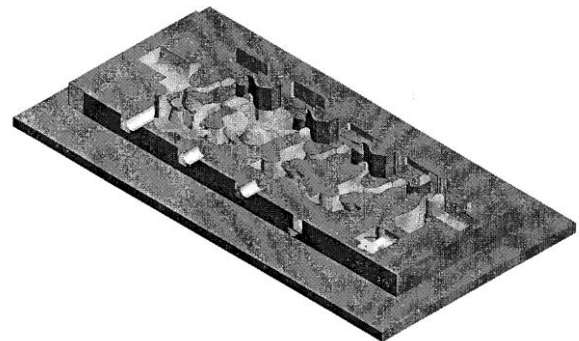


Figure 5. The pattern of water jacket for 1974cc Gray Cast Iron Alloy Engine head

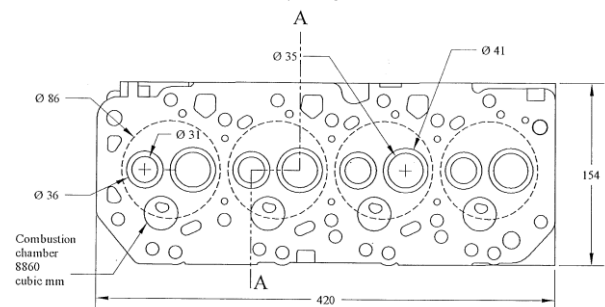


Figure 6. The lower view of 1974cc Gray Cast Iron Alloy Engine head

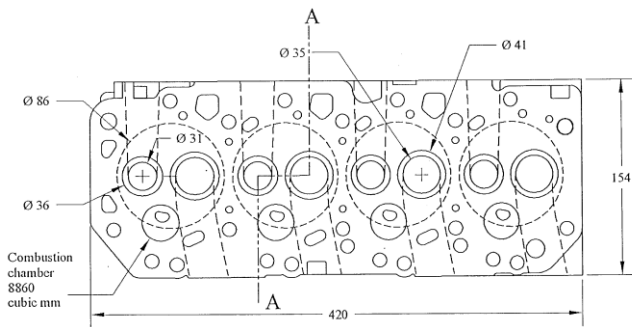


Figure 7. The lower view of 1974cc Gray Cast Iron Alloy Engine head with the exhaust and Inlet Passage

3. RADIATOR DESIGN

In the radiator design calculation, design amount of heat to the coolant, heat dissipation surface area, radiator face area and radiator design selection are described. It is assumed that all of the heat rejected to the cooling system should be dissipated by radiator surface.

The amount heat for an engine operation at rotated power is $Q_{des} = 58.66\text{kW}$.

The relation between the design amount of heat Q_{rad} and the heat dissipation surface A_t of the radiator is,

$$Q_{rad} = C_h \times \Delta t_{wa} \times A_t$$

where,

A_t = Heat dissipation surface

C_h = Heat transfer coefficient

$$C_h = \frac{1}{\frac{\epsilon}{\alpha_1} + \frac{\epsilon \times \delta}{\lambda} + \frac{1}{\alpha_2}} \quad (8)$$

α_1 = Heat transfer coefficient from the coolant to the metal of the tube = $4340 \text{ W/m}^2 \text{ }^\circ\text{C}$

α_2 = Heat transfer coefficient from the wall of the tube to the air = $100 \text{ W/m}^2 \text{ }^\circ\text{C}$

λ = Heat conductivity coefficient for copper = $330 \text{ W/m}^2 \text{ }^\circ\text{C}$ [5]

δ = Thickness of the tube wall = $0.13 \text{ to } 0.2 \text{ mm}$ [7]

= 0.165 mm

ϵ = Fining coefficient = $7.5 \text{ to } 10$
= $(7.5+10)/2 = 8.75$

Δt_{wa} = Temperature drop between the mean temperature of the cooling water and air passing through the radiator

$$t_{wm} = (t_{w,out} - t_{w,in})/2 = 86 \text{ to } 91 \text{ }^\circ\text{C}$$

$$t_{am} = (t_{a,out} - t_{a,in})/2$$

$$\Delta t_a = 20 \text{ to } 30 \text{ }^\circ\text{C}$$
 [8]

$$t_{am,b} = 15 \text{ }^\circ\text{C} = 288\text{K}$$

$$t_{a,in} = t_{am,b} + \Delta t_f$$

Δt_f = Amount by which the air is heated when pass through the shutter or the face of the oil cooler installed before the cooling system radiator = $3 \text{ to } 5 \text{ }^\circ\text{C}$

$$t_{a,in} = 15+4=19 \text{ }^\circ\text{C}$$

$$t_{a,out} = t_{a,in} + \Delta t_a/2 = 31.5 \text{ }^\circ\text{C}$$

$$t_{am} = 25.25 \text{ }^\circ\text{C}$$

$$\Delta t_{wa} = t_{wm} - t_{am} = 63.25 \text{ }^\circ\text{C}$$

By substituting in equation (8)

$$C_h = \text{Heat transfer coefficient} = 85.26 \text{ W/m}^2 \text{ }^\circ\text{C}$$

By substituting in Q_{rad} equation,

$$A_t = \text{Heat dissipation surface} = 10.87 \text{ m}^2$$

3.1 Radiator Face Area

It is important that temperature variation of the coolant be maintained within closed limits. This is a heat exchanger with two sets of passages. One set is for coolant and the other for outside air. This arrangement allows the radiator to remove heat from the engine coolant by passing through radiator to remove from the engine. The heat transfers from the hot coolant to the cooler outside air that also pass through the radiator.[9] The another formula of heat dissipated surface is

$$A_t = A_f \times l_{rad} \times \phi_{rad} \quad (9)$$

where

A_f = Face area of the radiator, m^2

l_{rad} = radiator depth $\text{m} = 44 \text{ mm}$

ϕ_{rad} = Volumetric coefficient of compactness = $1100/\text{m}$

By substituting in equation (9)

$$A_f = 0.22458 \text{ m}^2 = \text{radiator width} \times \text{radiator height}$$

In modern tubular constructions, appearance and provided by the ornamental grille which is now universal in passenger vehicles, and the radiator block can be designed simply as an efficient heat exchanger of the lightest possible weight. The cooling element consists of a nest of copper tubes soldered into brass upper and lower tube plates which are bolted to the top and bottom tanks. This construction is inexpensive and makes for accessibility and ease of repair.[9]

Choose Radiator width, $W_R = 550 \text{ mm}$

Radiator width, $H_R = 407 \text{ mm}$

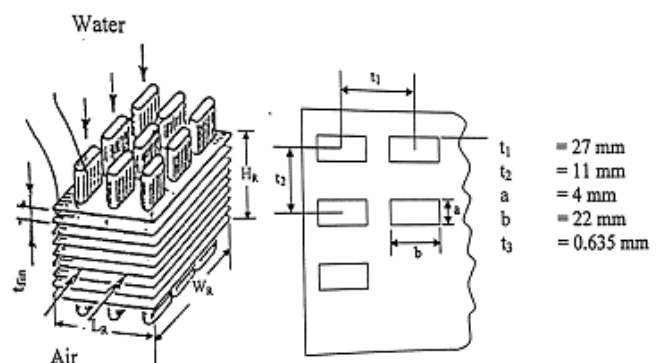


Figure 1. Basic dimensions of radiator

Number of tube row=3

N_T = Number of tube in transverse plane,

$$= \text{Width of radiator / tube pitch in transverse plane} = 21$$

Total Number of Tube = $N_T \times$ Number of row = 63

Also heat dissipated surface is determined

$$A_t = 2nf (A_{fi} - A_t \times N_t) + N_t P_t (L_f - n_f t_3) \quad (10)$$

where,

- A_{fi} = Fin area
- A_t = Tube Area
- P_t = Tube parameter
- t_3 = Fin thickness
- n_f = Number of fin
= 195

$$\text{Number of Fin, } n_f = \frac{\text{Height of radiator}}{\text{fin pitch}} \quad (11)$$

$$= 2$$

Table 1. Result Table of Cooling system Design

Item	Design Data
The amount of heat introduced into the engine with fuel, (Q_{total})	152.36 kW
Amount of heat rejected to the cooling system	53.32kW
The water pump capacity V_w	$2.004 \times 10^{-3} \text{ m}^3/\text{s}$
The velocity of water in the pump, v_w	2.8m/s
Amount of heat to the coolant (Q_w)	58.66kW
Heat dissipation area (A_t)	10.87 m^2
Radiator Face area (A_f)	0.22458 m^2
Width, (W_R)	550mm
Length, (L_R)	44mm
Height, (H_R)	407mm
Number of row	3
Number of table, N_1	$21 \times 3 = 63$
Number of fin, n	195
Tube shape, (a×b)	In line, rectangular (22×4)mm ²
Fin thickness, t_3'	0.635mm
Fin Pitch, t_3	2mm

3.2 Increment of Heat rate by designed radiator

Heat dissipation surface area of the original radiator

$$A_t' = A_f' \times l_{rad}' \times \phi_{rad} \quad (12)$$

$$= 7.55 \text{ m}^2$$

A_t' =original heat dissipated area of radiator of original engine,m²

A_f' = original face area of radiator, m²

ϕ_{rad} = original volumetric coefficient of compactness

The amount of heat disorient by the cooling system can be calculated,

$$Q_{des}' = A_t' \times C_h \times \Delta t_a \quad (13)$$

Q_{des}' = amount of heat absorbed by the original cooling system,,kW

C_h = Heat transfer coefficient
= 40.71 kW

Percentage increased by the design radiator,

$$\% \text{ increased} = \frac{(Q_{rad} - Q_{rad}')}{Q_{rad}'} \times 100$$

$$= 44\%$$

The amount of heat transfer by the water is circulated from

$$Q_{water} = \alpha_1 \times A \times \Delta T \quad (14)$$

where,

ΔT = Temperature difference of the water at the radiator outlet and inlet = 7°C

α_1 =Heat transfer coefficient from the metal to the coolant
=4340W/m²°C

A =Total coolant passing area through the tube
= $P_t \times N_T \times H_R$
= 1.339m²

By substituting in equation (14)

$$Q_{water} = 40.51 \text{ Kw}$$

3.3 Removal Amount of Heat to the Water and air

The warm water leaved the engine and passed through the radiator tube. The heat of warm water is transferred to the surrounding while it passed along the tube. At the same time, the fan gives cooling air to the radiator. So that engine heat transfer is due to the air and water to the cooling system .The amount of heat transfer by the water is 40.51 kW. Total heat removed amount by the cooling system is 58.66 kW.

Foe the design cooling system

Percentage amount of water removed = 70%

Percentage amount of air removed = 30%.

4. CONCLUSION

In this paper, the design engine is made of gray cast iron alloy and it can be studied on the engine cooling system. In closed type water cooling system the water is running through the passage in the engine (it absorbs the heat from the engine parts) and when it passes through the radiator, it cools. After getting cool again in the radiator, the water comes back through the engine. Therefore, this continues as long as the engine running, with the water absorbing and removing the engine heat and radiator cooling the water.

Cooling system efficiency is usually rated by the different in temperature between the water and surrounding air. Heat transfer analysis to the engine head with various water velocity, water flow rate, water jacket average length and radiator of cooling system for 1974cc gray cast engine head were calculated. In the radiator design, engine heat transfer is due to the air and water of the cooling system. The design water velocity is 2.8m/s. The limit of water velocity is 2.5 to 3 m/s for diesel engine [8].

The original radiator used in aluminum engine head can be released the amount of heat about 30.28 kW but the design radiator is rejected heat about 53.32 kW. In this paper ,the radiator size is changed and then the depth of radiator is increased from 4 mm, the width of radiator increased from 30mm and the height of radiator is increased from 75mm.The radiator size can be large about 75% and the amount of heat removed is increased to 44%. Today the percentage of the removed heat by the water is between 70% to 75%.

5. ACKNOWLEDGMENTS

First of all, the author is grateful to Dr. Thein Gi, Rector of Technological University (Thanlyin), for giving the permission to submit the paper.

The author would like to thank his supervisor, Dr. Mi Sandar Mon, Professor and Head of Mechanical Engineering Department, Yangon Technological University, for her close supervisions and words of inspiration that have always been a motivation to me during the paper work.

The author wishes to express her heartfelt thanks to each and every one who assisted in completing this paper.

Finally, the author deep gratitude and appreciation go to her parents for her moral supports, patience, understanding and encouragement.

6. REFERENCES

- [1] Spaniel,M., and Divis, M 2003. “Diesel Engine Head Steady State Heat Analysis”. Journal of Middle European Construction and Design of Cars. Moscow.
- [2] Heywood,J. B. No Date. Internal Combustion Engine Fundamentals. NewYork, McGraw-Hill Book Company
- [3] Stone, R.1972. Introduction to Internal Combustion Engines. 2nd Edition. Macmillon.
- [4] Lichty, L. C. 1951. Internal Combustion Engines. 6th Edition. Unite States of America..
- [5] A.T.J.Kersey,1947: Internal-Combustion Engineering. Third Edition, Blackie and Son Limited
- [6] Anonymous. 2005. Radiator Technical Information. 20th March 2009m<[http:// www. Toyotar Radiator.com.](http://www.ToyotarRadiator.com)>
- [7] Anonymous. 2005. Size of Radiator. 20th March 2009 [http://www.Chines Radiator.com.](http://www.ChinesRadiator.com)
- [8] Khovakh, M.1979.Motor vehicle Engine. Mir Publisher .Mascow
- [9] Heinz Heisler,1999.Vehicle and Engine Tecnology,2th Edition
- [10] Sein Lwin and Aung Kyaw Myint .1997.Design of Four Stroke Engine.BE Thesis ,YTU.

Design of Blade for 5kW Propeller Turbine

Lwin Lwin Oo
Department of Mechanical
Engineering,
Technological University
Thanlyin, Myanmar

Su Yin Win
Department of Mechanical
Engineering,
Technological University
Thanlyin, Myanmar

Khaing Zaw Lin
Department of Mechanical
Engineering,
Technological University
Thanlyin, Myanmar

Abstract: Hydropower is one of the most cost effective solution for the production of electricity and thus preventing global warming. Micro-hydro power scheme can be designed and build by local staff and small organizations by using materials that can be available at local marketing. In this paper, the design of 5kW propeller turbine is presented. The available head and flow rate for turbine are 2.2 m and 0.38 m³/s. The required speed to produce desired output power is 762rpm. The calculated specific speed for this turbine is 727. The main important parts of turbine such as runner, guide vanes, casing and draft tube. In this design the runner blade is mainly intend. The detail design of the runner blade profile is calculated by using Microsoft Excel .Runner blades are divided five sections and three dimensional blade profiles are drawn by SolidWorks software. The calculated runner diameter is 0.310 m and hub diameter is 0.124 m.

Keywords: propeller turbine; runner blade; guide vanes; blade profile; SolidWork.

1. INTRODUCTION

Water power has enormous potential. It is one of the most cost effective solution for the production of electricity and thus preventing global warming. By using of hydro-electric power , it no need to worry far environmental such as green house effect ad acid rain. Many countries in world are now encouraging the development of hydro power to full fill their electrical energy need.

Many new turbine manufacturers appearing and the older ones trying to a new expansion. Hydro power is a great option to choose instant of polluting energy sources. Hydraulic machine which convert either hydraulic energy (energy possessed by water) into mechanical energy (which is further converted into electrical energy) or mechanical energy into hydraulic energy.[3]

Turbines are defined as the hydraulic machine which converts hydraulic energy into mechanical energy. The kinetic energy of flowing water turns blades or vanes in hydro turbines, and then energy is change to mechanical energy. Depending on the capacity of water sources and flow of water by force of gravity, hydropower plant may be large, small, mini, micro and pico. Propeller turbines are low head and low cost for installation.

2. MAIN COMPONENTS OF PROPELLER TURBINE

There are four main components of propeller turbine. These are runner , guide vane , casing and draft tube.

i) Runner blades

Runner blades are main components of turbine that converts water power to the rotational of the shaft power.

ii) Guide Vanes

Guide vanes are fitted at entrance of runner. The primary section of the guide vanes is to convert the pressure energy of the fluid into the moment energy (kinetic energy). Flow which is coming from the casing, meets stay vanes, they are fixed.

iii) Casing

Spiral casing is the best type and provided at lower head as well. The runner is completely enclosed in casing. The casing and runner are always full of water.

iv) Draft Tube

The water, after passing through the runner, flow down through a tube called draft tube. It convert kinetic energy to flow energy because pressure different exist between the working fluid (water) in the turbine and atmosphere.[5]

3. APPLICATION OF PROPELLER TURBINE

When the vanes are fixed to the hub and they are not adjustable , the turbine is known as propeller turbine. This turbine is suitable where a large quantity of water at low head is available. In this turbine , allow the fluid to enter the runner axially and discharge the fluid axially.

The turbine having a propeller shape is known as propeller turbine ,which is an axial flow reaction turbine. The propeller turbine usually has three to six blades .On a vertical shaft and water flow parallel to the axis of turbine. The turbine wheel , which is completely under water , is turn by the pressure of water. Guide vanes regulated the amount of water reaching the wheel and the water flows from higher pressure to lower pressure.[8]

4. RUNNER DESIGN

After knowing the designed head, the specific speed can be calculated from the following equation

$$N_s = \frac{885.5}{H^{0.25}} \quad (1)$$

Speed of the turbine,

$$N = \frac{N_s H^{1.25}}{\sqrt{P}} \quad (2)$$

Where

N = speed of turbine, rpm

N_s = specific speed, rpm

And then the value of periphery coefficient can be determine by the following equation

$$\phi = 0.0242 \times N_s^{2/3} \quad (3)$$

The runner discharge diameter,

$$D = \frac{84.5 \times \phi \times \sqrt{H}}{N} \quad (4)$$

According to the specific speed, the number of blade and the ratio of hub and outer diameter of propeller turbine can be read from figure. The number of blade is four.

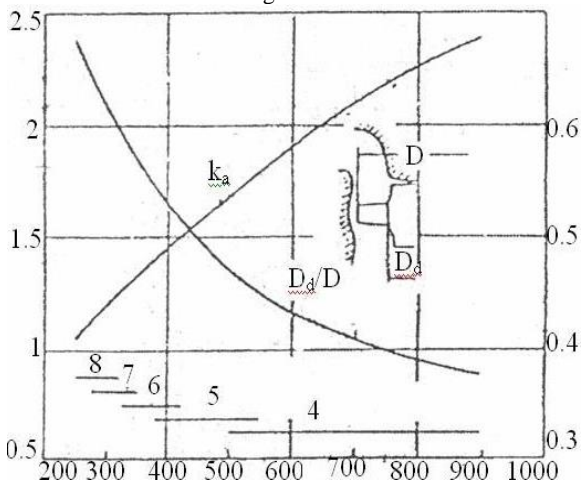


Figure 1. Relation Between Specific Speed and Number of Blade [1]

The power developed by a turbine is given by the following equation

$$P = \rho g Q H \eta_o \quad (5)$$

Where,

P = turbine output power, kW

Q = flow rate, m³/s

ρ = density of water, kg/m³

η_o = Overall efficiency of the turbine

H = Design head, m

Then, the flow velocity through with the runner can be determined from the following continuity equation[9].

$$Q = A V_f \quad (6)$$

Where,

A = Flow area, m²

V_f = Flow velocity, m/s

$$A = \frac{\pi}{4} (D^2 - d^2) \quad (7)$$

Where,

D = Runner diameter, m

d = Hub diameter, m

Table 1. Result Table of Propeller Turbine

Description	Symbols	Calculated Result	Units
Power output of turbine	P	5	kW
Speed of turbine	N	762	rpm
Runner discharge diameter	D	0.310	m
Runner hub diameter	d	0.124	m
Flow rate	Q	0.38	m ³ /s
Flow velocity	V _f	5.98	m/s
Number of blade	z	4	-

4.1 Guide vane design

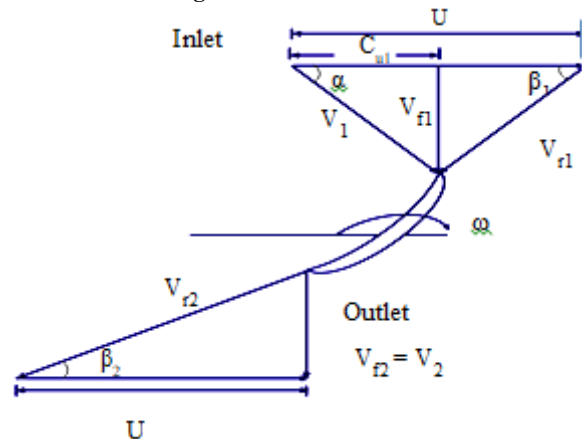


Figure .2 Inlet and Outlet Velocity Triangle of Propeller Turbine[7]

To calculate the Guide Vane angle α, it is need to know the flow velocity and inlet whirl velocity

$$\alpha = \tan^{-1} \frac{V_{f1}}{V \omega l} \quad (8)$$

Where the inlet whirl velocity can be calculate by the following equation,

$$V_{\omega l} = \frac{\eta_h g H}{U} \quad (9)$$

The hydraulic efficiency of turbine can be calculated,

$$\eta_h = \frac{\eta_o}{\eta_m} \quad (10)$$

The tangential velocity of outer runner diameter can be calculated by the following equation

$$U = \frac{\pi DN}{60} \quad (11)$$

The diameter of guide vane can be calculated,

$$D_v = 1.5D \quad (12)$$

So, The number of guide blade can be evaluated as follow

$$Z_1 = \frac{1}{4} \sqrt{D} + 5 \quad (13)$$

Then, the length of guide vane can be calculated by the following equation.

$$L = \frac{1.5D - D}{2 \sin \alpha} \quad (14)$$

5. DESIGN OF BLADE PROFILE

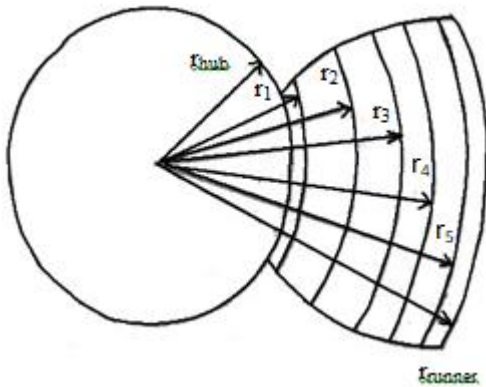


Figure . 3 Five Sections of Blade[4]

Runner can be divided into five cylindrical sections. These section can be calculated the following equation.

For section I,

$$r_1 = \frac{d}{2} + 0.015D \quad (15)$$

For section II,

$$r_2 = r_1 + \frac{r_3 - r_1}{2} \quad (16)$$

For section III,

$$r_3 = \frac{D}{2} \sqrt{\frac{1 + (\frac{d}{D})^2}{2}} \quad (17)$$

For section IV,

$$r_4 = r_3 + \frac{r_5 - r_3}{2} \quad (18)$$

For section V,

$$r_5 = \frac{D}{2} - 0.015D \quad (19)$$

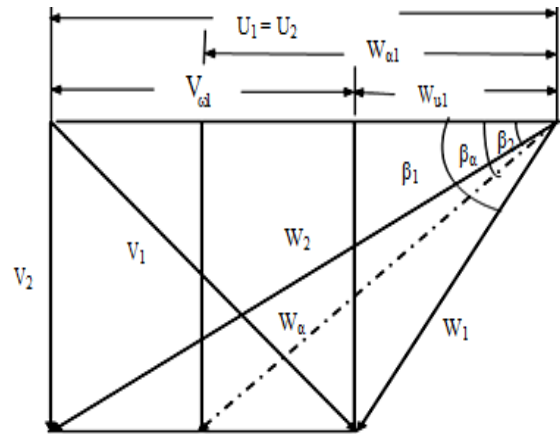


Figure. 4 Velocity Triangle of Propeller Turbine [6]

To find the Tangential speed,

$$U = \frac{\pi r_1 N}{30} \quad (20)$$

From Velocity diagram, The inlet whirl velocity, $V_{\omega 1}$ can be calculated

$$V_{\omega 1} = \frac{\eta_h g H}{U} \quad (21)$$

And then, the blade inlet angle and outlet angle at section I can be calculated as follow,

$$\tan \beta_1 = \frac{V_{f1}}{U - V_{\omega 1}} \quad (22)$$

$$\tan \beta_2 = \frac{V_{f2}}{U} \quad (23)$$

Then, the average blade angle is

$$\tan \beta_\alpha = \frac{V_f}{W_{\alpha 1}} \quad (24)$$

Where, $W_{\alpha 1}$ is the average value of tangential component of relative velocity and it can be determined by the equation;

$$W_{\alpha 1} = U - \frac{V_{\omega 1}}{2} \quad (25)$$

And then average relative velocity can be evaluated by the following equation,

$$W_\alpha = \frac{W_{\alpha 1}}{\cos \beta_\alpha} \quad (26)$$

The spacing of the blade can be determined by the following equation.

$$t = \frac{2r_1 \pi}{z} \quad (27)$$

Then, to obtain the angle of attack we have to consider the efficiency of turbine equation

$$\eta_h = uw_\alpha \frac{1}{t} \left(k_z - \frac{k_x}{\tan\beta_\alpha} \right) \quad (28)$$

From the above equation, it can be written by

$$\left(k_z - \frac{k_x}{\tan\beta_\alpha} \right) = \frac{\eta_h}{uw_\alpha \frac{1}{t}} \quad (29)$$

Where,

$$k_x = Mc_x$$

$$k_z = Mc_z$$

$$c_z M \tan\beta_\alpha - c_x + \frac{c_z}{6\pi} = \frac{\eta_h}{uw_\alpha \frac{1}{t}} \tan\beta_\alpha \quad (30)$$

To calculate the RHS of equation (29) we have to determine the following parameter

$$u = \frac{U}{\sqrt{2gH}} \quad (31)$$

$$w_\alpha = \frac{W_\alpha}{\sqrt{2gH}} \quad (32)$$

And then, select $\alpha = 14^\circ$,

The lattice angle, β will be greater by the angle of attack,

$$\beta = 90 - \beta_\alpha \quad (33)$$

And then, $\beta = 90 - \beta_\alpha + \alpha$

In this case, the following value can be obtained the appendix fig A.

$$t/l = 0.86, M = 0.55$$

Then, the value of above parameter can be substitute the RHS of the equation (29).

$$c_z M \tan\beta_\alpha - c_x + \frac{c_z}{6\pi} = 1.67$$

To satisfy the L.H.S and R.H.S of the equation (29)

Selected the profile N.A.C.A 2412 which satisfied the given direction for the selection of the cross section, by equations

$$c_z = \frac{\partial c_z}{\partial \alpha} (\alpha - \alpha_0) \quad (34)$$

$$c_x = c_{xv} + \frac{\partial c_x}{\partial c_z} c_z \quad (35)$$

From the figure in Appendix A

$$\alpha_0 = -2^\circ$$

$$\frac{\partial c_z}{\partial \alpha} = 0.075$$

$$c_{xv} = 0.0094$$

$$\frac{\partial c_x}{\partial c_z} = 0.0566$$

$$\alpha_\alpha = \alpha^\circ - 57.3 \times \frac{c_z}{6\pi} \quad (36)$$

And then, the lattice angle, β is

$$\beta = 90 - \beta_\alpha + \alpha_\alpha \quad (37)$$

Table. 2 Result Data of Blade Profile

Symbols	I	II	III	IV	V	units
R	0.067	0.092	0.118	0.134	0.150	m
U	5.32	7.37	9.42	10.70	11.99	m/s
V_{ol}	3.82	2.76	2.16	1.61	1.69	m/s
β_1	76	52	39	33	30	Degree
β_2	48	39	32	29	26	Degree
β_α	60	45	36	31	28	Degree
$W_{\alpha 1}$	3.14	5.99	8.34	9.90	11.15	m/s
W_α	6.88	8.46	10.26	11.56	12.65	m/s
t	0.105	0.145	0.185	0.211	0.236	m
Vf	5.98	5.98	5.98	5.98	5.98	m/s
l/t	1.16	0.99	0.91	0.88	0.86	-
l	0.121	0.144	0.169	0.186	0.204	m
β	40	48	56	59	63	degree
α_α	10.35	3.14	1.86	1.09	1.01	degree

After Calculating the blade profile , the three dimensional runner blade are drawn by SolidWorks Software. The standard NACA 2412 airfoil is used for blade profile.

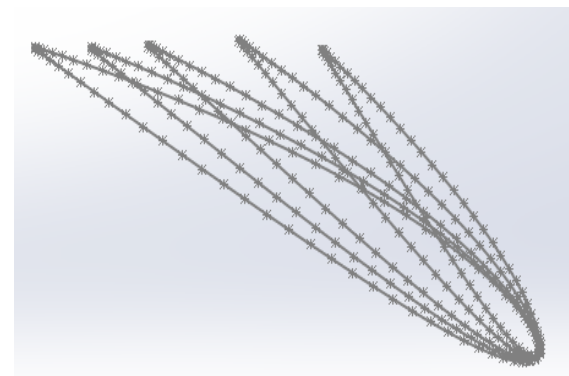


Figure . 5 Blade profile [11]

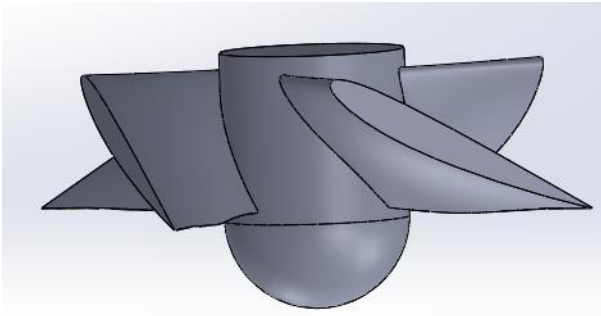


Figure . 6 Isometric View of Turbine Blade

6. CONCLUSION

Pico hydro power can be a suitable support to promote living standard and electrification development for rural area.[10] The required head and flow rate data are collected from the drop structure of irrigation canal of Ma Mya Dam in Irrawaddy Division, in Myanmar .In this paper, propeller has 4blade runner. The specification of turbine having rated capacity of 5kW , flow rate is 0.38m³/s and 2.2m head. The detail design of the blade that is divided in five cylindrical sections is presented. The next paper will describe the simulation result upon on the blade and compare with simulation result and theoretical result .

ACKNOWLEDGMENTS

First of all, the author is grateful to Dr. Thein Gi, Rector of Technological University (Thanlyin), for giving the permission to submit the paper.

The author would like to thank his supervisor, Dr. Su Yin Win , Professor and Head of Mechanical Engineering Department, Thanlyin Technological University for her kind supervisions ,encouragement , suggestion and valuable guidance for this paper.

Finally, the author would like to express my gratitude to my parents and friends for their support and encouragement to attain the attention without any trouble. I would like to thankful to all of my teachers who taught me everything from childhood until now and to each and everyone who assisted in accomplishing this paper.

7. REFERENCES

- [1] Frank M. White ,Fluid Mechanics (in SI Units) , Seventh Edition ,2011.
- [2] S.NAGARATNAM , Fluid Mechanics ,First Edition ,1995 April.
- [3] Dr. R. K. Bansal , Fluid Mechanics and Hydraulic Machines , Ninth Edition ,2010.
- [4] B C S RAO , Fluid Mechanics and Machinery Second Edition 2010.
- [5] Robert Simpson & Arthur Willians , Design of propeller Turbine for Pico Hydro , Version 1.1c , April (2011).
- [6] Pradhumna Adhikart , A Study on Developing Pico Propeller Turbine for Low Head Micro Hydropower Plants in Nepal , Journal of the Institute of Engineering ,Vol9.

- [7] ASHpetim Lajqi , Design and Construction of Mini Hydropower Plant with Propeller Turbine International Journal of Contemporary ENERGY , Vol .2 No.1 (2016).
- [8] Ms.M.Ujwala , Design and analysis of Low Head ,light weight Kaplan Turbine Blade (2017).
- [9] H.Zainuddin , Design and Developing of Pico-Hydro Generation System for energy Storage Using Consuming Water Distributor to House (2009).
- [10] Lejeune A. Professor and Topliceanu I. Sessution Hydroelectricity , May (2007).
<http://www.hydrowest.com/runners>

Comparative Study of Irregular-shaped RC Building with Different Lateral Load Resisting Systems

Phyu Thwe Thwe Tun
Department of Civil
Engineering
Technological University
(Thanlyin),
Myanmar

Dr. Kyaw Zeyar Win
Department of Civil
Engineering
Technological University
(Thanlyin),
Myanmar

Khaing Su Tin
Department of Civil
Engineering
Technological University
(Thanlyin),
Myanmar

Abstract: There has been a considerable increase in modern tall buildings due to the development in construction technology and structural systems. As the building height increase, lateral loads are important consideration and it is necessary to choose a structural system that can resist lateral load effectively. Lateral loads are often resisted by various lateral load resisting systems: Beam-Column System, Shear Wall and Frame System, Frame Tube System, Dia-grid System, Dual System, etc.....In this paper, a particular type of 16-storey Irregular-shaped RC building in Zone IIA is considered with different lateral load resisting systems (i.e – Beam-Column System, Rigid Frame with Shear Wall and Dual System). Modelling and Analysis of building with different load resisting systems are carried out with ETABS V 9.7.4 software. Structural members are designed according to ACI code 318-99 and load consideration is based on UBC-97. In dynamic analysis, Response Spectrum Method is used. The values of stability check such as storey drift, P- Δ effect, Overturning, Sliding in each system are compared. Since the building is irregular-shaped, torsional irregularity is also considered and soft storey and base shear are also check. All this points are considered and the results obtained are plotted and compared with graphs. This paper give information about various lateral load resisting systems and dual system gives better performance than other with same material consumption of lateral load resisting systems.

Keywords: Beam-Column System, Shear Wall, Dual System, Lateral Load, Dynamics Analysis Response Spectrum Method, ETABS, Stability, Torsional Irregularity.

1. INTRODUCTION

Nowadays, the construction of high-rise irregular-shaped residential and commercial buildings are increased in Myanmar. A building shall be considered as an irregular if it lacks symmetry and has discontinuity in geometry, mass or load resisting elements. Building having normal regular geometry in plan and in elevation suffers much less damage than irregular one. Buildings are subjected to two types of load; gravity load and lateral load. Taller the building, lateral loads such as wind load and earthquake load should be considered and it is necessary to choose an appropriate structural system. There are two components in structural system; (i) Horizontal framing system: consists of slabs and beam and (ii) Vertical framing system: consists of beams and columns. Using an appropriate structural system is critical for good seismic performance of building. Therefore, it is important for the structure to have sufficient strength against vertical loads together with adequate stiffness to resist lateral forces.

2. OBJECTIVES

- To investigate the lateral response of building in each system.
- To observe the performance of different lateral load resisting system
- To study the influence of lateral loading on structure

3. LATERAL LOAD RESISTING SYSTEMS

A typical lateral load resisting system consists of horizontal and vertical elements connected together so as to transfer lateral forces from the top of a building to the foundations. The

following sections present an overview of the behavior of various structural systems under lateral loading.

3.1 Beam-Column System

In beam-column system, frames are composed of columns and beams. Beam is a horizontal member and transfers the load to column. Column is a vertical member and transfers compressive load to the foundation. Due to the rigidities of the beam and column connections and moment resisting capacities of the individual members, it can resist the lateral loads.

3.2 Rigid Frame with Shear Wall

Wall-Frame structural system is a structural system having combination of rigid frame and shear wall. Shear wall is a constructed as a part of central elevator or service core and frames are arranged in plan in conjunction with the wall. This structural system can resist lateral loads effectively by producing interaction between shear wall and frames.

3.3 Dual System

Dual system is a system consisting of RC frames interacting with RC shear wall. This system resists both gravity and lateral loads using moment resisting frames and shear wall or braced frame. The two systems are designed to resist the total design force in proportion to their lateral stiffness considering the interaction of dual systems of all floor levels. The moment resisting frames are designed to independently resist at least 25% of design base shear.

4. PARAMETRIC STUDIES

In high-rise building, it is important to choose the suitable structural system which satisfy the strength and stiffness requirement. In this paper, the comparison of beam-column system, rigid frame with shear wall and dual system is presented. Analysis is carried out in ETABS and results are compared.

- (1) Model 1: Beam-Column System
- (2) Model 2: Rigid Frame with Shear Wall
- (3) Model 3: Dual System

4.1 Study Parameters

- (a) Type of building: Irregular-shaped RC building
- (b) Number of story: 16
- (c) Height of building: 168ft
- (d) Plan dimension: maximum length = 152.5ft
maximum width = 9ft

Table 1. Material properties

Modulus of elasticity, E	3600ksi
Poisson's ratio	0.2
Coefficient of thermal expansion	5.5x10 ⁻⁶ in/in per °F
Reinforcing yield stress, fy	50000psi
Shear reinforcement yield stress, fs	50000psi
Concrete strength, f'c	4000psi

(f) Design Loads

(i) Dead Loads

Dead loads are permanent and result from the weight of structure and all other permanently attached materials.

Table 2. Dead load data

4 ½" thick brick wall	50psf
9" thick brick wall	100psf
Weight of elevator	2tons
Superimposed D.L	20psf
Unit weight of concrete	150pcf

(ii) Live Loads

Live loads consist of temporary or short duration occupancy loads. They are moveable and their intensity may vary in locations.

Table 3. Live load data

For shopping center, restaurant, ballroom & staircase	100psf
For hotel room	50psf

(iii) Wind Loads

Wind loads shall be assumed to come from any horizontal direction.

Table 4. Wind load data

Exposure type	B
Leeward coefficient	0.5
Windward coefficient	0.8
Importance factor, I	1
Basic wind speed	100mph
Method	Normal Force Method

(iv) Earthquake Loads

Earthquake loads is the result from the shaking of foundation by seismic disturbance.

Table 5. Earthquake load data

Zone factor	0.2
Soil type	S _D
Importance factor, I	1
Response modification factor, R	5.5 (6.5 for dual)
Time period, Ct	0.03
Seismic coefficient, C _a	0.28
Seismic coefficient, C _v	0.4

4.2 Load Combination

There are 26-factored load combinations used in structural analysis based on ACI 318-99 and UBC-97.

Type of analysis – Dynamic Analysis

Table 6. 26 load combinations

COMB 1	1.4 TDL
COMB 2	1.4 TDL + 1.7 TLL
COMB 3	1.05 TDL + 1.275 TLL + 1.275 WX
COMB 4	1.05 TDL + 1.275 TLL – 1.275 WX
COMB 5	1.05 TDL + 1.275 TLL + 1.275 WY
COMB 6	1.05 TDL + 1.275 TLL – 1.275 WY
COMB 7	0.9 TDL + 1.3 WX
COMB 8	0.9 TDL – 1.3 WX
COMB 9	0.9 TDL + 1.3 WY
COMB 10	0.9 TDL – 1.3 WY
COMB 11	1.05 TDL + 1.275 TLL + SPX
COMB 12	1.05 TDL + 1.275 TLL – SPX
COMB 13	1.05 TDL + 1.275 TLL + SPY
COMB 14	1.05 TDL + 1.275 TLL – SPY
COMB 15	0.9 TDL + 1.02 SPX
COMB 16	0.9 TDL – 1.02 SPX
COMB 17	0.9 TDL + 1.02 SPY
COMB 18	0.9 TDL – 1.02 SPY
COMB 19	1.16 TDL + 1.275 TLL + SPX
COMB 20	1.16 TDL + 1.275 TLL – SPX
COMB 21	1.16 TDL + 1.275 TLL + SPY
COMB 22	1.16 TDL + 1.275 TLL – SPY
COMB 23	0.79 TDL + 1.02 SPX
COMB 24	0.79 TDL – 1.02 SPX
COMB 25	0.79 TDL + 1.02 SPY
COMB 26	0.79 TDL – 1.02 SPY

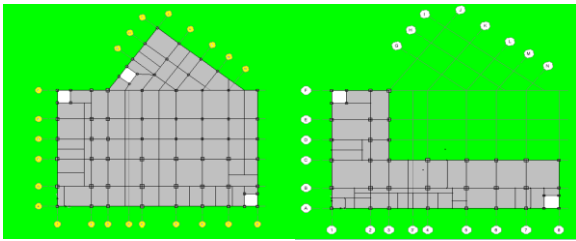
5. MODELLING IN ETABS

Table 7. Structural members sizes used in three models

Column size	16"x16", 18"x18", 20"x20", 22"x22", 24"x24", 26"x26", 28"x28", 30"x30", 32"x32", 34"x34", 36"x36", 38"x38"
Beam Size	10"x12", 12"x18", 14"x20", 14"x24", 16"x24"
Slab Thickness	6"
Shear Wall Thickness	14"

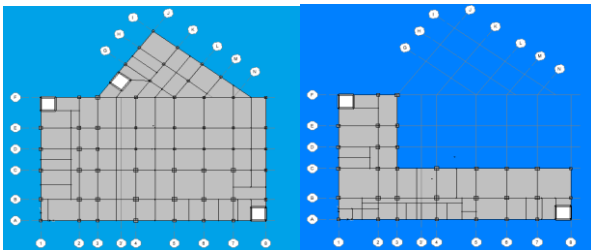
Column size change every fourth floor.

Three buildings of 16storey irregular-shaped are modelled in ETABS V 9.7.4 and plan of the building in each system and 3D model of structures are shown in figure 1, 2, 3, 4.



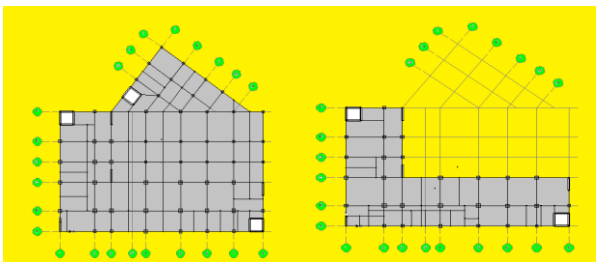
(a) (b)

Figure 1. Plan for beam-column system: (a) GF to 3rd floor & (b) 5th floor to roof



(a) (b)

Figure 2. Plan for rigid frame with SW: (a) GF to 3rd floor & (b) 5th floor to roof



(a) (b)

Figure 3. Plan for dual system: (a) GF to 3rd floor & (b) 4th floor to roof

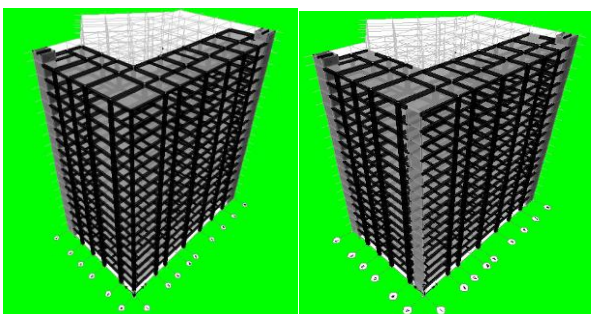
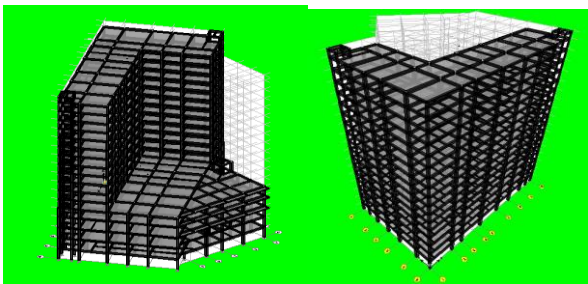


Figure 4. 3D models of structure in each system

6. ANALYSIS RESULTS

6.1 Storey Drift

Storey drift is the lateral displacement (deflection)

$$\Delta_m = 0.7R\Delta_s$$

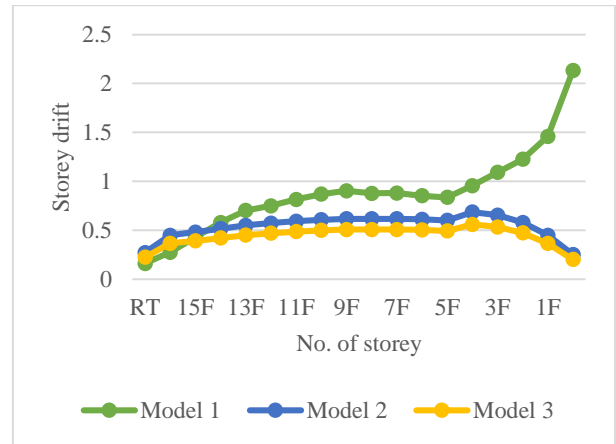


Figure 5. Storey drift in X-X direction



Figure 6. Storey drift in Y-Y direction

From figure 5 and 6, the results show that storey drift values in X-direction and Y-direction was found comparatively lesser in dual system than beam-column system and rigid frame with shear wall.

6.2 P-Δ Effect

When the structure is acted upon by a lateral (seismic load), the structure becomes laterally displaced and applied. According to UBC-97, the member forces, moments and story displacements are generated by P-Δ effect. It should be considered in the evaluation of overall structural frame stability.

$$\vartheta_x = P_x \Delta_{S_x} / V_x h_x$$

The stability coefficient is much smaller than allowable limit 0.1.

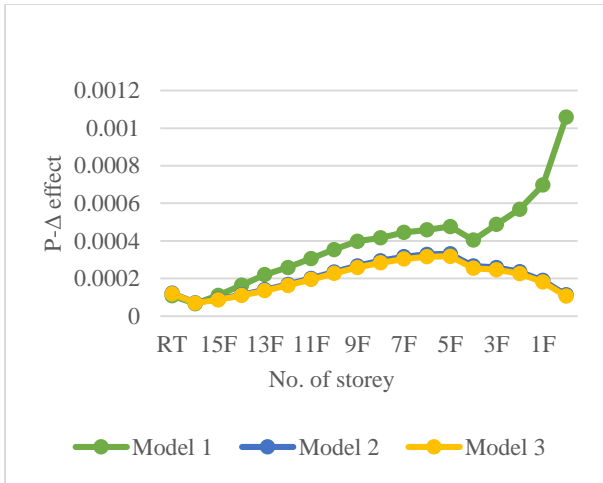


Figure 7. P-Δ effect in X-X direction

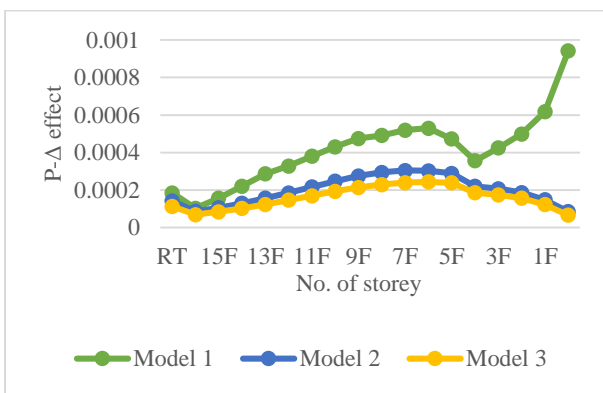


Figure 8. P-Δ effect in Y-Y direction

From above figure 7 & 8, it is observed that model 2 and model 3 gives less displacement compared to model 1.

6.3 Overturning Moment

The distribution of earthquake forces over the height of a structure cause the structure to experience overturning effect. According to UBC-97, every structure is to be designed to resist the overturning effects caused by seismic forces.

Safety Factor = Resisting Moment/Overturning Moment >1.5



Figure 9. Overturning check in X-X direction



Figure 10. Overturning check in Y-Y direction

6.4 Sliding Check

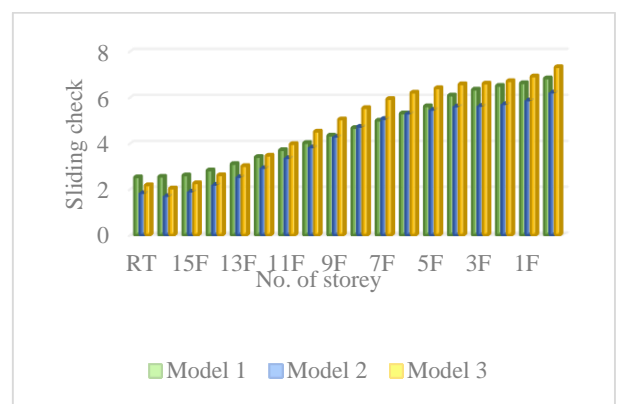


Figure 11. Sliding check in X-X direction

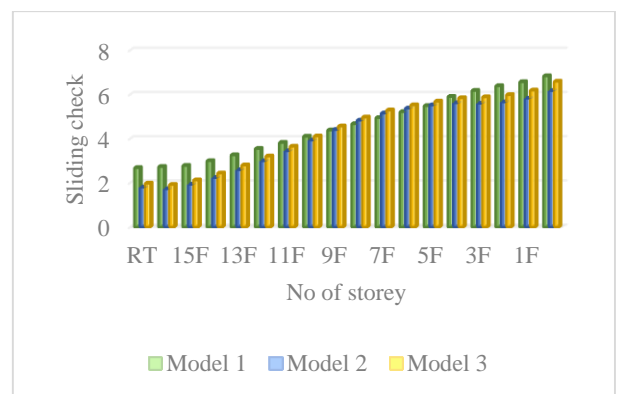


Figure 12. Sliding check in Y-Y direction

6.5 Base Shear

Base shear is an estimate of the maximum expected lateral force that will occur due to seismic ground motion at the base of the structure

Table 8. Base shear

Storey	Model 1	Model 2	Model 3
RT	4525.86477	4607.050573	4617.817
RB	3085.344054	3140.689528	3148.0291
15F	3085.344054	3140.689528	3148.0291
14F	3085.344054	3140.689528	3148.0291
13F	3085.344054	3140.689528	3148.0291
12F	3085.344054	3140.689528	3148.0291
11F	3085.344054	3140.689528	3148.0291
10F	3085.344054	3140.689528	3148.0291
9F	3085.344054	3140.689528	3148.0291
8F	3085.344054	3140.689528	3148.0291
7F	3085.344054	3140.689528	3148.0291
6F	3085.344054	3140.689528	3148.0291
5F	3085.344054	3140.689528	3148.0291
4F	2690.986069	2739.257477	2745.6589
3F	2690.986069	2739.257477	2745.6589
2F	2690.986069	2739.257477	2745.6589
1F	2690.986069	2739.257477	2745.6589
GF	2690.986069	2739.257477	2745.6589

6.6 Torsional Irregularities

Torsional irregularity is to be considered to exist when the maximum story drift, calculated with design eccentricity, at one corner of the structures transverse to an axis is greater than 1.2 times the average of the story drifts at the two ends of the structure.

Table 9. Torsional Irregularities Check

Model	Max: Story drift	Average story drift	$\Delta_{max}/\Delta_{avg} < 1.2$	Structural Irregularity
Model 1	3.4181	3.14625	1.09	Does not exist
Model 2	2.2133	1.87165	1.18	Does not exist
Model 3	1.8097	1.58115	1.15	Does not exist

7. CONCLUSION

From the above study of comparison between three lateral load resisting systems, the following results has been obtained. Story drift values in X-direction and Y-direction were found comparatively lesser in dual system than beam-column system and frame with shear wall system. Beam-column system produces greater deflection and drift. Shear wall produce large effects of overturning. Torsional irregularity can be avoided in building by providing proper shape and symmetry in structure. It is found that structure with dual system gives better performance than other with same material consumption of lateral load resisting systems. It may conclude that dual system gives result than other as in the case of time period, displacement, story force and stiffness.

8. ACKNOWLEDGEMENT

The author of this paper would like to thank to her supervisor Dr. Kyaw Zeyar Win, Professor, Head of the Department of Civil Engineering of the Technological University (Thanlyin) for carrying out the experimental work. The author would like express my deepest thanks to all who help her with necessary assistance for this study.

9. REFERENCE

- [1] International Conference of Building officials. 1997. Structural Engineering Design Provisions. Uniform Building Code. Volume 2. U.S.A.: International Conference of Building Officials.
- [2] Nilson, A.H., and Winter, G. 1991. Design of Concrete Structures. 11th ed. Singapore. McGraw Hill, Inc.
- [3] P.P. Hoogendoorn, "Lateral Load Design of Tall Buildings".
- [4] Tarant, B.S. 1998. Structural Analysis and Design of Tall Buildings. Singapore: McGraw. Hill Book Company.
- [5] American Concrete Institute. 1999. Building Code Requirement for Structural Concrete (ACI 318-99). U.S.A.: American Concrete Institute.
- [6] Bagheri B. et al., "Comparative Study of the Static and Dynamic Analysis of Multistorey Irregular Building International Scholarly and Scientific Research & Innovation, World Academy of Science, Engineering and Technology Vol:6.

Parametric Study on the Settlement of Piled Raft Foundation for High-Rise Building

Pwint Wai Wai Aung
Department of Civil Engineering
Technological University
(Thanlyin),
Myanmar

Nyan Phone
Department of Civil Engineering
Technological University
(Thanlyin),
Myanmar

Kyaw Lin Htat
Department of Civil Engineering
Technological University
(Thanlyin),
Myanmar

Abstract: Piled raft foundation is a composite construction consisting of three elements, piles, raft and subsoil. It has been commonly used for the foundation of high rise building in recent year. The combined effect of piles and raft can reduce the maximum and differential settlement and it can lead to more economical foundation design as compare to the conventional pile foundation. This paper focus on the settlement of piled raft foundation of a high-rise building resting on sandy soil in Yangon area. The critical column load of superstructure is obtained by using ETABs software and loading consideration for superstructure is based on UBC -97. Soil type is sandy soil and the upper soil layer where the raft located is sandy silt. This study considered the type of bored pile and the allowable bearing capacity is calculated by Hansen's method, Tomlison's methods and Meyerhof's Rule of Thumb method. The simplified analysis is made by Poulos – Davis - Randolph (PDR) method to estimate the load –settlement curve and load distribution between piled and raft. The piled raft foundation is analyzed by SAFE software, in which the raft is modelled as a thin plate and the piles and soils are treated as springs. In this study, a parametric study is made on raft thickness, pile length and number of piles. The increase in raft thickness do not have much significant effect in reducing maximum and differential settlement but it is uneconomical due to increasing of moment. The maximum settlement is reduced by increasing pile length and number of piles.

Keywords: piled raft foundation; parametric study; simplified approach; load distribution; settlement.

1. INTRODUCTION

The growth of population and the scarcity of land has been needed to build many high-rise building. These building impact huge axial load to the soil through their foundations. So the foundation of high -rise building needed to design to resist the superstructure load safety and to transfer these load to the soil. Moreover, it can be effectively supported the stability of the building. In conventional design, mat and pile foundations are used to support these heavy loaded buildings [1], [2], [3]. In recent years, piled raft foundations have been commonly used as a kind of foundation for high- rise buildings. Actually, it is a combination of raft foundation and pile foundation and it is composed of three elements raft, piles and subsoil. It is mostly used where the raft foundation alone provides nearly adequate bearing capacity but it can cause settlement. In piled raft foundation, load is distributed between piles and raft, so the load from the superstructure is taken partly by raft and piles [4]. The design process of piled raft foundation is described in three stage and the load-settlement curve of piled raft has been estimated based on stiffness of members [5], [6]. There are difference techniques that have been developed for analysis of piled raft foundation. The overall settlement and differential settlement are analyzed by hybrid method in [7]. Design method and simplified analysis based on stiffness of pile group stiffness and raft stiffness have been presented by many researchers in [8], [9]. Numerical analysis is made by finite element method in which raft are modelled as a plate and piles treated as non-linear springs in [10]. Behaviour of piled raft is also analyzed with pile of different lengths subjected to horizontal and vertical loadings by using finite layer method [11]. In piled raft foundation, the performance of parameters plays an important role for the stability of foundation. Parameters of piled raft foundation are raft thickness, piles length, piles diameter, piles spacing, piles configuration and number of piles. This

paper focus on the parametric study of raft thickness, piles length and number of piles and made a discussion the influence of these three parameter on the stability of foundation. In this study, firstly, parametric study is made on load distribution and found tri-linear load settlement curve by using simplified approach. Then, parametric study is made on settlement of piled raft foundation by using SAFE software and discuss the results. The rests sections are comparison of simplified analysis and software analysis and conclusion.

2. SOIL CONDITION

The type of soil in Bahan township, Yangon area is sandy soil. The groundwater table exists at 18 ft below the ground level. The underlain sand layer is covered by sandy silt layer near the surface. The layer of soil where the raft located is sandy silt. The allowable bearing capacity of subsoil below raft is 2.01 ton/ft² and the required bearing capacity is 2.69 ton/ft². Allowable capacity is nearly the required capacity but it cannot provide the satisfied bearing capacity values and can cause settlement. Piled raft foundation is suitable for this type of soil and it can improve bearing capacity and reduce the settlement. Liquefaction check must be taken for sandy soil but soil report has been proven that there is no liquefaction in the soil stratum. The allowable pile capacity is calculated by Hansen's method, Tomlison's method and Meyerhof's Rule of Thumb methods. The allowable pile bearing capacity is 500 tons at 41 m and it is about 100 tons at 12m.

3. PROPOSED SUPERSTRUCTURE

The superstructure is twenty-storeyed residential building and it is firstly analyzed by ETABs software. The overall height of the building is 63m, basement height is 3.5m, ground floor level height is 4m and typical floor height is 3m. The building is rectangular shape and its length is 43m and 23m width. Loading consideration is based on UBC-97 and the load

combinations are considered as per CQHP guideline. 3D model of superstructure which is analyzed in ETABs software is shown in Figure 1.

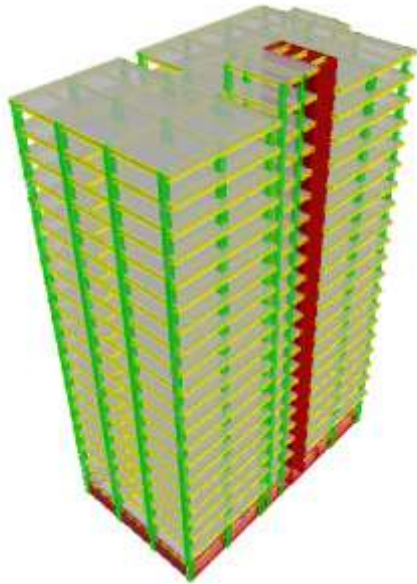


Figure 1. 3-D model of 20 storyed building

The total load of superstructure is 337.32 MN and maximum column point load is 14.508 MN.

4. MODELLING OF PILED RAFT

The philosophy of modelling of piled raft has been explained by using combined structural - geotechnical approach. To investigate the piled raft behavior, raft is modelled as a slab and piles are treated as springs. In this study, SAFE software is used for analysis of piled raft foundation. The layout of piled raft foundation in SAFE is shown in Figure 2.



Figure 2 . Layout of piled raft foundation

5. PARAMETRIC STUDIES

Parametric studies are planned to investigate the settlement of piled raft foundation under the changes of the parameter values such as raft thickness, pile length and number of piles. In this study, three cases study were taken into consideration to analyze the piled raft behavior. The raft was modelled as a concrete element and area of piled raft is 46m x 26m. The details of three cases are as follows;

Case 1: The effect of raft thickness was analyzed in Case 1 with constant other parameters. The constant pile diameter is 1m, 67 numbers, pile spacing is 3d and constant pile

length is 41m. In this case, pile raft with various raft thickness as 1.8m, 2m, 2.3m and 2.5m were analyzed to find the maximum moment and maximum and differential settlement on each thickness.

Case 2: The effect of various pile length was focus in Case 2 without changing other parameters. The constant raft thickness is 1.8m, constant 1m diameter, 67 numbers and the constant pile spacing is 3d. In Case 2, the maximum and differential settlement of piled raft foundation is observed by varying pile length such as 41m, 30m, 24m and 18m.

Case 3: Case 3 is mainly focus on the effect of number of piles by considering constant of other parameter. The constant raft thickness is 1.8m, 1m diameter and constant pile length is 41 m. In this case, the effect of maximum and differential settlement were observed with various number of piles such as 40, 60, 72 and 84. The configurations of various number of piles were shown in Figure 3.

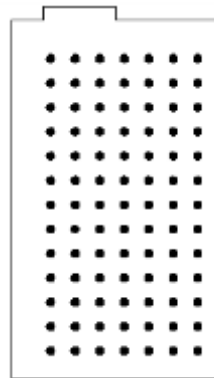


Figure 3. (a) 84 nos

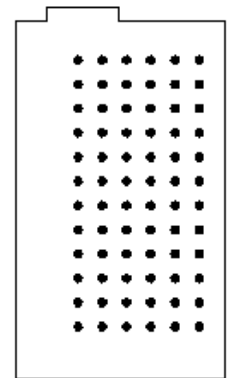


Figure 3. (b) 72 nos

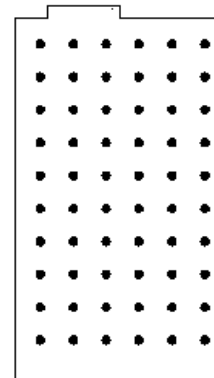


Figure 3. (c)60 nos

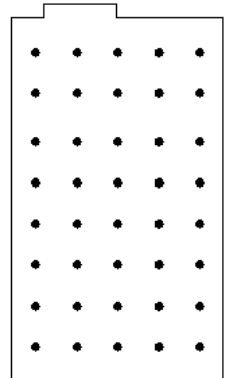


Figure 3. (d)40 nos

Figure 3. Piles location plan for Case -3

6. SIMPLIFIED ANALYSIS

Simplified approach is made by using Poulos - Davis-Randolph (PDR) method. In this method, the load – settlement relationship and load distribution between piled and raft are calculated based on the stiffness of each member. The stiffness of piled raft foundation is calculated by equation 1, where K_p is stiffness of pile group, K_r is stiffness of raft and α_{cp} is the raft-pile interaction factor.

$$K_{pr} = \frac{K_p + K_r(1 - \alpha_{cp})}{1 - \alpha_{cp} \frac{K_r}{K_p}} \quad (1)$$

The load sharing percent between piles and raft are calculated by equation 2, where P_r is the load carried by raft and P_t is the total applied load from the superstructure. The factor X is the the percent of load taken by raft and percentage of load carried by piles is obtained by 1- X.

$$X = \frac{P_r}{P_t} = \frac{K_r(1 - \alpha_{cp})}{K_p + K_r(1 - \alpha_{cp})} \quad (2)$$

The result of simplified analysis showed that the load distribution percent between piled and raft do not have significant changes with various raft thickness. But it was considerably effect on various pile length, the load sharing percent of piled and raft based on various pile lengths were showed in Figure 4. When increase in length, piles have been taken more percent of load because piles have more bearing capacity as increase in length.

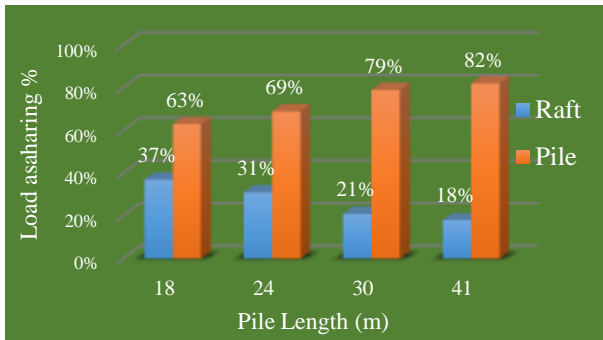


Figure 4. Load sharing (%) based on pile length

The effect of number of piles on load distribution ratio was indicated in Figure 5. It was found that the more number of piles in the group, the more percent of load can be taken by the pile group. Because the bearing capacity in the pile group is increased as increases in number in the group. But it was recognized that even the number of pile increased from 40 to 84, the load carrying percent increased about only 8 percent.

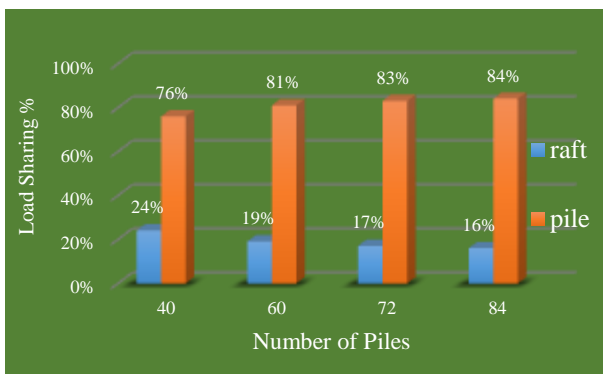


Figure 5. Load sharing (%) based on number of piles

Load – settlement curve of piled raft foundation that has been calculated by PDR method is shown in Figure 6 and Figure 7. The parameter of 1.8m raft thickness, 1m diameter ,41m pile length and 60 numbers were chosen as sampling for this load

–settlement curve. By this parameter, the stiffness of raft is 580.71 MN/m and pile group stiffness is 1979.16 MN/m. The interaction factor between raft and pile group is approximated as $\alpha_{cp} = 0.2347$. This lead to the overall stiffness of the piled raft is obtained 2463.387 MN/m by equation 1. Figure 5 showed that the maximum settlement was 5.8502 mm under maximum vertical column load of 14.508 MN.

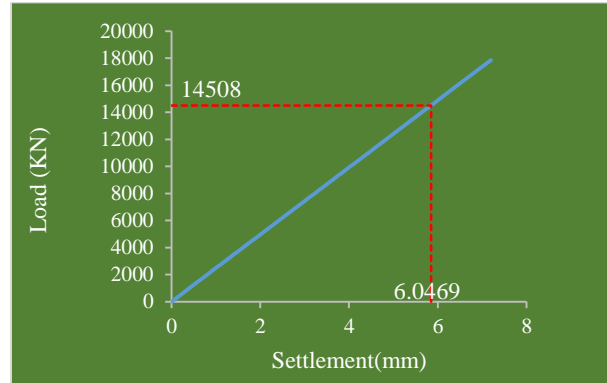


Figure 6. Load settlement curve for maximum load

The total applied load P_t at which the pile group capacity is reached its full capacity, it was calculated by equation 3, in which P_{up} is ultimate pile group capacity.

$$P_t = \frac{P_{up}}{1 - X} \quad (3)$$

The tri-linear load settlement curve calculated by PDR method is shown in Figure 7, it is showed that the total applied load of superstructure is 337.32MN and the stiffness of pile raft foundation was safety supported to this load. When total applied load further reached 928.34MN and the load – settlement curve beyond point A, the pile group capacity is fully utilized and the raft only elastic at this time.

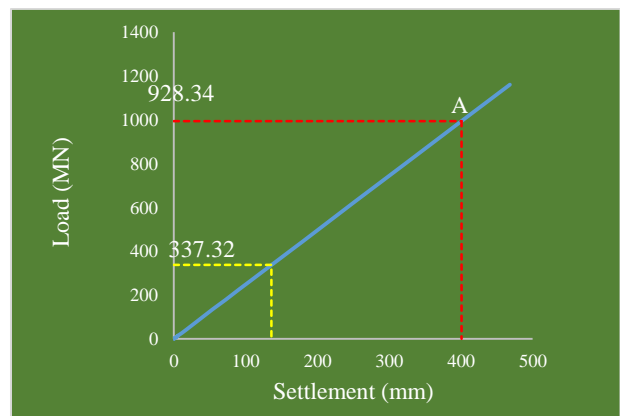


Figure 7. Tri – linear load settlement curve

The stiffness of pile raft foundation, K_{pr} , for various piles length is shown in Table 1. Where, the load P_t is the total applied load, under which the capacity of pile group reached its full capacity. Beyond this load, further applied load is supported by raft only. The value of settlement in this table is total settlement of piled raft foundation when the applied load increased to P_t and piles bearing capacity reached their ultimate limit at this time. The current applied load of superstructure in this study is 337.32 MN. Table 2 showed

that the stiffness of piled raft foundation for various number of piles.

Table 1. Stiffness of piled raft for various pile length

Pile Length	α_{cp}	K _{pr}	Pt	Se
m		MN/m	MN	mm
18	0.0565	1516	472	311
24	0.0759	1892	899	470
30	0.1495	2370	1017	429
41	0.2412	2488	1021	410

Table 2. Stiffness of piled raft for various number of piles

Pile number	α_{cp}	K _{pr}	Pt	Se
No		MN/m	MN	mm
40	0.1309	2116.0	658.0	311.0
60	0.2176	2399.0	928.0	386.0
72	0.2566	2549.0	1087.0	426.0
84	0.2895	2687.0	1245.0	463.0

7. RESULT OF SOFTWARE ANALYSIS

Analysis results of the effect of various parameters in piled raft foundation by using SAFE software are described detail in the following section.

7.1 Effect of raft thickness

The result of Case 1 analysis is shown in Figure 8, which indicate that the variation of maximum settlement with respect to various raft thickness. It can be conclude that the maximum settlement decreases when increase in raft thickness. Although raft thickness increase from 1.8m to 2.5m, settlement reduce only 0.44894 mm. The influence of raft thickness on differential settlement is shown in Figure 9. The increasing raft thickness is slightly effective in reducing differential settlement.

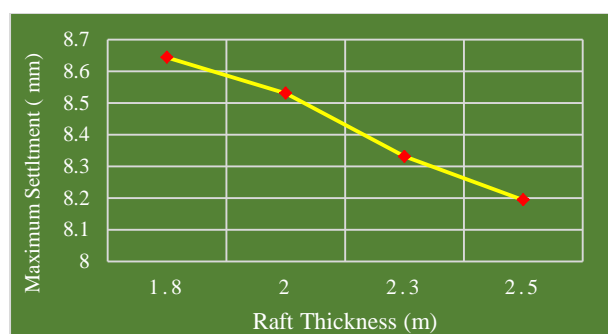


Figure 8. Effect of raft thickness on maximum settlement

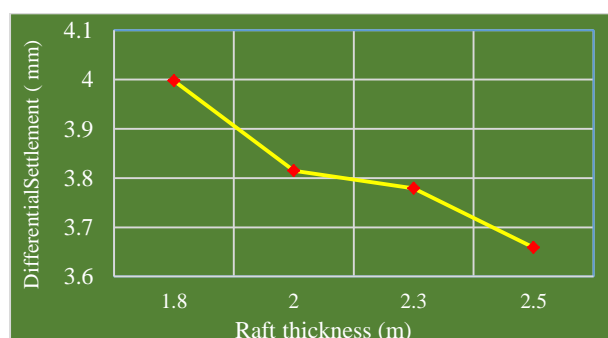


Figure 8. Effect of raft thickness on differential settlement
 The influence of raft thickness on the raft moment is described in Figure 10. There was a significant increase in moment as the raft thickness increase from 1.8m to 2.5m. Increasing moment lead to more steel area and it can cause uneconomical design. From above reason, it is shown that the increase in raft thickness have a little effect on maximum and differential settlement. But it is uneconomical because there is increase in raft moment , require more steel area and increase project cost.

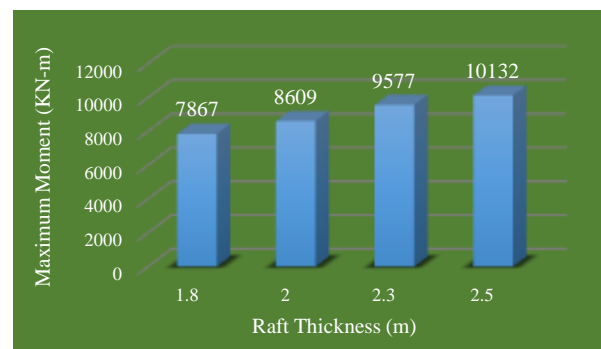


Figure 10. Effect of raft thickness on maximum moment.

7.2 Effect of pile length

The variation of settlements due to different pile length are shown in Figure 11 and Figure 12. The increase in pile length greatly reduced maximum settlement from 13.4125 mm to 8.64325 mm. As increase in length, the bearing capacity of pile is increase so it can more withsand the load over it and can reduce settlement. The value of differential settlement is slightly reduced when pile length increased from 12m to 41m. It can be summarized that maximum settlement was greatly affected by changing pile length whereas differential settlement has a little effect.

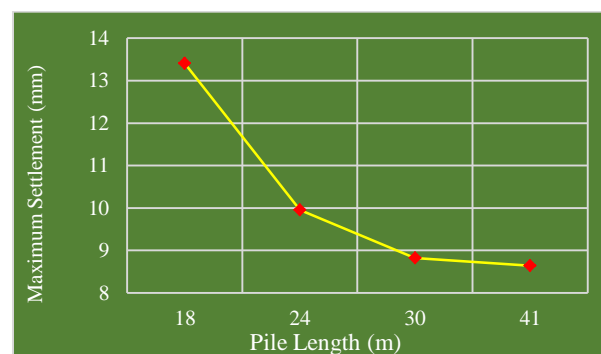


Figure 11. Effect of pile length on maximum settlement

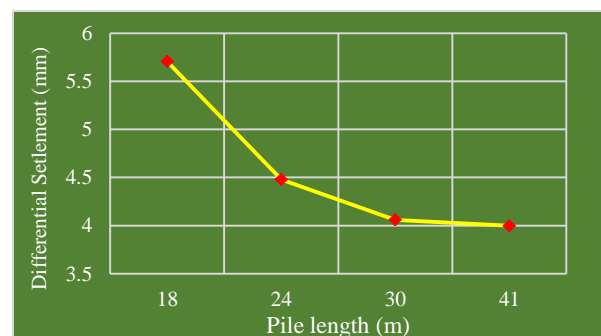


Figure 12. Effect of pile length on differential settlement

7.3 Effect of number of piles

The result of Case 3 analysis has shown in Figure 13 and Figure 14. It was showed that the increase in number of piles has a greatly effect on maximum settlement. The value of maximum settlement reduced from 11.1331mm to 7.70851 mm when the number of piles increase from 40 to 84. Bearing capacity of pile group is improved with increase in number in the group, so it can reduce maximum settlement. There was a little decrease in differential settlement with various number of piles. So, the number of piles more reduced maximum settlement than differential settlement. It was found that maximum settlement has greatly effect by increasing number of piles. But when it reached a certain limit, as 72 in this research, there was a slight effect on both settlement beyond this limit.

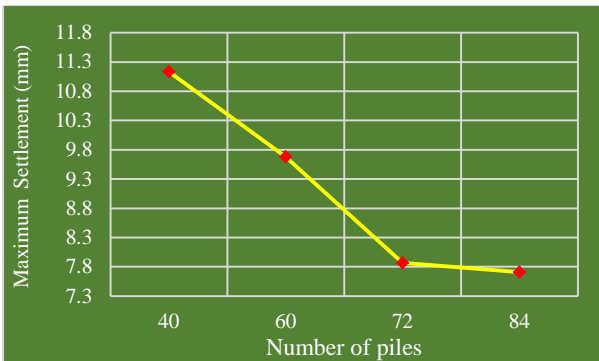


Figure 13. Effect of number of piles on maximum settlement

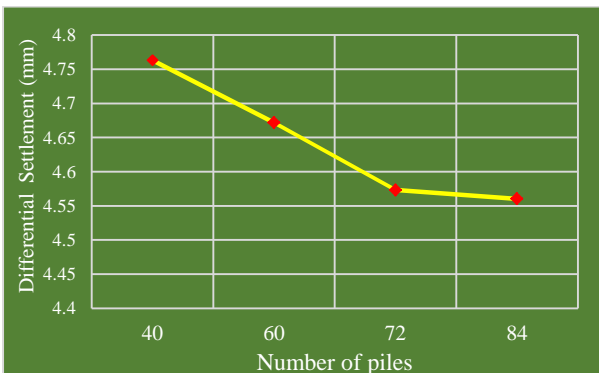


Figure 14. Effect of number of piles on differential settlement

8. COMPARISON OF SIMPLIFIED AND SOFTWARE ANALYSIS

In this study, simplified analysis is made by PDR method and this method is depended on stiffness of each member. Load distribution percent and settlement is calculated based on piles group stiffness, raft stiffness, soil stiffness and piled raft stiffness. In this method, soil stiffness is mainly depended on deformation parameter such as modulus of elasticity E_s and poisson's ratio μ . Software analysis is made by using SAFE program, in which piles spring stiffness and soil subgrade modulus is based on bearing capacity. Bearing capacity in these method is mainly depended on strength parameter of soil such as c and ϕ . Piles spring stiffness are obtained from bearing capacity/settlement and allowable settlement is 10mm. As a results, settlement values in simplified analysis is less than as compared to software analysis. The comparison of

settlement by these two methods analysis on various pile length and number of piles are shown in Figure 15 and Figure 16. So, it was recognized that the analysis based on bearing capacity gives more settlement values as compare to the analysis based on stiffness. Simplified analysis is suitable for primary analysis only and more detail analysis should be taken by software analysis.

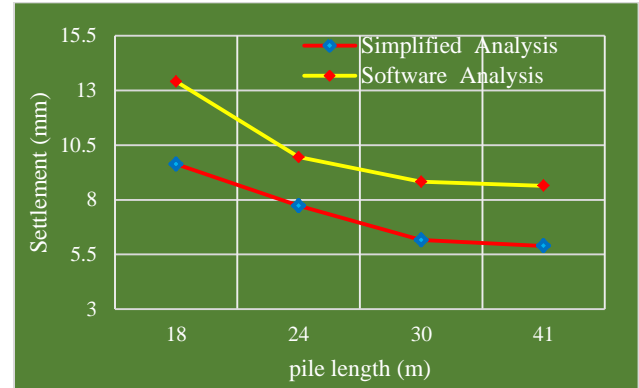


Figure 15. Comparison of settlement result from two analysis base on pile length

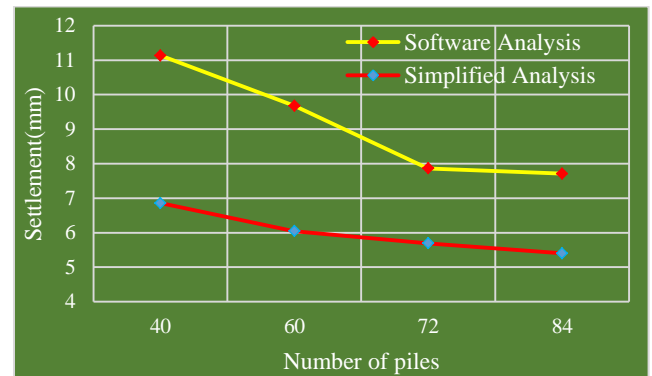


Figure 16. Comparison of settlement result from two analysis based on number of piles

9. CONCLUSION

Parametric study is made on three parameters by using finite element method and simplified analysis method. This study has found that the increase in raft thickness reduced maximum and differential settlement. But it has a slightly effect on both settlements and it is uneconomical due to increase in moment and stel area. The role of pile length is important in the piled raft foundation. Increasing pile length reduced both maximum and differential settlement. Especially, maximum settlement has a greater effect than differential settlement. The number of pile also has an important role in the performance of piled raft foundation. The increasing number of piles greatly reduced maximum settlement but it has not the great effect beyond the certain number. It was found that increase in pile length has more significant effect than increase in number of piles and increasing raft thickness, so pile length is the most important parameter in piled raft foundation. Software analysis give more settlement than simplified analysis. So, simplified analysis is suitable for primary analysis and software analysis give more satisfied result for detail analysis.

10. ACKNOWLEDGEMENT

The author would like to express my deepest thanks and gratitude to her supervisor Dr. Nyan Phone, Professor and

Head of the Department of Civil Engineering of the Technological University (Thanlyin). The author special thanks go to her co-supervisor Dr. Kyaw Lin Htat, Professor of the Department of Civil Engineering of the Technological University (Thanlyin), for his invaluable advice and suggestion throughout the study. The author would like to express her thanks to her member Dr. Kyaw Zeyar Win, Professor of the Department of Civil Engineering of the Technological University (Thanlyin), for his valuable comments and guidance during this study. Finally, her special thank goes to all who help her with necessary assistance for this study.

11. REFERENCE

- [1] Das, Braja M. “Principles of Foundation Engineering”, Seventh Edition.
- [2] M.J.Tomlison. “Pile Design and Construction Practice”, Fourth Edition, 1994.
- [3] Bowles, Joseph E. “Foundation Analysis and Design”, Fifth Edition. New York: McGraw Hill Co, 1996.
- [4] Poulos,H.G., “ Tall Building Foundation Design ”.
- [5] Poulos,H.G.(2001): Piled Raft foundation: Design and Applications. Geotechnique, 51 (2), 95-113.
- [6] Poulos, H.G., Small, J.C., Chow. H (2011). Piled Raft Foundation for Tall Building. Geotechnical Engineering Journal of the SEAGS & AGSSEA. Vol 42. No.2, 78-84.
- [7] Horikoshi, K., Randolph, M.F. (1994). “Estimation of Overall Settlement of Piled Rafts”. Japanese Geotechnical Society. Vol. 39, No.2,59-86.
- [8] Randolph., M.F. (1994). “Design Method of Pile Group and Piled Raft”. S.O.A. Report, 13 ICSMFE, New Delhi.5: 61-82.
- [9] Horikoshi, K., Randolph, M.F. (1998). “A Contribution of Optimum design of piled raft foundations”. Geotechnique 48, No.2, 301-317.
- [10] Russo, G. (1998). Numerical Analysis of Piles Rafts. Int. Jnl. Anal. & Num. Methods in Geomechs., 22(6): 477-493.
- [11] Chow, H.S.W., Small, J.C. (2006). “Analysis pf Pile Raft Foundations with Piles of Different lengths subjected to Horizontal and Vertical Loadings”. The University of Sydney, NSW 20.

Nonlinear Response of Reduced Beam Section Moment Connections with Box Columns

Mahmoud Ghaffari M.Sc.
Research Assistant
University of Tabriz
Tabriz, Iran

Yousef Ghaffari Ph.D.
Graduate Research Assistant
University of Memphis
Memphis, TN, USA

Fereshteh Nouri Zonouz M.Sc.
Graduate Research Assistant
University of Memphis
Memphis, TN, USA

Abstract: Before the Northridge earthquake, the flexural frames with welded flange-bolted web connections were used in numerous steel structures as a ductile and appropriate earthquake resisting system. During the 1994 Northridge and the 1995 Kobe earthquakes, which occurred one year later, many moment frames were deteriorated in the beam to column joint region. After earthquake investigations showed that concentration of stress at the location of beam to column connection was the main reason for failure, and subsequently, some methods were offered to mitigate the problem. One of the proposed solutions was a reduction of beam section near the column, which shifts the stress concentration far from critical region. In this paper the nonlinear response of moment connection with a reduction in beam section, and with the box column sections has been studied, and the stress distribution near the column have been compared for both welded and Reduced Beam Section (RBS) moment connections. Studying the results, showed that the reduced beam section connections exhibit a desirable response in comparing with the common connections. RBS force the beams plastification away from the column face and avoids stress concentrations and large deformation in the column. Furthermore, in this research some recommendations on the appropriate geometric parameter such as the connecting gap from the column edge, the length of the reduced section of beam flange, and the depth of reduced section of beam flange are provided.

Keywords: Nonlinear Analysis; Seismic Behavior; Steel Moment Frame; Plastic Hinge; Cyclic Response; Northridge Earthquake, Kobe Earthquake

1. INTRODUCTION

Investigation on damages imposed on buildings after the Northridge and Kobe earthquakes showed that most of the damage in steel moment resisting frames initiated from the bottom of the lower flange of beams [1-3] while mostly the upper flange was in good conditions because of the composite behavior between steel beam and concrete slab. The concentration of stress in the lower flange led to the failure of the connection in the event of an earthquake. Several solutions to fix the problem were suggested in literature.

Reduced Beam Section (RBS) connections are among the solutions that have been shown to exhibit satisfactory levels of ductility in numerous experimental tests [4-7]. In RBS connection, a portion of the flange in a beam is removed at a particular radius. The radius depends on the geometrical shape of the section. The moment capacity of reduced beam section should be greater than the required moment under combination of seismic and gravity loads. By doing this, in case of an earthquake, the plastic hinge in the beam is forced away from the beam-column intersection. As results, a higher ductility and seismic performance can be achieved [8-13].

Although an extensive body of knowledge exists on the performance of the RBS connection systems, the recommendation for the geometry of the connections design and verifying code recommendations for of seismic parameters such as deflection amplification factor, response modification factor, ductility, and over strength factor need more research [14-17]. This lack would become a major significance especially for the RBS connection system that is linked to box columns, since most of the previous studies were conducted on the connection systems linked to I-column sections.

Since the framed structures are usually designed in a way that some of their components enter into the nonlinear region during severe earthquake excitations to attenuate the imposed earthquake energy, it is of importance to evaluate and study the structural nonlinearity through numerical modeling. Different nonlinear analysis methods such as pushover, incremental dynamic [18-25], and cyclic analysis have been utilized to investigate the seismic behavior of structures in global scale e.g. an entire building frame or local scale e.g. structural connections. In this study, the nonlinear response of mentioned moment connections has been studied by using finite element method analysis. For this purpose, a numerical model of the proposed connection was developed by using an application that has been used previously by other researchers in this field [7]. In this model, it is assumed that beam-column connections are welded. The response of RBS connection has been compared with common connection systems, and then the design parameters for this connection system has been investigated.

2. MODELING

2.1 Materials and Loading

All steel sections and elements were made up of ST37 grade steel in accordance with DIN 17100:1966-09 [26], and the stress-strain curve of steel was considered as a bilinear curve resembling an actual stress-strain curve of steel. The cyclic loading pattern has been used to control the displacement up to 15 centimeters with gradual increasing in 2.5-centimeter steps [7].

2.2 Specification of Specimens

As shown in Figure 1, IPE30 sections were selected as beam sections and the columns are chosen from box sections with dimensions of 30 x 30 centimeters with a wall thickness of 2 centimeters. For the design of RBS connection, three significant geometric parameters of connecting gap from the column edge (a), the length of the reduced section of beam flange (b), and the depth of reduced section (c) as shown in Figure 1 are considered. For each parameter, a group of specimens has been considered and different values are considered for each parameter as shown in the Table 1 to 3. The parameters are defined concerning the section properties so they can be potentially extended to other connections with different dimensions. Parameters “a” and “c” are defined as a portion of flange width (b_f) and parameter b is defined as a portion of section depth (d). The specimen indicated by MA1 was selected for comparing RBS connection with the connections that were common before 1994 with no reduction in section.

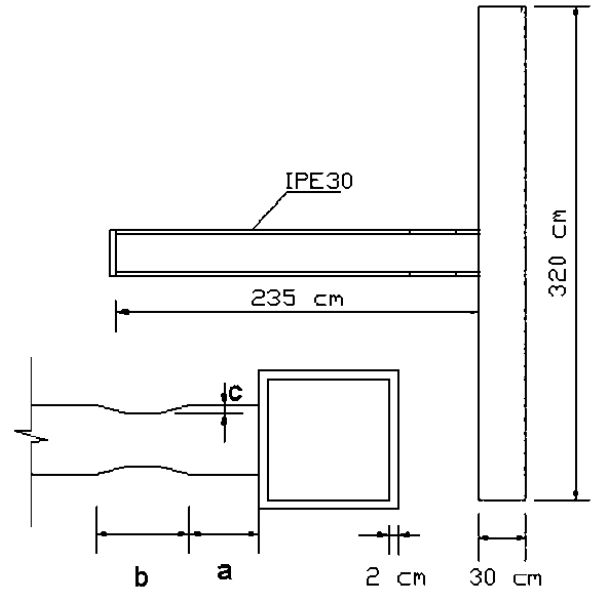


Figure 1: Geometry of RBS connection used in the analytical

Table 1: Connection specifications to determine optimized “a” parameter.

Specimen	Column	Beam	a	b	c
MA1	30×30×2×2	IPE30	-	-	-
MA2	30×30×2×2	IPE30	0.4 b_f	0.75 d	0.2 b_f
MA3	30×30×2×2	IPE30	0.5 b_f	0.75 d	0.2 b_f
MA4	30×30×2×2	IPE30	0.6 b_f	0.75 d	0.2 b_f
MA5	30×30×2×2	IPE30	0.75 b_f	0.75 d	0.2 b_f
MA6	30×30×2×2	IPE30	0.8 b_f	0.75 d	0.2 b_f
MA7	30×30×2×2	IPE30	0.9 b_f	0.75 d	0.2 b_f

Table 2: Connection specifications to determine optimized “b” parameter.

Specimen	Column	Beam	a	b	c
MB1	30×30×2×2	IPE30	0.6 b_f	0.55 d	0.2 b_f
MB2	30×30×2×2	IPE30	0.6 b_f	0.65 d	0.2 b_f
MB3	30×30×2×2	IPE30	0.6 b_f	0.75 d	0.2 b_f
MB4	30×30×2×2	IPE30	0.6 b_f	0.85 d	0.2 b_f
MB5	30×30×2×2	IPE30	0.6 b_f	1.0 d	0.2 b_f
MB6	30×30×2×2	IPE30	0.6 b_f	1.1 d	0.2 b_f
MB7	30×30×2×2	IPE30	0.6 b_f	1.2 d	0.2 b_f

Table 3: Connection specifications to determine optimized “c” parameter.

Specimen	Column	Beam	a	b	c
MC1	30×30×2×2	IPE30	0.6 b_f	0.75 d	0.2 b_f
MC2	30×30×2×2	IPE30	0.6 b_f	0.75 d	0.25 b_f
MC3	30×30×2×2	IPE30	0.6 b_f	0.75 d	0.3 b_f

model.

3. RESULTS

3.1 Comparing RBS and Ordinary Connections

Analysis of the MA1 specimen; the connection without any reduction in section; shows that the maximum stress has occurred just beside the column, which is not favorable (see Figure 2a). To make a comparison, specimen indicated by MA4 is selected from the group of RBS connection, which is considered as a RBS connection representative. In MA4 connection, the maximum stress has occurred at the reduced section of the beam, which is desired (see Figure 2b). In addition, despite the reduction of beams flanges, the load-displacement hysteretic curve has a stable state (see Figure 3).

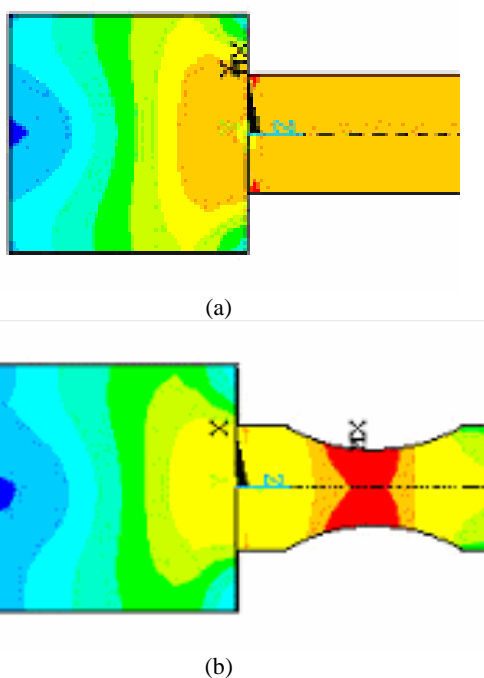


Figure 2: (a) MA1 stress contour, (b) MA4 stress contour.

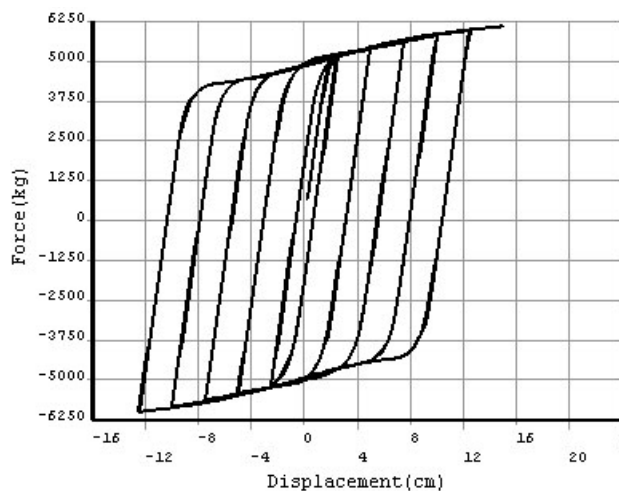
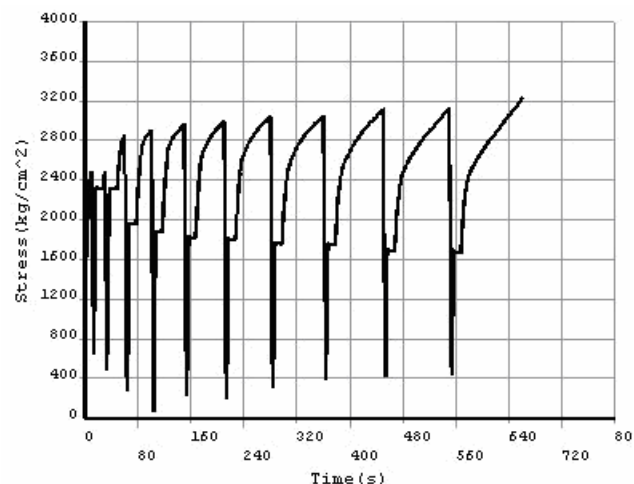
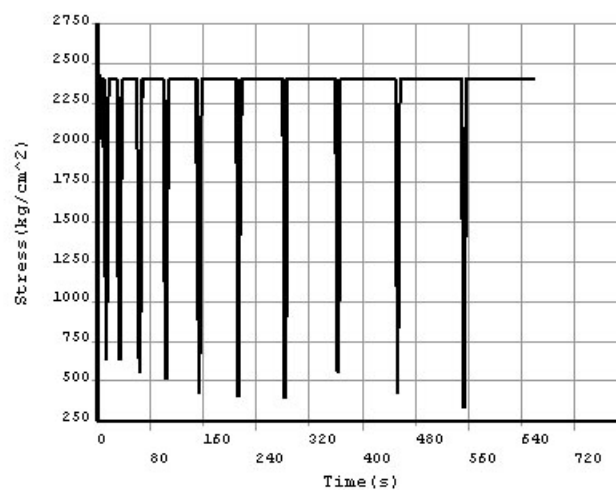


Figure 3: MA2 load-displacement curve.



(a)



(b)

Figure 4: (a) MA1 stress-time curve, (b) MA2 stress-time curve.

Stress distributions just at beside columns differ in these two specimens. The stress-time curves for these two specimens have been shown in Figures 4a and 4b. Note that the time has a virtual concept in this analysis. For more comparisons for these two specimens, the stress distribution within the width of the beam flange has been shown in Figure 5.

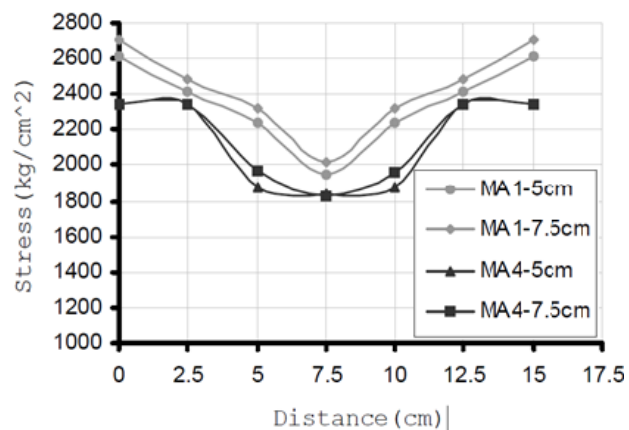
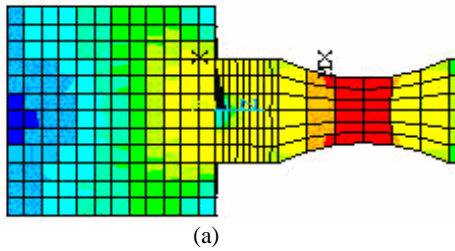


Figure 5: Stress distribution within the width of the beam flange.



(b)

Figure 6: (a) MA2 stress-time curve, (b) MA7 stress-time

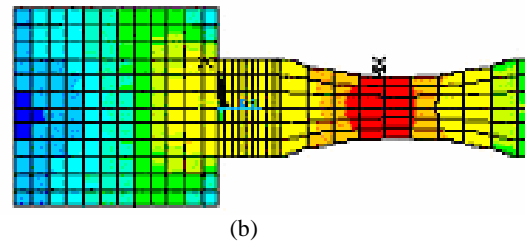
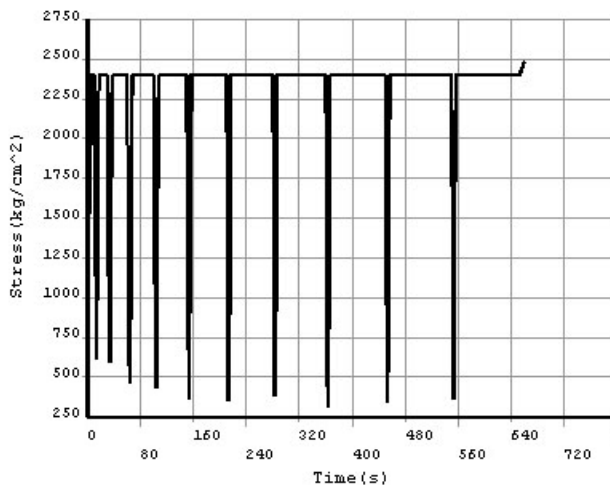


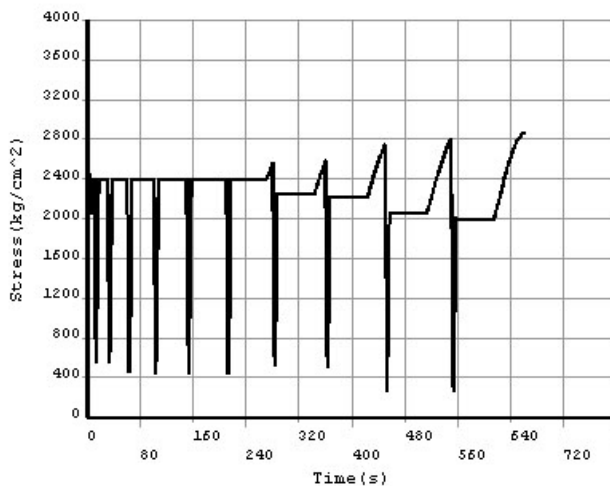
Figure 8: (a) MB5 stress counter, and (b) MB7 stress counter.

3.2 Determining Range of Parameter “a”

From the specimens in Table 1, appropriate values of parameter “a” is obtained. MA2 and MA7 results have been shown in Figures 6a and b. Results for MA3, MA5, and MA6 showed that their treatments similar to MA4. There is a concentration of stress just at beside of the column in MA2 and MA7. To more comparison of the response of specimens, the maximum absorbed strain energy and maximum absorbed plastic energy in width of one flange has been shown in Figure 7a and b.



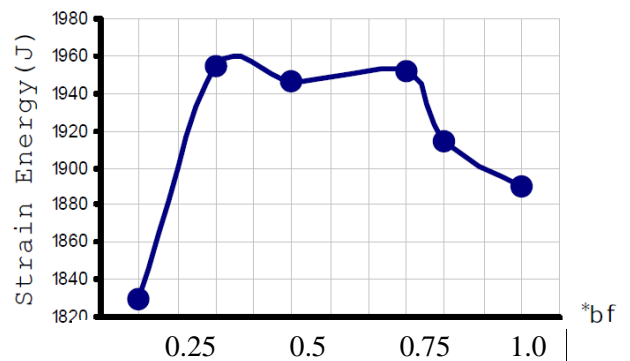
(a)



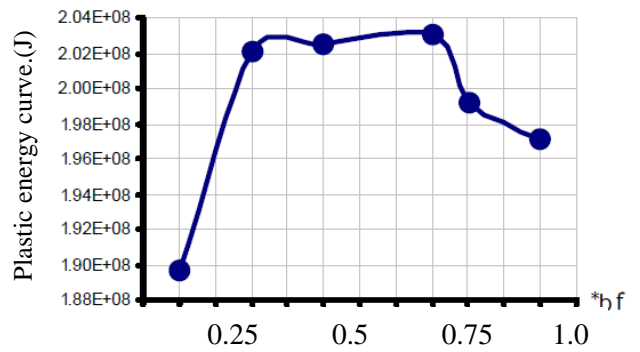
curve.

3.3 Determining Range of Parameter “b”

For investigating the length of the reduced section of beam flange (parameter “b”), the specimens of Table 2 have been analyzed. There was a concentration of stress just at beside of column at the ending stage of loading in MB1 (see Figure 2a). MB2 and MB5 had similar and desirable responses. The curve load-displacement and stress distribution just beside the column for MB2 has been shown in Figures 8b and c, but the separation of plastic hinges in MB6 and MB7 have a fundamental difference with specimen MB2 and MB5s. The plastic hinge is nonsymmetrical corresponding to the middle of the reduced part, Figure 9.



(a)



(b)

Figure 7: (a) Strain energy curve, and (b) Plastic energy curve.

For more comparison of the response of specimens, the maximum absorbed strain energy and maximum absorbed plastic energy in the flange width has been shown in Figure 10. The differences of these curves with Figures 8 and 9 are

For more comparison of the response of specimens, the maximum absorbed strain energy and maximum absorbed plastic energy in the flange width has been shown in Figure 10. The differences of these curves with Figures 8 and 9 are

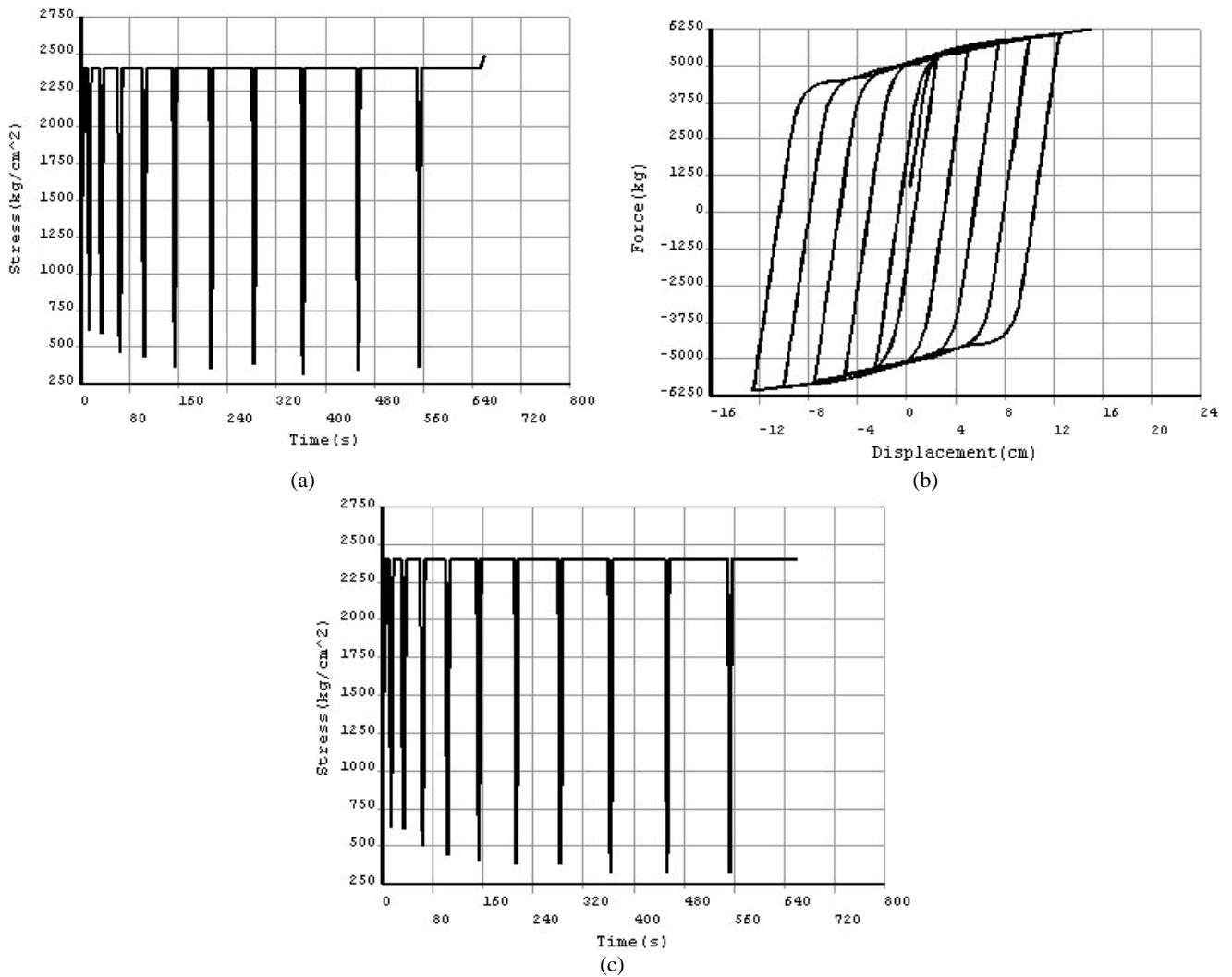


Figure 9: (a) MB1 stress-time curve, (b) MB2 load-displacement curve, and (c) MB2 stress-time curve.

due to their element size.

due to their element size.

3.4 Determine the range of parameter “c”

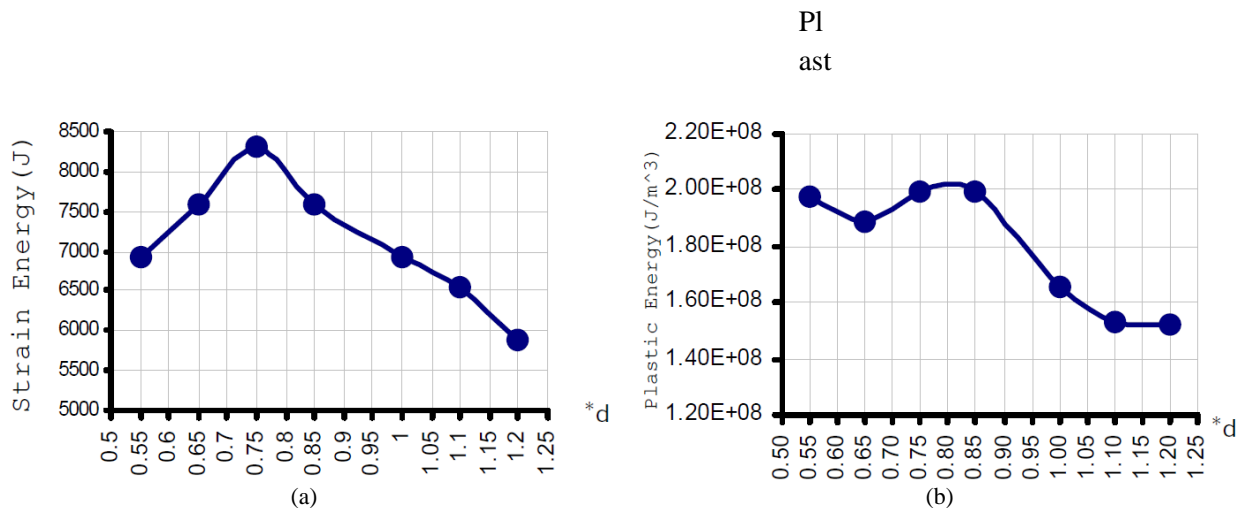


Figure 10: (a) Strain-energy curve, and (b) Plastic energy curve.

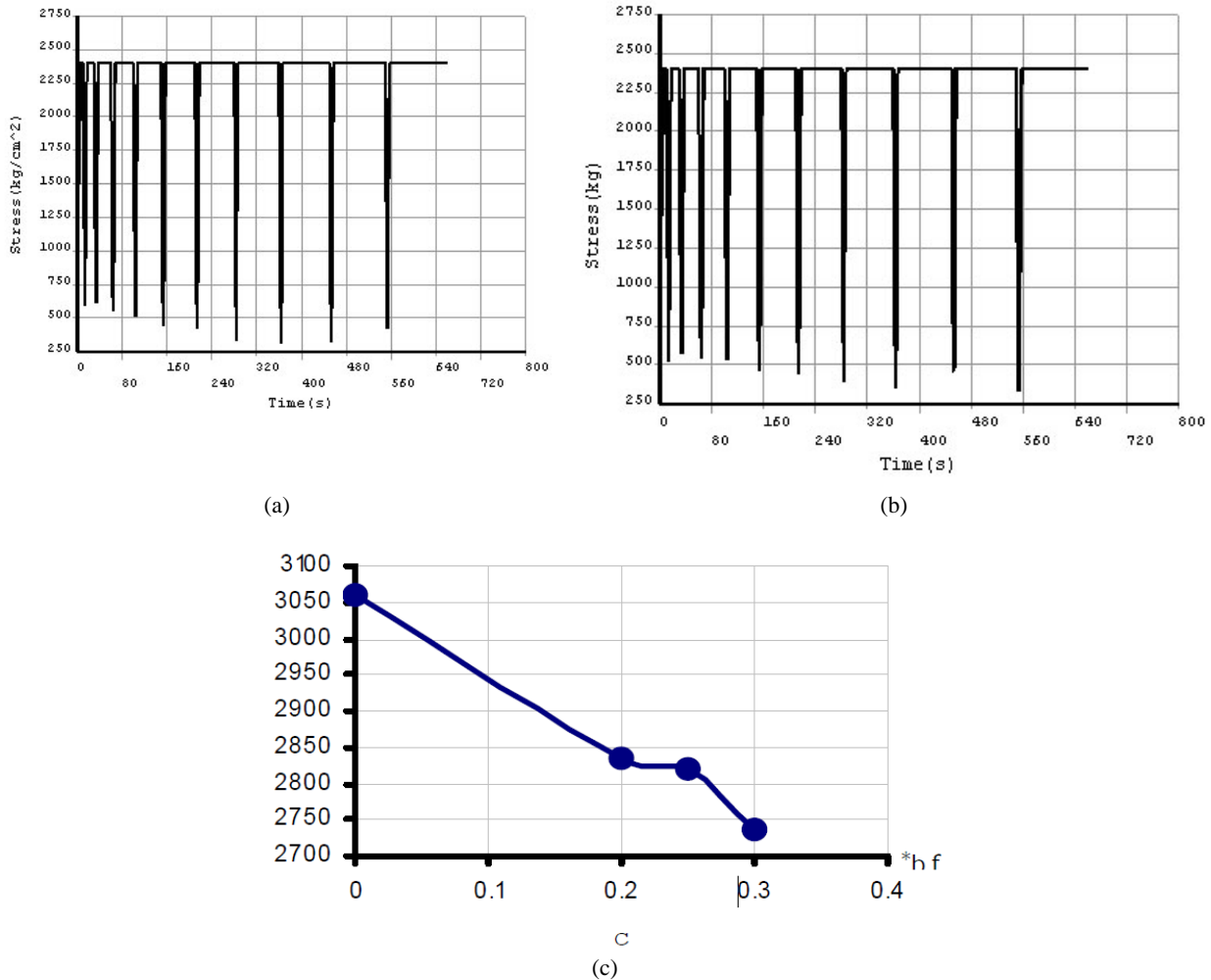


Figure 11: (a) MC2 stress-time curve, (b) MC3 stress-time curve, and (c) stiffness versus c parameter.

To investigate the depth of reduced section of beam flange (parameter “c”), the specimens of Table 3 have been analyzed. The analysis of MC1 showed that it was similar to MB3 (explained in section 3.3). For MC2 and MC3, stress-time curves have been shown in Figures 11a and b. Although in these two cases, the stress concentration did not occur at just beside the column, the system stiffness decreased considerably. For more comparison, the connection system stiffness has been shown for various values of c in Figure 11c.

4. CONCLUSION

The nonlinear response of RBS moment connections, with the column sections of the box, has been studied, and the stress distribution just near the column have been compared for the both welded and Reduced Beam Section (RBS) moment connections. The following conclusions were made:

1. The RBS connections have a desirable response in comparing with the common connections were utilized before 1994 Northridge earthquake. Using RBS connections, the problem of stress concentration at just beside of column can be mitigated.

2. Based on the analysis results on the geometric parameters of the RBS connections, the appropriate ranges for each parameter were determined. The gap from the column edge (“a”) should be in range of $0.5 b_f \leq a \leq 0.8 b_f$, the length of reduced section of beam flange (“b”) should be in range of $0.65d \leq b \leq d$, and the depth of reduced section (“c”) should be in range of $C \leq 0.25 b_f$. It is worth noting to mention that the section with $a = 0.75 b_f$ and $b=0.75d$ showed the best seismic performance.

5. REFERENCES

[1] Masayoshi Nakashima, Charles W. Roeder, Yoshiomi Marouka,(2000). Steel Moment frames for Earthquakes in the United States and Japan. Journal of Structural Engineering (ASCE), Vol. 126, No. 8. pp. 861-868.

[2] Charles J. Carter, Nestor R. Iwankiw(1998), Improved Ductility in Seismic Steel Moment frames with Dogbone connections. Proceeding: 2nd world conference on steel in construction San Sebastian.

[3] Charles J. Carter, Nestor R. Iwankiw(1998), Improved Ductility in Seismic Steel Moment frames with Dogbone

- connections. *Journal of Constructional Steel Research*, Vol. 46, No 1-3.
- [4] Chen, S. J., Yeh, C. H., and Chu, J. M. (1996). "Ductile steel beam-to-column connections for seismic resistance." *J. Struct. Engrg., ASCE*, 122(11), 1292-1299
- [5] Plumier, A. (1997). "The dogbone: back to the future." *Engrg. J.* 34(2), 61-67
- [6] Zekioglu, A., Mozaffarian, H., Chang, K. L., and Uang, C.-M. (1997). "Designing after Northridge." *Modern Steel Constr.*, 37(3), 36-42
- [7] Engelhardt, M. D., Winneberger, T., Zekany, A. J., Potyraj, T. J., (1998). "Experimental Investigations of Dogbone Moment Connections." *Engrg. J.*, 35(4), AISC, Fourth Quarter, 128-139
- [8] Popov, E. P. (1998), Design of Steel MRF Connections before and after Northridge Earthquake. *Engineering Structures*, Vol. 20, No. 12, pp. 1030-1038.
- [9] Popov, E. P., Toader A. Balan, and Tzony-shuah Yang (1998), Post- Northridge Earthquake Seismic, Steel Moment Connections. *Earthquake Spectra*, pp. 659-677.
- [10] Engelhardt M. D., Winneberger T., Zckany A. J., and Potyraj T. J. (1998), Experimental Investigation of Dogbone Moment Connections. *Engineering Journal Fourth Quarter*, pp. 128-139,
- [11] Iwankiw N.(1997), Ultimate Strength consideration for Seismic Design of the Reduced Beam section (Internal Plastic Hinge). *Engineering Journal First Quarter*, pp 3-10.
- [12] J. Shen, A. Astaneh- Asl, and D. B. McCallen, (2002). Used of Deep Columns in Special Steel Moment Frames. *Steel TIPS Report*, ASCE.
- [13] Kevin S. Moore, James O. Mally, Michael D. Engelhardt, (1999). Design of Reduced Beam Section (RBS) Moment frames Connections. *Steel TIPS Report*, ASCE.
- [14] Ramin Taghinezhad, Arash Taghinezhad, Vahid Mahdaviifar and Vafa Soltangharaei, 2018. Evaluation of Story Drift Under Pushover Analysis in Reinforced Concrete Moment Frames, *International Journal of Research and Engineering*, 5(1), 296-302, 2018.
- [15] Mahdaviifar, V., Barbosa, A.R. and Sinha, A., 2016. Nonlinear layered modelling approach for cross laminated timber panels subjected to out-of-plane loading. *Albufeira, Algarve, Portugal*.
- [16] Eiden, C.M., 2003. Nonlinear dynamic analysis of heavy timber frame structures including passive damping devices, PhD dissertation, University of Oxford, Oxford, United Kingdom.
- [17] Mahdaviifar, V., Sinha, A., Barbosa, A.R., Muszynski, L. and Gupta, R., 2018. Lateral and Withdrawal Capacity of Fasteners on Hybrid Cross-Laminated Timber Panels. *ASCE Journal of Materials in Civil Engineering*, 30(9), p.04018226.
- [18] Soltangharaei, V., Razi, M., & Gerami, M. (2016). Comparative evaluation of behavior factor of SMRF structures for near and far fault ground motions. *Periodica Polytechnica. Civil Engineering*, 60(1), 75.
- [19] Vamvatsikos, D., & Cornell, C. A. (2002). Incremental dynamic analysis. *Earthquake Engineering & Structural Dynamics*, 31(3), 491-514.
- [20] Vamvatsikos, D., & Cornell, C. A. (2004). Applied incremental dynamic analysis. *Earthquake Spectra*, 20(2), 523-553.
- [21] Ramin Taghinezhadbilondy, Aaron Yakel, and Atorod Azizinamini, Deck-pier connection detail for the simple for dead load and continuous for live load bridge system in seismic regions, Volume 173, 15 October 2018, Pages 76-88.
- [22] Soltangharaei, V., Razi, M., & Vahdani, R. (2016). Seismic fragility of lateral force resisting systems under near and far-fault ground motions. *International Journal of Structural Engineering*, 7(3), 291-303.
- [23] Chomchuen, P., & Boonyapinyo, V. (2017). Incremental dynamic analysis with multi-modes for seismic performance evaluation of RC bridges. *Engineering Structures*, 132, 29-43.
- [24] Ghaffari, Y., S. Pezeshk, and A. Abdelnaby. "Improved Value for Load Increase Factor in Disproportionate Collapse." In *Structures Congress 2015*, pp. 1130-1137.
- [25] Taghinezhadbilondy, Ramin. "Extending Use of Simple for Dead Load and Continuous for Live Load (SDCL) Steel Bridge System to Seismic Areas." (2016), Ph.D. dissertation.
- [26] DIN 17100:1966-09, (1966) Steels for general structural purposes; quality specifications Title in German: Allgemeine Baustähle – Gütevorschriften.

Design and Thermal Analysis of Shell and Tube Heat Exchanger

Lai Yi Cho Oo
Department of Mechanical
Engineering,
Technological University
Hmawbi, Myanmar

Myo Zaw Min
Department of Mechanical
Engineering,
Technological University
Hmawbi, Myanmar

Su Su Mar
Department of Mechanical
Engineering,
Technological University
Hmawbi, Myanmar

Su Yin Win
Department of Mechanical
Engineering,
Technological University
Thanlyin, Myanmar

Maung Maung Yi
Department of Mechanical
Engineering,
Technological University
Thanlyin, Myanmar

Abstract: Heat exchangers are used in a number of applications in various industries. The present study focus on calculation of shell and tube heat exchanger design with minimum pressure drop. Calculation of heat exchanger design has been done by considering with two case of different coolant are used 98°C of water is enter to the exchanger and its outlet at 60°C. Water is used in case one and another case R134a is used for coolant. This study also including different coolant temperature use and MATLAB software is used to analyze for distribution of pressure drop. When a heat exchanger is placed into a thermal transfer system a temperature drop is required to transfer heat. The magnitude of this temperature drop can be decrease by utilizing a larger heat exchanger but this will be large pressure drop, increase the cost of the heat exchanger. Economic considerations are important in engineering design, and in a complete engineering equipment, not only the thermal performance characteristics but also the minimum pressure drop are requirement.

Keywords: over all heat transfer coefficient, heat transfer rate, heat transfer area, pressure drop, pressure distribution.

1. INTRODUCTION

A heat exchanger is a device in which heat is transferred between a warmer and a colder substance, usually fluid. There are various types of heat exchanger

- (1)The type of heat exchanger (a) recuperator and (b) regenerator.
- (2) The type of heat exchanger process between the fluids (a) indirect or transmural and (b) direct contact.[1]
- (3)Thermodynamic phase or state of the fluids (a) single phase (b) evaporation or boiling (c) condensation[1].
- (4) The type of construction or geometry (a) tubular (b) plate and (c) extended or finned surface.[1]

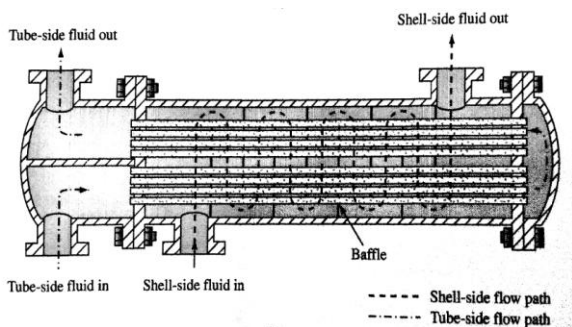
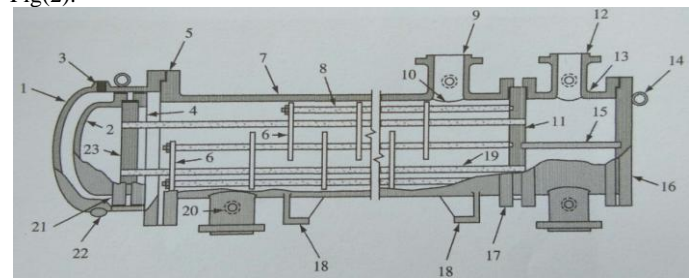


Figure 1. Shell and Tube Heat Exchanger with Segmental baffles: Two Tube Pass, One Shell Tube[1]

In the design of heat exchanger it is important to specify whether the fluids are mixed or unmixed, and which of the fluid is mixed. It is also important to balance the temperature drop by obtaining approximately equal heat

transfer coefficient on the exterior and interior of the tubes. If this is not done, one of the thermal resistances may be unduly large and cause an unnecessarily high overall temperature drop for a given rate of heat transfer, which in turn demands larger equipment and results in poor economics. The shell-and-tube heat exchanger illustrated in Fig (1) has fixed tube sheets at each end, and the tubes are welded or expanded into the sheets.[1]

This type of the construction has the lowest initial cost but can be used only for small temperature differences between the hot and cold fluids because no provision is made to prevent thermal stresses due to the differential expansion between the tubes and the shell. Another disadvantage is the tube bundle cannot be removed for cleaning. These drawbacks can be overcome by modification of the basic design in Fig(2).



1. Shell cover
2. Floating head
3. Vent connection
4. Floating head backing device

5. Shell cover end flange
6. Transverse baffles or support plates
7. Shell
8. Tie rod and spacers
9. Shell nozzle
10. Impingement
11. Stationary tube sheet
12. Channel nozzle
13. Channel
14. Lifting ring
15. Pass partition
16. Channel cover
17. Shell channel end flange
18. Support saddles
19. Heat transfer tube
20. Test connection
21. Floating head flange
22. Drain connection
23. Floating tube sheet

Figure 2. Shell and Tube Heat Exchanger with Floating Head [1]

In this arrangement one tube sheet is fixed but the other is bolts to a floating-head cover that permits the tube bundle to move relative to the shell. The floating tube sheet is clamped between the floating head and flanges so that it is possible to remove the bundle for cleaning. The heat exchanger shown in Fig (2) has one shell pass and two shell passes.

In the design and selection of a shell-and-tube heat exchanger, the power requirement and the initial cost of the unit must be considered. Show that the smallest possible pitch in each direction result in the lowest power requirement for a specified rate of heat transfer, since smaller values of pitch also permit the use of a smaller shell, the cost of the unit is reduced when the tubes are closed packed. There is little difference in performance between inline and staggered arrangement, but the former are easier to clean. [1]

Heat transfer in a heat exchanger usually involves convection in each fluid and conduction through the wall separating the two fluids. In the analysis of heat exchangers, it is convection to work with an overall heat transfer coefficient U that account for the contribution of all these on heat transfer.

The rate of heat transfer between the two fluids at a location in heat exchanger depends on the magnitude of the temperature difference at that location, which varies along the heat exchanger. In the analysis of heat exchangers, it is usually convection to work with the logarithmic mean temperature difference LMTD, which is an equivalent mean temperature difference between the two fluids for the entire heat exchanger. [5]

2. LOG MEAN TEMPERATURE DIFFERENCE

The temperature of fluids in a heat exchanger are generally not constant but vary from point to point as heat flows from the hotter to the colder fluid.

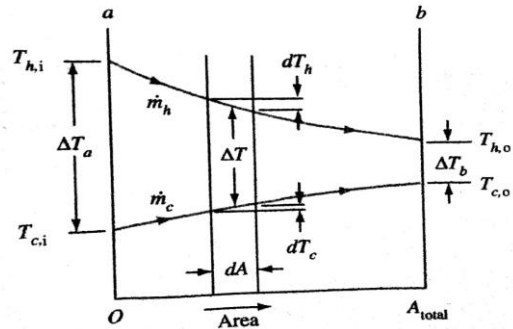


Figure 3(a) Temperature Distribution in Single Pass Parallel Flow Heat Exchanger [1]

Even for a constant thermal resistance, the rate of heat flow will therefore vary along the path of the exchangers because its value depends on the temperature difference the cold fluid and hot fluid in that section. Fig (3) illustrate the changes in temperature that may in either or both fluid in a simple shell and tube exchanger.[1]The distances between the solid lines are proportional to the temperature differences ΔT between the two fluids.

$$\Delta T = (\Delta T_a - \Delta T_b) / \ln(\Delta T_a / \Delta T_b)$$

Where the subscripts a and b refer to the respective ends of the exchanger and ΔT_a is the temperature difference between the hot and cold fluids streams at the inlet while ΔT_b is the temperature difference at the outlet end as shown in Fig (3)..

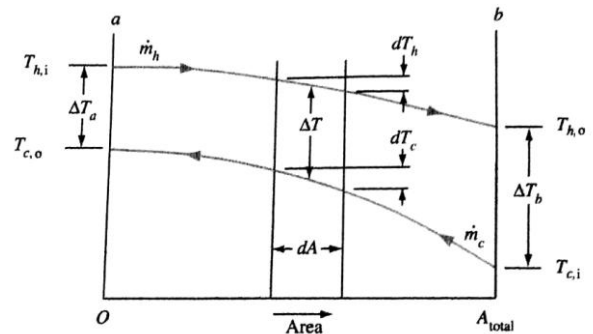


Figure 3 (b) Temperature Distribution in Single Pass Parallel Flow Heat Exchanger [1]

The distances between the solid lines are proportional to the temperature differences ΔT between the two fluids.

$$\Delta T = (\Delta T_a - \Delta T_b) / \ln(\Delta T_a / \Delta T_b)$$

Where the subscripts a and b refer to the respective ends of the exchanger and ΔT_a is the temperature difference between the hot and cold fluids streams at the inlet while ΔT_b is the temperature difference at the outlet end as shown in Fig (3)..In practice, it is convenient to use an average effective

temperature difference ΔT for the entire heat exchanger, defined by

$$Q = UA \Delta T$$

The ordinate of each is the correction factor F . to obtain the true mean temperature for any of these arrangements, the LMTD calculate for correction factor, that is

$$\Delta T_m = LMTD \times F$$

The values shown on the abscissa are for the dimensionless temperature-difference ratio temperature-difference ratio

$$P = (T_{h,o} - T_{h,i}) / (T_{c,i} - T_{h,i})$$

$$Z = (T_{c,i} - T_{c,o}) / (T_{h,o} - T_{h,i})$$

Where the subscripts h and c refer to the hot and cold fluid respectively

$T_{h,o}$ = outlet temperature of hot fluid

$T_{h,i}$ = inlet temperature of hot fluid

$T_{c,o}$ = outlet temperature of cold fluid

$T_{c,i}$ = inlet temperature of cold fluid [1]

The ratio P is an indication of the heating and effectiveness and can vary from zero for a constant temperature of one of the fluid to unity for the case when the inlet temperature of the hotter fluid equal to the outlet temperature of the cooler fluid. The parameter for each of the curves, Z , is equal to the ratio of the temperature changes of the shell fluid divided by the temperature change of the fluid in the tube. Fig (4) show the correction factor F chart for common shell and tube and cross flow heat exchanger. [1]

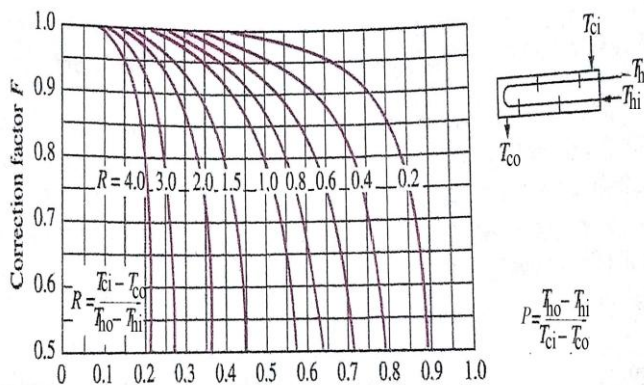


Figure 4. Correction Factor F Chart. [5]

3. OVERALL HEAT TRANSFER COEFFICIENT

A heat exchanger typically involve two flowing fluids separated by a solid wall. Heat is first transferred from the hot fluid to the wall by convection, through the wall by conduction, and from the wall to the cold fluid again by convection. Any radiation effects are usually included in the convection heat transfer coefficients. The thermal resistance network associated with this heat transfer process involves two convection and one conduction resistances, as shown in Fig(5). The subscripts i and o represent the inner and outer surfaces of the inner tube. [5]

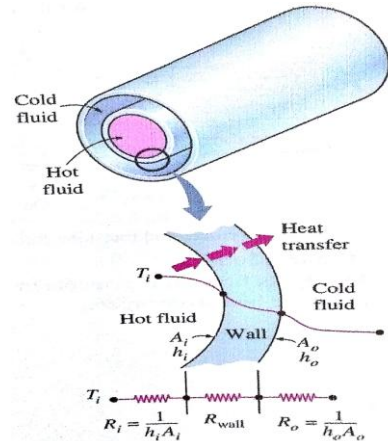


Figure 5. Thermal Resistance Network Associated with Heat Transfer [5]

$$Q = U A F \Delta T_m$$

$$UA = 1 / [(1/h_i A_i) + (x/kA_k) + (1/h_o A_o)]$$

Where,

h_i = convection heat transfer hot coefficient = 7500 W/m²K

h_o = convection heat transfer cold coefficient for water = 8000 W/m²K

A_i = area of hot fluid

A_o = area of cold fluid

A_k = area of copper tube

x = thickness of copper tube

= 5 × 10⁻³ m

k = thermal conductivity of copper tube

= 399.375 W/mK

$U = 3692.04$ W/m²K

4. FOULING FACTOR

The overall heat transfer coefficient of a heat exchanger under some operating conditions, especially in the process industry, often cannot be predicted from thermal analysis alone. During operation with most liquids and some gases, a deposit gradually builds up on the heat transfer surface. The deposit may be rust, boiler scale, silt, coke, or any number of things. Its effects, which is referred to as fouling, is to increase the thermal resistance. The manufacturer cannot usually predict the nature of the deposit or the rate of fouling. Therefore, only the performance of clean exchanger can be guaranteed. The thermal resistance of the deposit can generally be obtained only from actual tests or from experience. If performance tests are made on a clean exchanger and repeated later after the unit has been in service for some time, the thermal resistance of the deposit (or fouling factor) R_d can be determined from the relation. [1]

$$R_d = 1/U_d - 1/U$$

Where,

U = overall heat transfer coefficient of clean exchanger = 3692.04 W/m²K

U_d = overall heat transfer coefficient after fouling has Occurred

R_d = fouling factor (or unit thermal resistance) of Deposit

= 0.0002

Table 1 is shown typical fouling factor .A
convection working from is
 $U_d = 1/[R_d+(1/U)]$

Table 1. Typical Fouling Factors [2]

Type of Fluid	Fouling Factor, (m ² °C/W)
Seawater	
below 125°F	0.00009
above 125°F	0.002
Treated boiler feedwater above 125°F	0.0002
Fuel oil	0.0009
Quenching oil	0.0007
Alcohol vapors	0.00009
Steam, non-oil-bearing	0.00009
Industrial air	0.0004
Refrigerating liquid	0.0002

5. CALCULATION OF HEAT TRENSEFER RATE

Heat exchanger usually operate for long periods of time with no change in their operating conditions. Therefore they can be modeled as steady-flow devices. As such, the mass flow rate of each fluid remains constant, and the fluid properties such as temperature and velocity at any inlet or outlet remain the same. Also, the fluid streams experience little or no change in their velocities and elevations, and thus the kinetic and potential energy changes are negligible. The specific heat of a fluid, in general, changes with temperature. But, in a specified temperature range, it can be treated as a constant at some average value with little loss in accuracy. Axial heat conduction along the tube is usually insignificant and can be considered negligible. Finally, the outer surface of the heat exchanger is assumed to be perfectly insulated, so that there is no heat loss to the surrounding medium, and any heat transfer occurs between the two fluids only. [5]

The idealization state above are closely approximated in practice, and they greatly simplify of a heat exchanger with little sacrifice of accuracy. Therefore, they are commonly used. Under these assumptions, the first law of the thermodynamics requires that the rate of heat transfer from the hot fluid be equal to the rate of heat transfer to the cold one. That is,

$$Q = m_c C_{p,c}(T_{c,o} - T_{c,i})$$

Where,

m_c = mass flow rate of cold fluid

$C_{p,c}$ =specific heat of cold fluid

$T_{c,o}$ =outlet temperature of cold fluid

$T_{c,i}$ =inlet temperature of cold fluid

$$Q = m_h C_{p,h}(T_{h,i} - T_{h,o})$$

$$Q = 326.87 \text{ kW}$$

m_h = mass flow rate of hot fluid

$$= 2.05 \text{ kg/s}$$

$C_{p,h}$ =specific heat of hot fluid

$$= 4.196 \text{ kJ/kgK}$$

$T_{h,o}$ =outlet temperature of hot fluid

$$= 60^\circ\text{C}$$

$T_{h,i}$ =inlet temperature of hot fluid

$$= 98^\circ\text{C}$$

Where the subscripts c and h stand for cold and hot fluids, respectively. Note that the heat transfer rate Q is taken to be a positive quantity, and its direction is understood to be from the hot fluid to the cold one in accordance with the second law of thermodynamics. In heat exchanger analysis, it is often convection to combine the product of the mass flow rate and the specific heat of a fluid into a single quantity.

The heat capacity rate of a fluid stream represents the rate of heat transfer needed to change the temperature of the fluid stream by 1°C as it flows through a heat exchanger. Note that in a heat exchanger, the fluid with a large heat capacity rate will experience a small temperature change, and the fluid with a small heat capacity rate will experience a large temperature change. [5]

That is, the heat transfer rate in a heat exchanger is equal to the heat capacity rate of either fluid multiplied by the temperature change of that fluid. Note that the only time of temperature rise of a cold fluid is equal to the temperature drop of the hot fluid is when the heat capacity rates of the two fluids are equal to each other. [5]

5.1. Calculation of Heat Transfer Area

Heat transfer of hot water is determined by the following equation,

$$Q = m_h C_{p,h}(T_{h,i} - T_{h,o})$$

$$= U A F \Delta T_m$$

Where,

U =overall heat transfer coefficient

$$= 3692.04 \text{ W/m}^2\text{K}$$

F =correction factor

$$= 0.98$$

ΔT_m =log mean temperature difference

$$= 30.04$$

Q =heat transfer rate

$$= 326.87 \text{ kW}$$

A = heat transfer area

$$= 3 \text{ m}^2$$

Table 2. Comparison Result Table of H₂O and R 134a

Name	Symbol	H ₂ O	R.134a	Unit
Coolant inlet temperature	T_{ci}	40	-41	°C
Coolant outlet temperature	T_{co}	55	-26	°C
Heat Loss	Q	326.87	326.87	kW
Convection heat transfer for cold Fluid	h_{cold}	8000	2261.307	W/m ² K
Thermal conductivity	k	399.375	403.425	W/mK
Over all heat transfer coefficient	U	3692.04	1700.8	W/m ² K
Heat transfer area	A	2.82	1.71	m ²

Length of tube	L_{tube}	38	22	m
Volume of tube	V_{tube}	0.192	0.011	m^3
Volume of cold fluid	V_{cold}	0.012	0.022	m^3
Pressure drop for hot fluid	ΔP	2.69	1.56	m

5.2 Pressure Drop for Heat Exchanger

Pressure drop is a major constraint in thermal design of shell and tube heat exchanger is meaningful only when it is optimum and the extent of the optimality is constrained by the pressure drop. Optimization of thermal design requires maximization of overall heat transfer coefficient and effective mean temperature difference. So as to minimize the heat transfer area subject to constraints, pressure drop being the major one [4]. Tube side pressure drop can be lowered in following ways;

- Increasing the shell diameter. Increasing the shell diameter increases tube flow area due to increased number of tubes and, thereby reduces tube flow velocity and, hence, reduces tube side pressure drop. Further—, it also means reduced tube length which, too, leads to reduced pressure drop.
- Increasing the tube diameter. Increasing the tube diameter reduces velocity and, thereby, reduce pressure drop. However, tube diameters are standardized and standard outside diameters are limited. Further tube outside diameters more than 1.0inch is generally not desirable as higher tube diameter means higher shell diameter to accommodate required number of tubes due to increased tube pitch which, in turn, means higher cost.
- Increasing the nozzle size. If the nozzles are too small in diameter, their diameter can be increased reasonably to lower the pressure drop.
- Using the shells in parallel. Multiple shells can be used in parallel so that total tube side flow is split and flow velocity is reduced. Consequently, pressure drop is reduce. However, it increases the cost due to the reasons as mentioned for shell side pressure drop.

The pressure drop can be relatively straightforward in a single-pass pipe-in tube heat exchanger or extremely difficulty in, say a shell and tube exchanger. Table (3) and (4) are shown pressure drop for water and R134a coolant with varies tube length and diameter. The pressure drop in a straight run of pipe, given by

$$\Delta P = fLv^2/2gD$$

Where,

f=friction loss

= 0.023

L=length of tube

v=velocity of hot fluid

=1.24m²

g=gravity

=9.81m/s²

D=diameter of tube

ΔP =pressure drop

Table 3. Pressure Drop for Water with Various Length and Diameter

No	Length(m)	Diameter(m)	Pressure drop(m)
1	38	0.0254	2.6631
2	34	0.0279	2.2009
3	31	0.0305	1.8493
4	29	0.0330	1.5758
5	27	0.0356	1.3587
6	25	0.0381	1.1836
7	24	0.0406	1.0403
8	22	0.0432	0.9215
9	21	0.0457	0.8219
10	20	0.0483	0.7377

Table 4. Pressure Drop for R134a with Various Length and Diameter

No	Length(m)	Diameter(m)	Pressure drop(m)
1	19.5497	0.0254	1.3848
2	17.7725	0.0279	1.1445
3	16.2915	0.0305	0.9617
4	15.0383	0.0330	0.8194
5	13.9641	0.0356	0.7065
6	13.0332	0.0381	0.6155
7	12.2186	0.0406	0.5409
8	11.4998	0.0432	0.4792
9	10.8610	0.0457	0.4274
10	10.2893	0.0483	0.3836

Figure 6 shown the pressure drop with varies tube diameters and figure 7 shown the tube length with varies tube diameters.

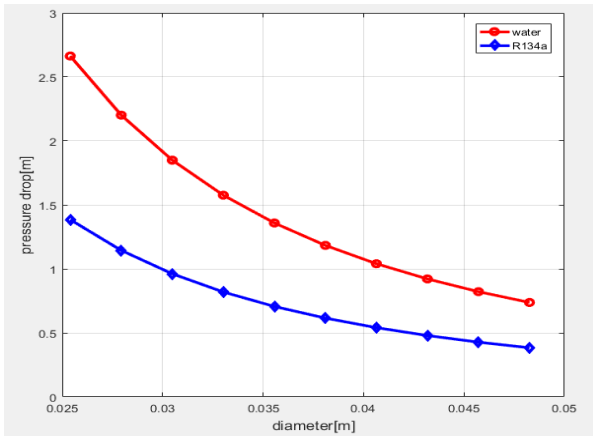


Figure 6. Pressure Drop with Varies Tube Diameters

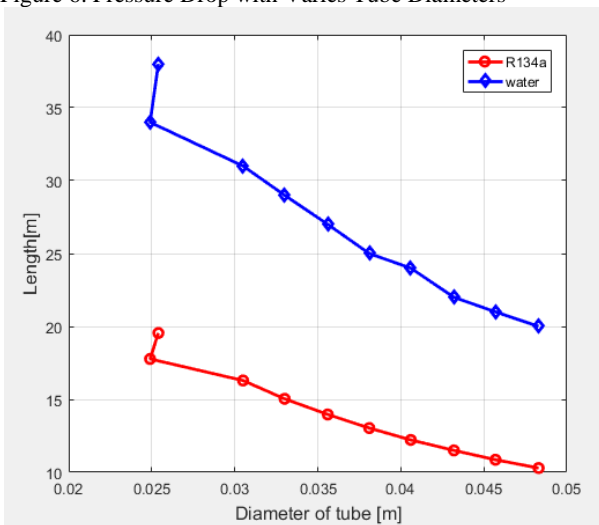


Figure 7. Tube length with Varies Tube Diameters

6. CONCLUSION

In this paper, counter flow shell and tube heat exchanger design are calculated. Hot water enter at 98°C and at exist 60°C. Density of the working fluid is used average temperature. Tube material is copper .Tube diameter and length are varies with the calculation of pressure drop .Firstly, cold water is used for coolant inlet temperature 40°C and outlet temperature 55°C. The velocity of the hot water is 1.24m/s and flow is turbulent. The roughness of the copper pipe is 0.0015mm. finally, the coolant is R134a. Inlet temperature of the coolant is -41°C and outlet temperature is -26°C. In this condition the heat transfer area of R134a is less than using the water coolant. Pressure drop is also less than coolant is water for the same diameter. Now a day in shell and tube heat exchanger, tube side pressure drop is 7m used.

7. ACKNOWLEDGMENTS

First of all, the author is grateful to Dr. Kay Thi Lwin, Rector of Technological University (Hmawbi), for giving the permission to submit the paper.

The author wishes to express her heartfelt thanks to each and every one who assisted in completing this paper.

Finally, the author deep gratitude and appreciation go to her parents for her moral supports, patience, understanding and encouragement.

8. REFERENCES

- [1] Frank Kreith, Raj M. Manglik, Mark S. Bohn, Principles of Heat and Transfer, Seventh Edition
- [2] J.P Holman, , Heat Transfer, Tenth Edition
- [3] Incropera/De witt/Bergman, Lavine, Fundamentals of Heat and Mass Transfer, Sixth Edition
- [4] Warren M. Rohsenow, James P. Hartnett, Young I. Cho, Hand book Of Heat Transfer
- [5] Yunus A. Cengel, Heat Transfer A Practical Approach 2nd edition

Study on the Behavior of Bored Pile Foundation for Sixteen-Storeyed RC Building

Nan Thida Htway
Department of Civil Engineering
Technological University
(Thanlyin),
Myanmar

Nyan Phone
Department of Civil Engineering
Technological University
(Thanlyin),
Myanmar

Kyaw Lin Htat
Department of Civil Engineering
Technological University
(Thanlyin),
Myanmar

Abstract: Pile foundation are used extensively for the support of bridges and other structures to transfer structure loads to the ground and to avoid excess settlement or lateral movement. It can be installed without appreciable noise or vibration. This paper presents the behavior of bored pile foundation for sixteen-storeyed reinforced concrete building. Superstructure analysis and design are carried out by using ETABs software. All reinforced concrete members are designed by ACI (318-99) and load considerations are based on UBC-97. Necessary checking is carried out for the stability of the superstructure. All checking for stability of superstructure are within the limits. Required soil properties are obtained from soil report. The allowable bearing capacity is calculated by Meyerhof's Method, Vesic's Method and SPT Method and the average value of these result is finally selected. Analysis and design of pile foundation are made by using ETABs software and pile caps are designed by SAFE software. In design of pile foundation, the required pile length and pile diameter is 50m and 800mm. Number of pile in the group are varied depending on column load and total required number of pile is 114 nos. The required thickness of pile caps are 1.4m, 1.8m and 2m. The tensile strength of bored pile is greater than the pullout capacity for single and group pile. And then checking the pile settlement, lateral load and deflection is within the allowable limit. Therefore, the design of bored pile foundation for this proposed building is satisfactory.

Keywords: bored pile foundation; soil bearing capacity; pullout capacity; lateral load; settlement; deflection

1. INTRODUCTION

Nowadays, the rate of population is increased and the cost of lands is very expensive. Its lead to construct many high-rise building in urban areas. The tall building must have strength and safety, so bored pile foundation is widely used over the world. The design of bored pile foundation has been established by many researchers [1], [2], [3], [4]. The effect of installing the piles reduced the soil stiffness within the bored pile group, making the soil less efficient in resisting lateral pile movements than in the driven pile group. Structurally, however, bored piles were more resistant to flexural loading. The net effect was that the system of bored piles was stiffer than the system of driven displacement piles [5]. The comparisons of experimental results and theoretical analysis for laterally loaded pile showed encouraging results for the prediction of ultimate lateral load, but the prediction of lateral deflection was not satisfactory and needs further work [6]. Elastic solution for laterally loaded piles are analyzed using the fourier FEM [7]. The comparisons of ultimate uplift capacity of pile developed by Kulhawy et al (1979); Das (1983) and Chattopadhyay and Pise (1986) [8]. This study considers the behavior of bored pile foundation for sixteen-storeyed reinforced concrete building. Superstructure is analysis by ETABs software. Allowable bearing capacity is calculated by Meyerhof's Method, Vesic's Method and SPT Method. Analysis and design of pile foundation is made by ETABs software and pile cap is designed by SAFE software. Pullout capacity is calculated from piles for resisting uplift equation and settlement of single pile and group pile by semiempirical method. And then lateral load capacity is calculated by using Brom's method. The rest section is compared the result on single and pile group.

2. IMPLEMENTATION PROGRAM

Firstly, a 16th storeyed superstructure is modelled by ETABs software and checked the stability of superstructure. To get foundation design, the bearing capacity of soil on each type is

calculated and then chosen the foundation type. And the compression capacity, settlement, deflection and pullout capacity are checked. And then lateral loads and bending moment are calculated and checked. Finally, the figure of axial force, shear force, bending moment and deflection along the length of pile are showed.

3. PROPOSED SUPERSTRUCTURE

The superstructure is sixteen-storeyed residential building and it is firstly analyzed by ETABs software. It is situated in seismic zone 2B in Kamaryut township, Yangon Region. In these building concrete strength, f_c' is 4000psi and reinforcing yield strength, f_y is 50000psi. The intermediate moment resisting frame and dynamic analysis procedure are used. The overall height of the building is 57m, basement height is 3.66m, ground floor level height is 3.66m and typical floor height is 3m. The building is square shape and its length is 33m and 33m width. Loading consideration is based on UBC-97 and the load combinations are considered as per CQHP guideline. 3D model of superstructure which is analyzed in ETABs software is shown in Figure 1.

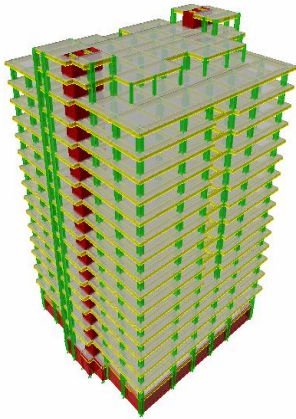


Figure 1. 3-D model of 16th storyed building

4.RESULT OF STABILITY CHECKING

Overturning moment, sliding, storey-drift and P-Δ effect are checked for the stability of superstructure. All checking of superstructure stability are within the allowable limit. So, the superstructure is stable. The result of checking is shown in Table 1.

Table 1

Checking	X-Direction	Y-Direction	Limit	Remark
Overturning Moment	7.82	7.01	1.5	satisfied
Sliding	4.4	4.9	1.5	satisfied
Storey-Drift	0.49065	0.03888	2.16	satisfied
P-Δ Effect	0.00209	0.00261	0.1	satisfied

5. STUDY ON SOIL REPORT

The proposed building is located in Kamaryut township, Yangon Region. The required soil parameters such as C, Ø, Y_{sat} and Y_r are taken from soil report. Three number of borehole are used. The depth of borehole is 72m and the water table is found at 16.5m below the ground surface.

5.1 Calculation of Allowable Bearing Capacity of Soil

The allowable bearing capacity is calculated by Meyerhof Method, Hansen Method and Vesic Method. The allowable bearing capacity is finally taken the average value of these three methods. The value of allowable bearing capacity are shown in Table 2.

Table 2

Methods	Q _{all} (ton/m ²)
Meyerhof	13.3
Hansen	12.3
Vesic	16.7
Average	14.1

5.2 Selection of Foundation Type

Foundation type is chosen by comparison the allowable bearing capacity of soil and the required bearing pressure of structure.

$$\text{Allowable bearing capacity} = 14.1 \text{ ton/m}^2$$

$$\text{Unfactor column load} = 31257.08 \text{ ton}$$

$$\text{Foundation Area} = 1089 \text{ m}^2$$

$$\text{Required bearing pressure} = \frac{31257.08}{33 \times 33} = 28.7 \text{ ton/m}^2$$

The required bearing pressure is greater than the allowable bearing capacity of mat foundation. Therefore, mat foundation is not suitable for the proposed building So, pile foundation should be used.

6.LOAD CARRYING CAPACITY OF SINGLE PILE AND GROUP PILE FOUNDATION

The unfactored column load are taken from superstructure. According to the critical unfactored column load, single pile and four pile group are chosen to design pile foundation. The values of critical unfactored column loads are shown in Table 3.

Table 3

Point	Critical Unfactored Column Loads (tons)	Remark
13,20,21,22,27,28,30,35,36,37,44	316.94	Single pile
14,15,16,17,18,19,38,39,40,41,42,43	542	Group-1
1,2,3,4,5,6,7,9,10,12,45,47,48,50,51,52,53,54,55,56	604.55	Group-2
8,11,46,49	683.53	Group-3
(69+70+71+72+282+283+287+288+1197+1198+1201+1202+1203),(73+74+75+76+284+285+290+291+1199+1200+1204+1205+1206)	2795.765	Group-4

7.DESIGN OF BORED PILE FOUNDATION

To design the bored pile foundation, ETABs software is used and all of piles are satisfied with compression capacity checking, settlement checking and deflection checking. The results of pile foundation from software represent in Table 4.

Table 4

Name	Single pile	Group 1	Group 2	Group 3	Group 4
Diameter (mm)	800	800	800	800	800
Length(m)	50	50	50	50	50
All: Bearing Capacity	334	334	334	334	334

(tons)					
Control Point	20	3054	3019	3063	3095
Load Per Pile (Tons)	330	289	320	250	303
Settlement (mm)	9.49	8.96	9.79	8.82	9.13
Deflection in X-Direction (mm)	3.22	3.17	3.73	3.51	2.97
Deflection in Y-Direction (mm)	3.56	2.91	3.60	3.01	3.44
All: Settlement (mm)	10	10	10	10	10
Remark	OK	OK	OK	OK	OK

7.1 Design Result of Pile Cap

According to design analysis result from SAFE software the maximum punching shear ratio is 0.95 and this value is lower than the allowable limit. And required reinforcement for the pile caps are obtained. For single pile and group pile required pile cap size and steel schedule are shown in Table 5 and Table 6. Pile cap foundation plan is shown in Figure 2.

Table 5

Name	No of Pile	Length (m)	Width (m)	Thickness (m)
Single pile	1	1.8	1.8	1.4
Group 1	2	3.6	1.8	1.8
Group 2	2	1.8	3.6	2
Group 3	3	3.6	3.28	2
Group 4	10	10.8	4	2

Table 6

Name	Top Steel		Bottom Steel	
	X-Strip	Y-Strip	X-Strip	Y-Strip
Single pile	#8@4"c/c	#8@4"c/c	#8@4"c/c	#8@4"c/c
Group 1	#8@3"c/c	#8@3"c/c	#8@3"c/c	#8@3"c/c
Group 2	#8@3"c/c	#8@3"c/c	#8@3"c/c	#8@3"c/c
Group 3	#8@3"c/c	#8@3"c/c	#8@3"c/c	#8@3"c/c
Group 4	#8@3"c/c	#8@3"c/c	#8@3"c/c	#8@3"c/c

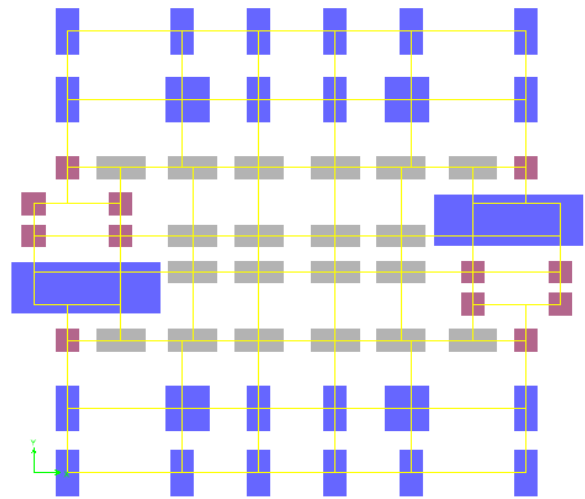


Figure 2. Cap Foundation Plan

7.2. Allowable Pullout(uptift) Capacity of Bored Pile

The uplift capacity of piles is generally controlled by the unit shearing resistance, either adhesion or friction, available at the interface of pile and soil. The design of bored pile foundation should be considered checking the pullout capacity. In checking the allowable pullout capacity is not greater than tensile capacity of pile. Furthermore, the uplift capacity of the pile group must also be checked. The pullout capacity for single pile is estimated from equation 1.

$$\text{Pullout Capacity, } P_{tu} = \sum P_{si} + P_{pb} + W \quad (1)$$

In equation (1) $\sum P_{si}$ is skin resistance from the several strata over the embedment depth, P_{pb} is pullout capacity from base enlargement and W is total weight of pile. The allowable pullout capacity of single pile and pile groups are shown in Table 7. Since the tensile strength of bored pile is greater than the ultimate uplift capacity of pile. So, the design is satisfied.

Table 7

Name	All: Pullout capacity of pile (Tons)	Tensile capacity of pile (Tons)
Single pile	44.14	173.96
Group 1	88.28	347.92
Group 2	88.28	347.92
Group 3	132.42	521.88
Group 4	441.38	1739.6

7.3 Settlement of Single Pile and Group Pile

The settlement analysis plays an important role in building foundation. The settlement of pile is calculated by semiempirical method. The calculated value of settlement is lower than the allowable limit(25mm). The results of settlement for single pile and pile group are described in Table 8.

Table 8

Name	Single Pile Settlement(mm)	Group Pile Settlement(mm)
Single Pile	11.08	11.08
Group 1	9.47	14.21
Group 2	10.56	15.84
Group 3	7.96	16.12
Group 4	9.77	21.84

7.4. Lateral Load Capacity of Bored Pile

Lateral loadings are included wind loads, earthquake loads, wave loads and inclined loads. Many different methods of analysis have been proposed to solve the problem of a laterally loaded pile. For this paper the analysis is done with Brom’s method. The actual values of lateral load, lateral deflection, and bending moment are taken from ETABS result and it value is lower than the allowable value. So, the pile can resist the imposed lateral load. The results of pile capacities under lateral load are as shown in Table 9.

Table 9

Pile Capacity		Lateral Load (tons)	Lateral Deflection (mm)	Bending Moment (ton. m)
Single pile	Actual	2.87	3.56	5.03
Group 1	Actual	2.21	3.17	1.45
Group 2	Actual	3.13	3.73	3.97
Group 3	Actual	2.31	3.51	2.78
Group 4	Actual	2.36	3.44	5.31
Allowable		21.20	10.00	42.55
Remark		OK	OK	OK

8. ANALYSIS RESULT DESCRIPTION

The following figures are shown axial force, shear force, bending moment deflection and settlement of pile.

8.1 Axial force along pile

The following Figure 3 shows the axial load distribution in the pile. The axial force is maximum at the top portion of the pile, it reduces with depth and is minimum at the bottom portion of the pile. The maximum axial force of the pile is 319.62tons which is occurred in group 2. The minimum axial force of the pile is 282.42tons which is occurred in group 3.

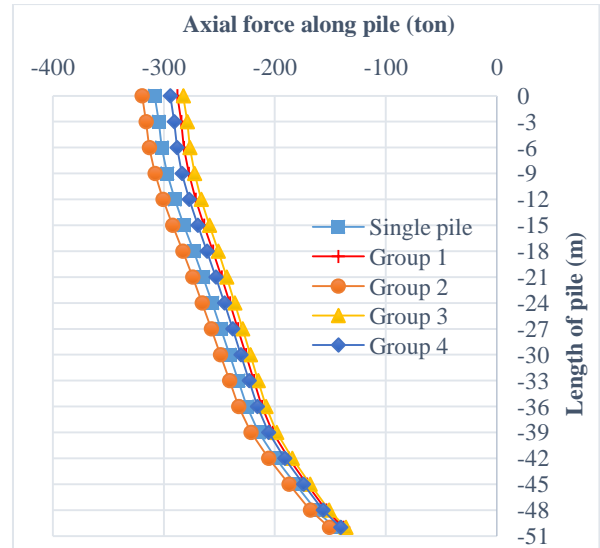


Figure 3 Axial Force of Pile

8.2 Shear Force along pile

Figure 4 describes shear force along the pile. The maximum shear force is occurred at the top portion of pile and the minimum at the bottom portion of pile. The maximum shear force of the pile is 2.04 tons which is occurred in group 4 and the minimum value is 0.37 tons which is occurred in group 1.

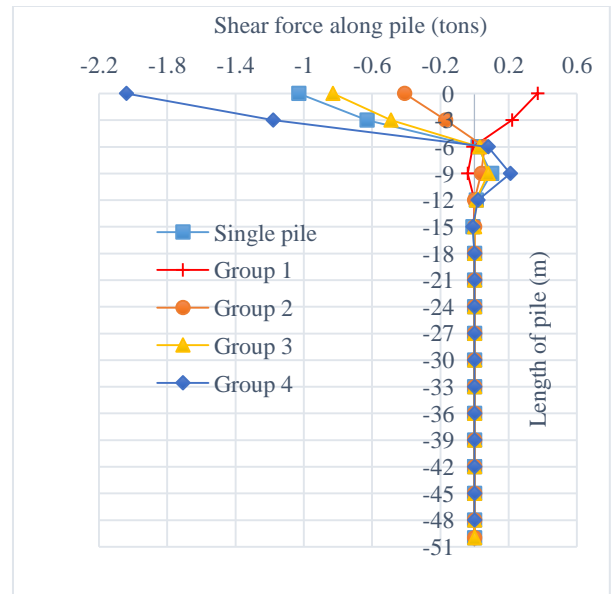


Figure 4 Shear Force of Pile

8.3 Bending Moment along pile

The effect of bending moment along the pile length is described in Figure 5. The maximum bending moment of pile is occurred at the top portion of pile and the minimum at the bottom portion of pile. The maximum bending moment of the pile is 8.745 ton-m which is occurred in group 4 and the minimum value is 1.44 ton-m which is occurred in group 2.

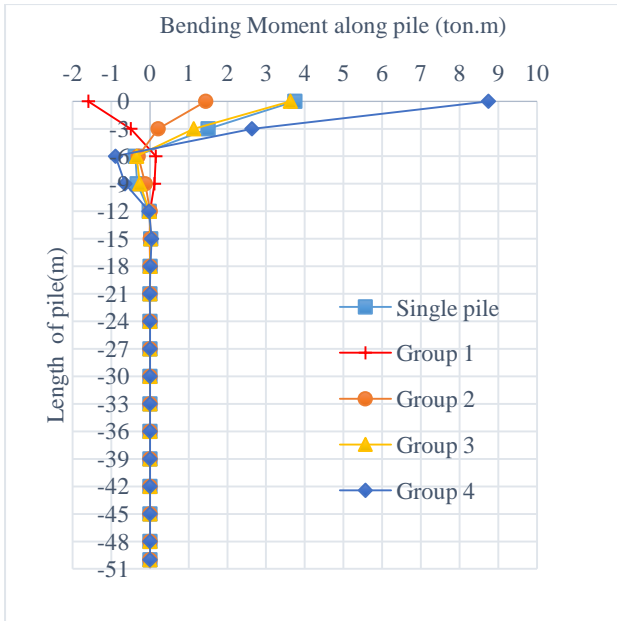


Figure 5 Bending moment of Pile

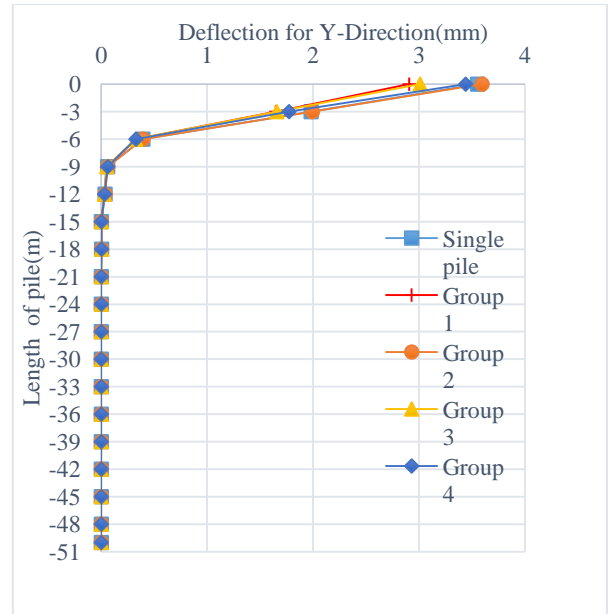


Figure 7 Pile deflection in X-Direction

8.4 Pile Deflection in X-Direction

The value of deflection along pile for X-Direction is shown in Figure-6. It was found that the deflection value is decreased with increase in length of pile. The maximum deflection is 3.73mm which is occurred at group2 and the minimum values is 2.97mm which is occurred at group 4.

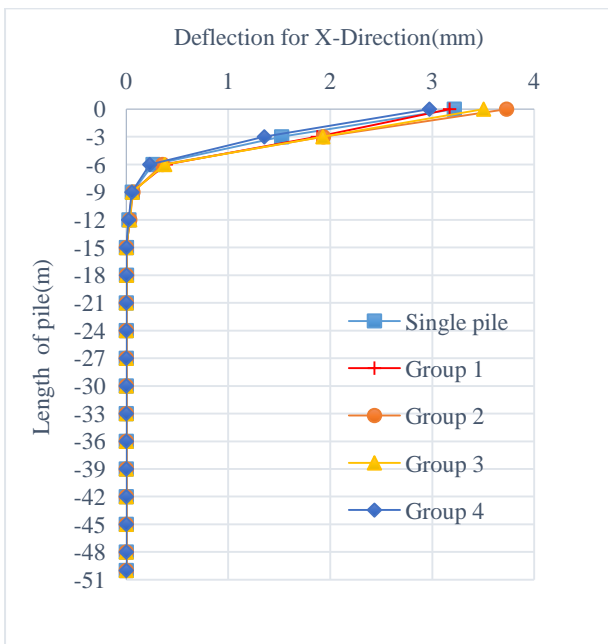


Figure 6 Pile deflection in X-Direction

8.5 Pile Deflection in Y-Direction

The value of deflection along pile for Y-Direction is shown in Figure-7. It was found that the deflection value is decreased with increase in length of pile. The maximum deflection is 3.6mm which is occurred at group2 and the minimum values is 2.91mm which is occurred at group 1.

8.6 Settlement

The value of settlement is shown in Figure 8. The maximum value of settlement is 9.79mm which is occurred in group 2 and the minimum is 8.96 mm which is occurred in group 1.

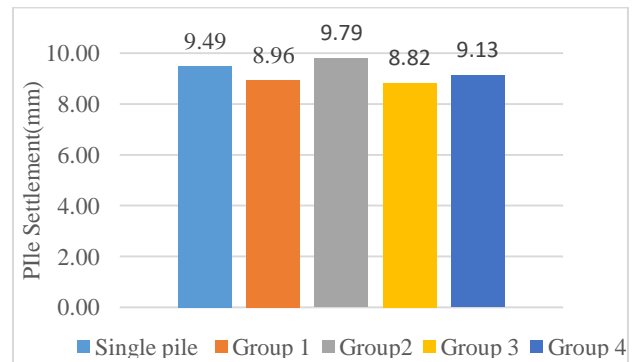


Figure 8 Settlement

9. PILE REINFORCEMENT

For piles, a minimum amount of vertical steel reinforcement is 1% of the cross sectional area of pile. According to ACI code, spirals should consist of a continuous bar or wire not less than 5/8" in diameter and clear spacing between turns of spirals must not exceed 3" nor less than 1". For this proposed building the required reinforced bars are 10#8 longitudinal reinforcement with 3" clear cover @ 8" c/c spacing and 5/8" spiral bar diameter @ 3" c/c is used throughout the length of pile.

10. DISCUSSION AND CONCLUSION

In this study 16th storeyed building is designed in seismic zone 2B and bored pile foundation is considered. Single pile and four pile groups are used. In the pile design, the diameter of pile is 800mm and the length of pile is 50m. The reinforced design is 10#8 longitudinal bar with 3" clear cover @ 8" c/c spacing and 5/8" spiral bar diameter @ 3" c/c is used throughout the length of pile. Pile cap are designed with 3D

spacing and checking punching shear ratio by SAFE software. They are satisfactory in punching shear ratio. Reinforcement design for pile cap is #8 bar but number of pile are varied according to the pile cap size. The value of settlement, deflection in X&Y direction and lateral load are less than the allowable limit. The tensile strength of bored pile is greater than the pullout capacity for single and group pile. So, the bored pile foundation is satisfied for the proposed building. According to the result, the axial force in group 2 is maximum and minimum is occurred in group 3. The shear force and bending moment in group 4 is maximum and minimum is occurred in group 2. The maximum deflection in X-direction and Y-direction is occurred at group 2 but the minimum is occurred at group 4 in X- direction and at group 1 in Y-direction. The base settlement is maximum at group 1 and the minimum is occurred at group 3.

11.ACKNOWLEDGEMENT

The author would like to express my deepest thanks and gratitude to her supervisor Dr. Nyan Phone, Professor and Head of the Department of Civil Engineering of the Technological University (Thanlyin). The author special thanks go to her co-supervisor Dr. Kyaw Lin Htat, Professor of the Department of Civil Engineering of the Technological University (Thanlyin), for his invaluable advice and suggestion throughout the study. The author would like to express her thanks to her member Dr. Kyaw Zeyar Win, Professor of the Department of Civil Engineering of the Technological University (Thanlyin), for his valuable comments and guidance during this study. Finally, her special thank goes to all who help her with necessary assistance for this study.

12.REFERENCES

- [1] Das, Braja M. "Principles of Foundation Engineering", Eighth Edition.
- [2] M.J.Tomlison. "Pile Design and Construction Practice", Fourth Edition, 1994.
- [3] Bowles, Joseph E. "Foundation Analysis and Design", Fifth Edition. New York: McGraw Hill Co, 1996.
- [4] Ruman Rajapakse "Pile Design and construction rules of Thumb"
- [5] Michael W.O'Neill.An-Bin Huang"Comparative Behaviour of Laterally Loaded Groups of bored and Driven Piles in Cohesionless Soil" The International Society of Offshore and Polar Engineering Conference.
- [6] P.J.Anathanathan, S.Gajan, T.Kanagalingam and H.N.Seneviratne. "Behaviour of Laterally Loaded Piles.
- [7] William Higgins, Celio Vasquez, Dipanjan Basu, and D.V.Griffiths,(2013)."Elastic Solution for Laterally Loaded Piles."Journal of Geotechnical and Geoenvironmental Engineering July 2013.
- [8] Weeraya Chim-oye and Narin Marumdee(2012) "Estimation of Uplift Pile Capacity in the sand layers". International Transaction Journal of Engineering, Management, Applied Sciences and Technologies.(2013)
- [9] U Nyi Hla Nge, "Reinforced Concrete Design" 2010.
- [10] H.Nilson, "Design of concrete structures",Twelfth Edition.

Client Server based Fault Management System for LAN

Khin Khin Su

Lecturer

University of Computer Studies (Dawei)
Dawei, Myanmar

Abstract: This paper aims to implement the client server based fault management system. The user who uses this system can ping the clients within a network and the user can view the result of the message. It also provides to check the network card and this system can show the Network Card Setting. This system has two portions: client side and server side. The server listen the entire requests of the clients and response to them,

Keywords: Fault management system, Network Management System, Client/Server Network, Local Area Network

1. INTRODUCTION

The International Organization for Standardization (ISO) network management model defines five functional areas of network management. Among many types of Network Management Systems today, the purpose of fault management is to detect, isolate, notify, and correct faults encountered in the network. Network devices are capable of alerting management stations when a fault occurs on the systems. An effective fault management system consists of several subsystems.[1] This objectives of this paper is to integrate network management information, to manage fault, configuration and security management, to track the client/server information and to detect hardware and software port of the server and USB.

2. METHODOLOGY

2.1 Overview of Network Management System

Network management involves a distributed database, auto polling of network devices, and high-end workstations generating real-time graphical views of network topology changes and traffic. In general, network management is a service that employs a variety of tools, applications, and devices to assist human network managers in monitoring and maintaining networks. The combination of equipment, hardware and software used in monitoring, controlling and managing a data communication network. The overall purpose is to provide practical recommendations on each functional area to increase the overall effectiveness of current management tools and practices. It also provides design guidelines for future implementation of network management tools and technologies. The early 1980s saw tremendous expansion in the area of network deployment. As companies realized the cost benefits and productivity gains created by network technology, they began to add networks and expand existing networks almost as rapidly as new network technologies and products were introduced. By the mid-1980s, certain companies were experiencing growing pains from deploying many different (and sometimes incompatible) network technologies. The problems associated with network extension affect both day-to-day network operation management and strategic network growth planning. Each new network technology requires its own set of experts. In the early 1980s, the staffing requirements alone for managing large, networks created for many organizations. An urgent need for automated network management (including what is typically called network capacity planning) integrated across diverse environments..

2.2 Network Management Functional Areas

The ISO network management model's five functional areas each of which represents a set of activities performed by operations personnel or customers. The network management system and the Intelligent Network Elements are involved in accomplishing the functioned task. These areas are

- Configuration Management
- Fault Management
- Performance Management
- Security Management
- Accounting Management

2.2.1 Fault management

Detect, isolate, notify, and correct faults encountered in the network. Fault Management applications include processing all events and determining if a fault is detected. Fault detection requires other functions including filter events, logging to maintain historical records that detect long-term trends, monitoring, notification, and reporting by generating alarms. The goal of fault management is to fix network problems to keep the network running effectively. Because faults can cause downtime or unacceptable network degradation, fault management is perhaps the most widely implemented of the ISO network management elements. Fault management involves first determining symptoms and isolating the problem. Then the problem is fixed and the solution is tested on all-important subsystems. Finally, the detection and resolution of the problem is recorded.

Fault management is the process of identifying and correcting network problems, otherwise known as faults. Faults typically manifest themselves as transmission errors or failures in the equipment or interface. Faults result in unexpected downtime, performance degradation and loss of data. Generally, fault conditions need to be resolved as quickly as possible. Comprehensive fault management is the most important task in network management. Fault management tools can help increase the reliability of the network by quickly identifying the fault, and then help initiate the recovery process. The first step is to identify the fault, isolate the cause of the fault, and then, if possible, correct the fault. This three step process requires predetermining which faults should be managed and be given higher priorities than others, and then utilizing a set of tools to resolve the fault through the network manager.

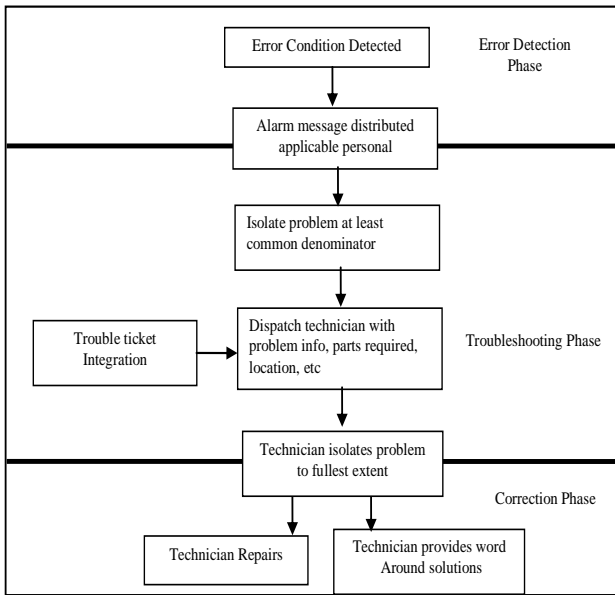


Figure 1. Fault Management System

2.3 Local Area Network

In general terms, LAN (Local Area Network) refers to a group of computers interconnected into a network so that they are able to communicate, exchange information and share resources (e.g. printers, application programs, database etc). In other words, the same computer resources can be used by multiple users in the network, regardless of the physical location of the resources.

Each computer in a LAN can effectively send and receive any information addressed to it. This information is in the form of data 'packets'. The standards followed to regularize the transmission of packets, are called LAN standards. There are many LAN standards as Ethernet, Token Ring and FDDI etc. Usually LAN standards differ due to their media access technology and the physical transmission medium.

A local area network (LAN) is a group of computers and associated devices that share a common communications line or wireless link. Typically, connected devices share the resources of a single processor or server within a small geographic area (for example, within an office building). Usually, the server has applications and data storage that are public in common by multiple computer users. A local area network may serve as few as two or three users (for example, in a home network) or as many as thousands of users (for example, in an FDDI network). Major local area network technologies are: Ethernet, Token Ring and FDDI.

Ethernet is by far the most commonly used LAN technology. A number of corporations use the Token Ring technology. FDDI is sometimes used as a backbone LAN interconnecting Ethernet or Token Ring LANs. Another LAN technology, ARCNET, once the most commonly installed LAN technology. A suite of application programs can be kept on the LAN server. Users can order printing and other services as needed through applications run on the LAN server. A user can share files with others at the LAN server; read and write access is maintained by a LAN administrator. A LAN server may also be used as a Web server if safeguards are taken to secure internal applications and data from outside access.

A Local Area Network (LAN) is the result of connecting a number of computers or other IP devices together in a

localized geographic area – for example in one room, building or several buildings. LANs are typically connected to each other via cable and more recently via radio waves. In an office building for example, workstations and personal computers (PCs) are commonly connected to each other with a Local Area Network. This allows an employees' equipment to communicate - send and receive files, share access to the files or data on another workstation even share applications. One obvious benefit of building a LAN is the efficiency of transporting data from one location to another. The transmission speed of data, across the LAN, can be measured at more than 1,000 times the speed in which transfer files using a standard 56k modem. [2]

2.4 Client Server Network

Client/Server network uses a network operation system designed to manage the entire network from a centralized point, which is the server. Clients make requests of the server and the server responds with the information or access to a resource. Client/Server networks have some definite advantages over peer-to-peer networks. It is easier to find files and resources because they are stored on the server. Also have much tighter security .All usernames and passwords are stored in the same database (on the server), and individual users can't use the server as a workstation. The server holds the database of user accounts, passwords, and access rights.

Establishing the right kind of network for the user's organization is important to make the most of their time and money. While peer-to-peer network is often a good choice for small networks, in an environment with more than 10-15 computers, a peer-to-peer network begins to become more trouble than it is worth: their computers start to slow down, they can never find the file they are looking for, and security is non-existent. If this is happening in their organization, it is probably time to switch to a client-server network by bringing in a dedicated server to handle the load. The server is called "dedicated" because it is optimized to serve requests from the "client" computers quickly. The diagram below shows a simple client-server network. [3]

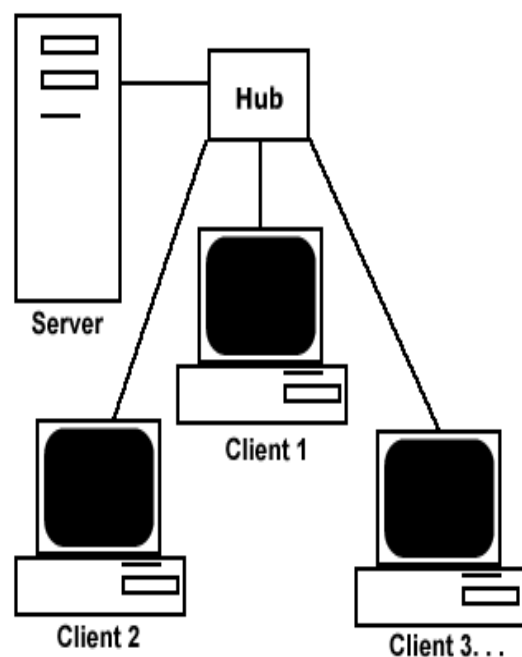


Figure 2. Simple Client Server Network

3. DESIGN AND IMPLEMENTATION OF FAULT MANAGEMENT SYSTEM

3.1 Overview System of Fault Management

There are many managements such as configuration management, fault management, performance management, security management, accounting management and etc. These are essential and useful in any fields. Among them, this system is designed for fault management system. Fault management is to detect and troubleshoot the system.

This system can track the all of the fault event of the client server network management system. It provides the user authentication fault and network card fault.

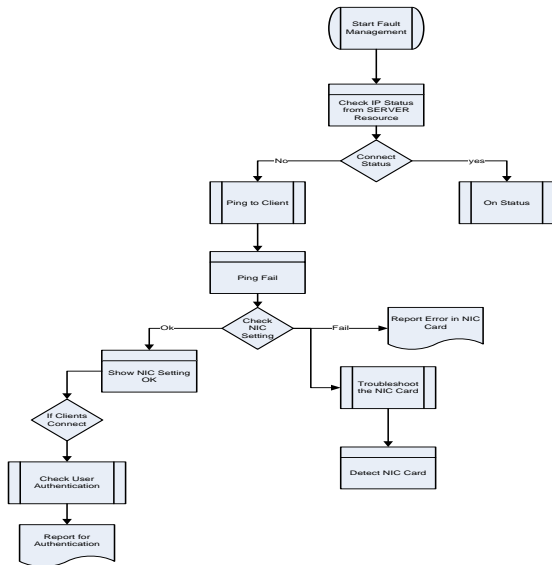


Figure 3. Fault Management System Design

4. TEST AND RESULTS OF CLIENT SERVER FAULT MANAGEMENT SYSTEM

In this system, there are two main components such as server program which is listening the entire request of the clients and client which are sending request to server. In the fault management, this system can trace which invalid user is connecting and connected and user authentication.

4.1 NIC Card menu Program

In this program when the user press the check NIC card button this program will show the history of the network card.

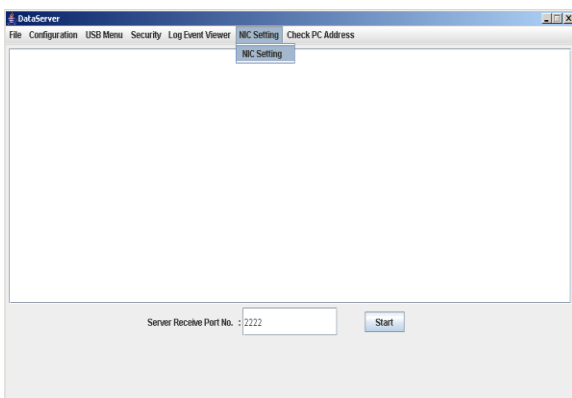


Figure 4. NIC Card Menu

From this menu, NIC setting checking program will show when the NIC setting sub menu will be clicked.

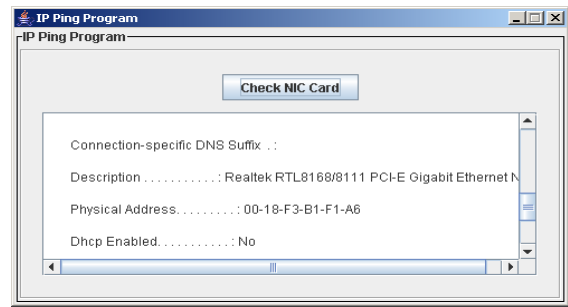


Figure 5. NIC Card Setting Menu

4.2 Check PC Address Menu Program

From this menu, PC address checking program will show when the Check PC Address sub menu will be clicked.

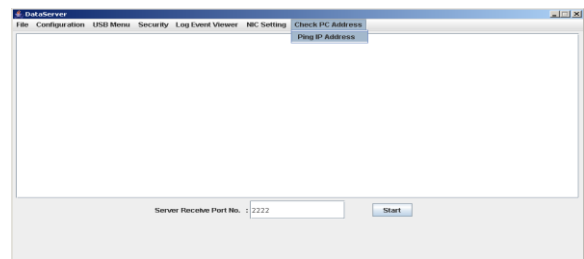


Figure 6. PC Address Check Menu

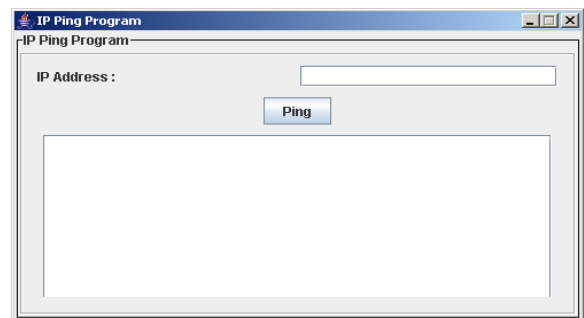


Figure 7. IP Ping Program Menu

In this program, if the user wants to know which PC is reached on the network, the user must to enter the required IP at the IP Address text box and press ping button. The result of the message will show at the text box area of the program.

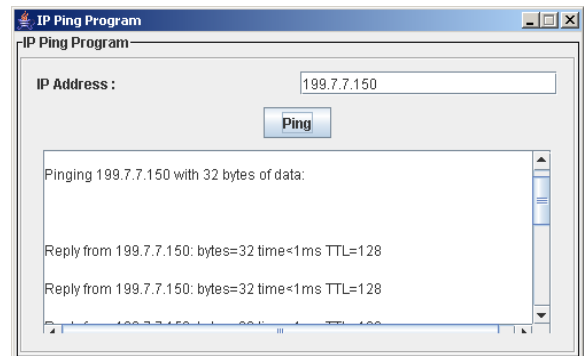


Figure 8. IP Checking Program Menu

4.3 Starting the Server

When the user want start the server, press start button and the server will start. And listen all of the request of the client.

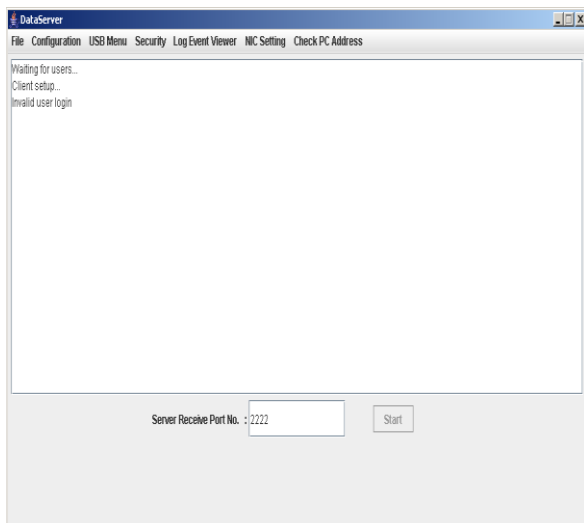


Figure 9. Starting the Server Menu

4.4 Starting the Client Program

When the user wants to start the client program, the user must be run the client program. The client program will run like this.

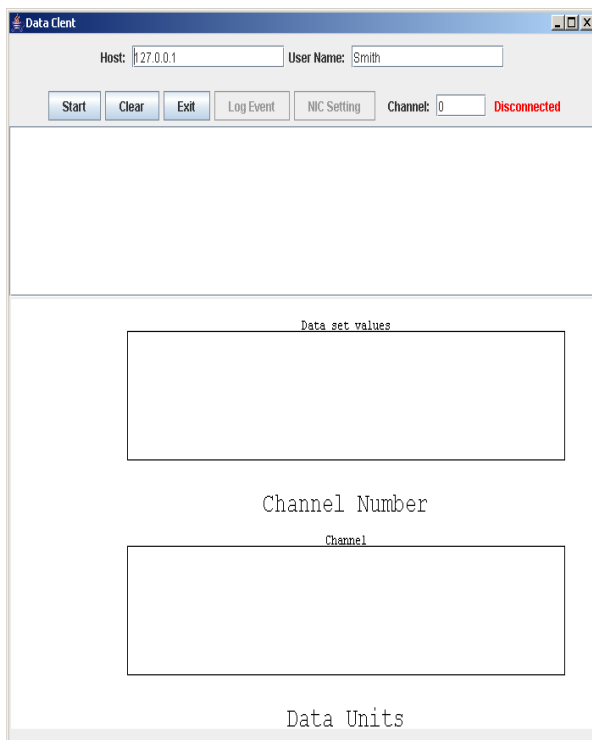


Figure 10. Starting the Client Menu

In this program the user must be enter the server IP address at the host text box and at user name textbox, the user must be typed the user id which are reserved at the server. If the user id is invalid or user is disabling at the server side, the user cannot connect the server and get the message from the server. If the user want to start the client program, user must be pressed the start button and if the user want to clear all of the message the user must pressed clear and if the user want to exit the client, press the exit button.

5. DISCUSSIONS AND CONCLUSION

In this client server based fault management system, the server can listen all of the requests of the clients and response to the clients. And when the server is start up, the server listen the client request and can show the message about which client connect with which user and which client are connecting and which cannot connect. The data channel is to register in the server. And when the client is start up and connect to the server, the client request the server with the user name, if the server accept the request the response message of the server will show at the display area of the client. And also show the message of the client is connecting with how many data channel to server.

This system is suit to use in the client server network system with java environment. Because all of the programs in the system are developed by java language and native dll file. So in the client server data sending environment and client server messaging environment, this system can give fully support and moreover for the USB data access, this system can support the USB ports and devices to detect and read devices configuration.

6. ACKNOWLEDGMENTS

The author would like to express thanks to the people who help her to support and valuable knowledge to do this paper.

REFERENCES

- [1] Network Management System: Best Practices White Paper
<<https://www.cisco.com/c/en/us/support/docs/availability/high-availability/15114-NMSbestpractice.html#faultde>>
- [2] Local Area Network
<http://en.wikipedia.org/wiki/Local_area_network>
- [3] Client Server Network
<<http://compnetworking.about.com/od/networkdesign/l/a050201a.htm>>
<http://compnetworking.about.com/od/basicnetworkingconcepts/g/network_servers.htm>
<<http://compnetworking.about.com/cs/clientserver>>

Design Comparison for Rectangular and Round Winding Distribution Transformer (1000kVA)

Ei Ei Chaw
Department of Electrical Power
Engineering
Technological University
(Thanlyin),
Myanmar

Myo Thet Tun
Department of Electrical Power
Engineering
Technological University
(Thanlyin),
Myanmar

Hnin Wint Aung
Department of Electrical Power
Engineering
Technological University
(Thanlyin),
Myanmar

Abstract: The transformer is the most efficient of transmission and distribution system, with efficiencies typically in the high 90s, it is possible to reduce transformer costs and losses by using round and rectangular conductor winding. This journal presents the result of the difference between round conductor winding and rectangular conductor winding of distribution transformer. The most substation transformers are utilized either circular or rectangular in core and coil assembly. The transformers manufacturing industry improve transformer efficiency and reliability. This paper intended to prove the product would have improved outcomes, a higher standard and sustainability by adapting the product development to the road condition of the country of manufacture. In design consideration, selection of magnetic frame, choice of conductor size, choices of current density are considered.

Keywords: Distribution Transformer, Step Core, Core Type, Round and Rectangular winding, Tank and Losses

1. INTRODUCTION

A transformer is a static piece of apparatus used for transferring power from one circuit to another without change in frequency. Transformer can raise or lower the voltage with a corresponding decrease or increase in current. The voltage levels at the primary and secondary windings are usually different and any increase or decrease of the secondary voltage is accompanied by corresponding decrease or increase in current. A transformer consists of two conducting coils having a mutual inductance. When one of the windings is connected to an AC supply, an emf is induced on the other winding which is proportional to the number of turns. Transformers are commonly employed in the chain of electric power supply from generating stations to consumers of electric energy. Distribution transformers are used in the distribution networks in order to transmit energy from the medium voltage network to low voltage network of the consumers. Distribution transformers are energized for 24 hours with wide variation in load; therefore they are designed for low no-load losses.

2. BASIC PRINCIPLE OF DISTRIBUTION TRANSFORMER

A transformer is basically electromagnetic static equipment based on the principle of Faraday's Law of electromagnetic induction. The transformer is an electromagnetic conversion device in which electrical energy received by primary winding is first converted into magnetic energy which is reconverted back into a useful electrical energy in other circuits (secondary winding, tertiary winding, etc.). A transformer consists of laminated magnetic core forming the magnetic frame. The primary and secondary coils are wound up the three cores for three-phase of the magnetic frame, linked by the common magnetic flux. When an alternating voltage is applied across the primary coil, a current flow in it and the magnetic flux is produced in the transformer core. And then the secondary coil produces the output voltage. Thus, the primary and secondary windings are not connected

electrically, but coupled magnetically. A transformer is termed as either a step-up or step-down transformer depending upon whether the secondary voltage is higher or lower than the primary voltage respectively.

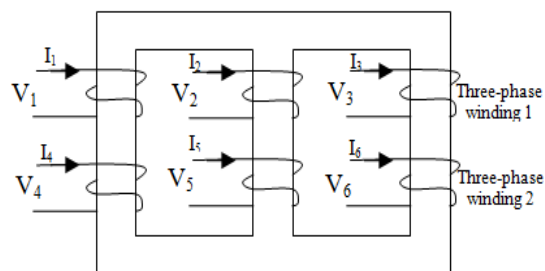


Figure 1. Three-phase two winding transformer

3. CONSTRUCTION OF TRANSFORMER

- (i) Core
- (ii) Windings
- (iii) Tank
- (iv) Off-load Tap Changer

3.1 Type of core

The core, which provides the magnetic path to channel the flux, consists of thin strips of high-grade steel, called laminations, which are electrically separated by a thin coating of insulating. Grain-Oriented Silicon Steel is used as the core material for transformer. The usual thickness of laminations are 0.23 mm, 0.27 mm and 0.3 mm. The core cross section can be classified in circular core, rectangular core, stepped core and triangular core. Rectangular cores are used for smaller ratings and as auxiliary transformers used within a power transformer. Rectangular cores use a single width of strip steel, while circular cores use a combination of different strip widths to approximate a circular cross-section. Stepped

core can be reduced the two losses due to varying flux occur the eddy current and the hysteresis losses in the core.

There are two type of core construction used in transformer; core form and shell form. In a single phase core form, the windings are on the outside, a single path for the magnetic circuit. In the three-phase core form, the windings of a particular phase are typically on the same core leg. In a single-phase shell form, the windings are on the inside, multiple paths for the magnetic circuit. In the three-phase shell-form construction include five and seven-legged cores, depending on size and application. The Figure (2) shows the type of cores.



Figure 2.Type of cores

3.2 Winding

Winding form, the electrical circuit of a transformer. The windings must be electrically and mechanically strong to withstand both over-voltages under transient surges, and mechanical stress during short circuit. The winding that is connected to the source is called the primary winding. The winding that is connected to the load is called the secondary winding. For core-type transformers, the windings are cylindrical, and are arranged concentrically. According to the voltage ratings and current ratings, we adopt one of the following types of windings.

- High Series Capacity Winding
- Continuous Disc Winding
- Helical Winding
- Cylindrical Winding

High Series Capacity Winding for transformer above highest system voltage 72.5kV, the series static capacitance of the windings is increased to such an extent that the initial potential distribution of incoming impulse voltage is made nearly linear. Continuous disc winding is most commonly used for coils above 24kV and these windings consist of number of disc wound from a single wire or number strip in parallel. In Helical Winding, the coil consists of a number of rectangular strips wound in parallel radially.

3.3 Coil Insulation and Insulation Paper

For oil immersed transformers, the insulation system comprises a mixed dielectric, oil and cellulosic material. The insulation structure must be arranged into major insulation and minor insulation. Major insulation comprises insulation of

windings to earth and transformer core, other winding of the same phase (e.g. HV winding to LV winding) and between one phase and another. The insulation between different windings and inner winding to core consists of pressboard cylinders separated by oil ducts. Minor insulation refers to insulations between different parts of one winding, like insulation between turns, layers, etc. The insulation of the conductors is generally of paper, which is wrapped around the conductor. Pressed, oil ducts, spacers and insulating cylinders of high dielectric strength are used between low voltage winding and core, low and high voltage windings and layers of windings.

3.4 Tank

Transformer tank is to provide a protective cover to the core, windings and other internal parts including transformer oil. The transformer tank also provides external surface for dissipating heat. The tank surface cools by both radiation and convection. The oil provides a medium for insulation and heat dissipation. The heat from core and windings is dissipated by means of the circulating oil. The tank and cooling system contribute to the heat dissipation. Normally transformers up-to 50kVA could be manufactured without external cooling tubes. For transformers of higher rating, tanks are constructed with external cooling tubes to provide additional surface for heat dissipation.

3.5 Off-load Tap Changer

Off-load tap changer is the simplest arrangement. The changes are made when the transformer is isolated from the supply on both sides, in order to avoid arcing at the point of break. Thus, for changing the taps, energy supply has to be interrupted quite frequently, which is highly undesirable. As such, this method of tap changing is generally used in small and medium size transformers. Larger rating transformers are provided with on-load tap changer, because frequently discontinuity of power cannot be tolerated by the power system network. On-load tap changer is used to control large high-voltage distribution networks and to maintain correct system voltages.

4. DESIGN THEORY OF TRANSFORMER

The design of the distribution transformer is to obtain main dimensions of the magnetic circuit (core), yoke and window, low voltage and high voltage windings, performance characteristics and the cooling tank.

The selection of number of turns with the equation is

$$\text{The e.m.f per turn, } E_t = k\sqrt{Q}$$

$$\text{The e.m.f per turn, } E_t = 4.44 \times f \times B_m \times A_g \times 10^{-4}$$

Where,

B_m = maximum flux density in the core, Tesla

f = rated frequency, 50Hz

A_g = gross core area in sq.cm

Number of turn per phase in low voltage winding,

$$T_2 = \frac{V_2}{E_t}$$

Number of turn per phase in high voltage winding,

$$T_1 = T_2 \times \frac{V_1}{V_2}$$

The design is to select the number of turns of coils and proceed further towards estimating the coil configuration till

arriving at the window height of the core frame. Based on the calculated window height, the design of the low voltage coil is done.

Output of transformer for three-phase,

$$Q = 3.33f B_m d' K_w A_w A_i 10^{-6} \text{ Volt} - \text{A}$$

Where, d' = average value of current density, A/mm^2

The window space factor depends upon the voltage rating of the windings, mainly the highest voltage and kVA rating of the transformer.

Window area, $A_w = L(D - d)$

Overall length of the yoke, $W = 2D + d_1$

Gross yoke area, $A_y = 1.15 \times A_i$

Width of the yoke, $b_y = 0.9d$

Height of the yoke, $h_y = \frac{A_y}{b_y}$

The core cross-section is rectangular in the case of a small capacity transformer or polygonal, inscribing a circle, in the case of a large capacity transformer in order to utilize fully the space available, which mean smaller diameter of the circle over the stepped core. The number of steps depends upon the kVA rating of the transformer and its gross core section. Figure (3) describes the inscribing polygonal of 7steps core form. In Figure (4), main dimension of window consists of the height and the width of the window. Main dimension of the yoke consists of overall length (W), width of the yoke and the height of the yoke.

Volume of the core = $N_c \times A_c \times L$

Weight of the core = Volume of the core x density of steel

Iron losses in the cores = Weight of the core x losses per kg

Volume of the yoke = $N_y \times A_y \times W$

Iron losses in the yokes = Weight of the yoke x losses per kg

Total iron losses = Iron losses in the core + Iron losses in the yoke

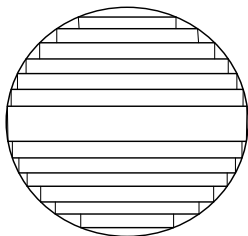


Figure 3. Main dimensions of magnetic frame

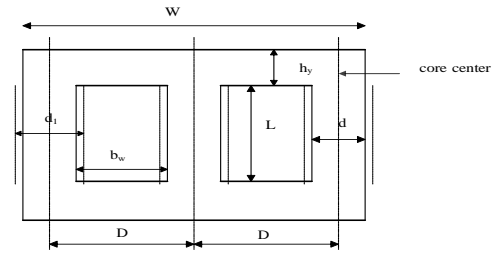


Figure 4. Main dimension of magnetic frame

The magnetizing component of no-load current,

$$I_m = \frac{\text{VA/kg} \times \text{kg}}{3 \times \text{phase voltage}}$$

Hysteresis and eddy current component from no-load loss and rated secondary phase voltage,

$$I_{h+e} = \frac{\text{No-load loss}}{3 \times \text{Phase voltage}}$$

No-load current, $I_o = \sqrt{I_m^2 + I_{h+e}^2}$

For rectangular conductor,

Cross sectional area, $a = \frac{I}{\delta}$

For round conductor,

Cross sectional area, $a = \frac{\pi D^2}{4}$

Outer diameter of insulating cylinder,

$$d_{i0} = d + 2t_i$$

Inner diameter of L.V winding,

$$D_{i2} = d_{i0} + 2t_0$$

Outer diameter of L.V winding,

$$D_{o2} = D_{i2} + 2b_2$$

Mean diameter of L.V winding,

$$D_{m2} = \frac{D_{i2} + D_{o2}}{2}$$

Mean length of L.V turn, $l_{m2} = \pi D_{m2}$

Resistance per phase of L.V winding,

$$r_2 = \frac{\rho L_{m2} T_2}{a_2} \times 10^{-3}$$

Total copper losses = $3I^2R$

Total losses = Total iron losses + Total copper losses

$$\text{Efficiency of transformer} = \frac{Q}{Q + \text{Total losses}}$$

Percentage reactance of high voltage winding,

$$E_x = \frac{7.91 \times f \times I_s \times T_1 \times \pi \times D}{V_s \times A_L} \times \left(a + \frac{b_1 + b_2}{3}\right) \times 10^{-6} \Omega$$

Percentage reactance of low voltage winding,

$$E_x = \frac{7.91 \times f \times I_s \times T_1 \times \pi \times D}{V_s \times A_L} \times \left(a + \frac{b_1 + b_2}{3}\right) \times 10^{-6} \Omega$$

Percentage resistance, $E_r = \frac{IR}{V}$

Percentage impedance $E_z = \sqrt{R^2 + X^2}$

Percentage regulation,

$$(n.E_r \% \cos\theta + n.E_x \% \sin\theta) + \frac{(n.E_r \% \cos\theta + n.E_x \% \sin\theta)^2}{200}$$

The length of the tank for three-phase transformer,

$$l_t = 2D + D_{o1} + \Delta l$$

The width of the tank for three-phase transformer,

$$b_t = D_{o1} + \Delta b$$

The height of the tank for three-phase transformer,

$$h_t = L + 2h_y + \Delta h + h_1$$

Where Δl , Δb , Δh are total clearance length-wise, width-wise and height-wise

5. ROUND AND RECTANGULAR WIRE OF DISTRIBUTION TRANSFORMER DESIGN

To calculate the transformer design, first step is based on the main data and the properly assumed values

Table 1. Specifications of Distribution Transformer Design

Specifications	Symbol	Unit	Rating
Output	Q	VA	1×10^6
Number of phase	-	-	3
H.V winding voltage	V1	V	11000
L.V winding voltage	V2	V	400
Frequency	F	Hz	50

Connection of H.V/L.V	-	-	Delta/Star
Limit of oil temperature	Θ	$^{\circ}\text{C}$	60
Limit of winding temperature	Θ	$^{\circ}\text{C}$	65

Table 2. Specifications of Distribution Transformer Magnetic Frame Design

Specifications	Symbol	Unit	Design Values
Diameter of circumscribed circle	D	mm	206
Length of core	L	mm	570
Length of yoke	W	mm	980
Height of yoke	h_y	mm	190
Width of window	b_w	mm	205
Distance between core center	D	mm	395
Weight of cores and yokes	-	kg	866.042

Table 3. Design Comparison of Distribution Transformer for L.V Winding Design

	Specifications	Symbol	Unit	Design Values
Rectangular	Turn per phase	T_2	-	20
	Phase current	I_2	A	1443.37
	Conductor section	a_2	mm^2	456.7
	Conductor size	d_2	mm	3.8 x 10
	Copper weight	-	kg	187.03
	Inner diameter of Windings	D_{i2}	mm	215.78
	Outer diameter of	D_{o2}	mm	273.2

Rectangular	Windings			
	Radial width of Windings	b_2	mm	28.71
	Resistance per phase	r_2	Ω	0.000727
	Turn per phase	T_2	-	20
	Phase current	I_2	A	1443.37
	Conductor section	a_2	mm^2	456.7
	Conductor size	d_2	mm^2	3.8 x 10
	Copper weight	-	kg	187.03
	Inner diameter of Windings	D_{i2}	mm	215.78
	Outer diameter of Windings	D_{o2}	mm	273.2
Radial width of Windings	b_2	mm	28.71	
Resistance per phase	r_2	Ω	0.000727	

Table 4. Design Comparison of Distribution Transformer for H.V Winding Design

	Specifications	Symbol	Unit	Design Values
	Turn per phase	T_1	-	976
	Phase current	I_1	A	30.3
	Conductor section	a_1	mm^2	9.6
	Conductor size	d_1	mm^2	1.6 x 6

Rectangular	Copper weight	-	kg	258.687
	Inner diameter of Windings	D_{i1}	mm	287.8
	Outer diameter of Windings	D_{o1}	mm	370.5
	Radial width of Windings	b_1	mm	41.35
	Resistance per phase	r_1	Ω	2.27
Round	Turn per phase	T_1	-	976
	Phase current	I_1	A	30.3
	Conductor section	a_1	mm^2	5.939
	Conductor size	d_1	mm	2.75 x 2
	Copper weight	-	kg	260.689
	Inner diameter of Windings	D_{i1}	mm	286.5
	Outer diameter of Windings	D_{o1}	mm	377.08
	Radial width of Windings	b_1	mm	45.29
	Resistance per phase	r_1	Ω	1.849

Table 5. Performance Summary of Distribution Transformer

Specifications	Symbol	Unit	Design Values(rect-rect)	Design Values(round-rect)
No load current	I_o	A	0.3	0.3
Iron losses	P_i	kW	1.2098	1.2098
Copper losses	P_c	kW	11.88	10.604
Total losses	P_t	kW	13.089	11.814
Full load efficiency	η	%	98.39	98.54

Table 6. Design Summary of Transformer for Regulation

Specifications	Symbol	Unit	Design Values (Rect-Rect)	Design Values(Round-Rect)
Per unit reactance	E_x	p.u	0.0585	0.06
Per unit resistance	E_r	p.u	0.0119	0.0106
Per unit impedance	E_z	p.u	0.0597	0.0609
Regulation at full load	-	p.u	0.0425	0.0417

Table 7. Design Comparison for Calculation Results and Experimental Test Results (Rectangular-Rectangular)

Specifications	Calculation Results	Experimental Test Results
Winding resistance for L.V	0.000727 Ω	0.0007716 Ω
Winding resistance for H.V	1.51 Ω	1.36 Ω
No-load losses	1209.85W	1303 W
No-load current (%)	0.31%	0.38%
Load losses	11880 W	13642 W
Voltage impedance (%)	5.969%	6.38 %

Table 8. Design Comparison for Calculation Results and Experimental Test Results (Round-Rectangular)

Specifications	Calculation Results	Experimental Test Results
Winding resistance for LV	0.000727 Ω	0.0007299 Ω
Winding resistance for H.V	1.23 Ω	1.35 Ω

No-load losses	1209.85W	1266 W
No-load current	0.31%	0.37%
Load losses	10604.54 W	13748 W
Voltage impedance	6.09 %	6.08

6. CONCLUSION

In this journal, 1000kVA, 50Hz, 11/0.4kV, three-phase two winding, and delta-star connected, core type distribution transformers are already designed by using round and rectangular conductor. But magnetic frame designed is used the same type for both transformer. The design is carried out to reduce losses of transformer and in turn improve efficiency of power system. This transformer design is utilized to step down the transmission voltage to the low voltage for the power distribution requirement with minimize losses and cost, and improve efficiency of power system components. Transformer efficiency is improved by reducing load and no-load losses and transformer reliability is improved mainly by the accurate evaluation of the short-circuit reactance and the resulting forces on transformer windings under short-circuit, since these enable the avoidance of mechanical damage and failures during short-circuit tests and power system faults.

7. ACKNOWLEDGEMENTS

The author is deeply grateful to Dr. Myo Thet Tun, my dissertation supervisor and Daw Hnin Wint Aung, my co-supervisor. The author also thanks to all teachers at Technological University (Thanlyin) and all who provided her with HISEM Electric & Machinery Co., LTD. The author wishes to express her guidance to all persons who helped directly or indirectly towards the successful completion of paper. Finally, the author wishes to express her special thanks to her parents for their support and encouragement to attain her destination without any trouble.

8. REFERENCES

- [1] Indrajit Dasgupta. : Tata McGraw-Hill Publishing Company Limited: Design of Transformers,(2002)
- [2] Kulkarni,S.V. And Khaparde, S.A. “Transformer Engineering Design and Practice” Indian Institute of Technology, Bombay Mumbai, India, (2004).
- [3] S.RAO, M.E,M.I.E. : Power Transformers and Special Transformers, Principle and Practice, 3rd Ed, July,(1996).
- [4] R.FEINBERG,Dr.Ing, M.Sc. F.I.E.E. : Modern Power Transformer Practice, 1st Ed, (1979)
- [5] Mittle, V.N. and Arvind Mittal. “Design of Electrical Machine” 4th Edition, Standard Publishers Distributors, New Delhi, (1996).
- [6] Dr. Sankar Sen.: Bharat Heavy Electricals Limited Bhopal (MP),: Transformer , 2nd Ed.

Design Calculation of Automatic Voltage Stabilizer Control System

Hnin Hnin Aye
Department of Electrical Power
Engineering
Technological University
(Thanlyin), Myanmar

Abstract: Voltage fluctuation always occurs in electrical supply system. Due to voltage fluctuation, life of electrical equipment consumed electricity is shorted really. To solve this problem, automatic voltage stabilizer is needed for domestic and industries. Both single phase and three phases are available. In this journal intend to know that automatic voltage stabilizer plays efficient role in all type of load i.e. resistive, inductive and capacitive loads. This journal present control circuit for automatic voltage stabilizer provides voltage comparator, relays and servo controlled motor that compare instantaneous input and output voltage. Automatic voltage stabilizer consists of two unit; measuring unit and regulating unit. In this stabilizer, toroidal type variable auto transformer is used for regulating unit and electronic control circuit is used for sensing unit. Electromechanical or servo control system is used for measuring unit to sense the supply voltage. This electronic control circuit will operate within the fluctuation range from 120V to 250V. The rating of this automatic voltage stabilizer is 7kVA (single phase) and its frequency range is 50Hz. The output sensitivity is $\pm 1\%$. If input voltage is lower than 120V or higher than 250V, the system will be automatic shutdown. The main purpose of this research is design calculation of control circuit.

Keywords: voltage stabilizer; LM324; sensing unit; relays; controller design

1. INTRODUCTION

Servo controlled voltage stabilizer is a useful and effective device used to maintain a constant power supply. Voltage fluctuation is a common problem in Myanmar, which can cause damage in electronic devices used in home and in industries. To solve these appliances safe is to use voltage stabilizers. The automatic voltage stabilizers are widely used in industrial application to obtain the stability and good regulation for the sophisticated electrical and electronic equipments such as communication equipments and system, process controller, computer equipment etc[1]. Servo controlled is a closed loop systems for electric motors. The motor used in servo control is usually DC motor used in servo is also possible. The servo system uses a sensor to sense motor position/speed. Servo control has a feedback circuit which changes the drive power going to motor according to the control input signals and signal from sensors[2]. There are various type of stabilizers available in market. Based on the change in main voltage, the automatic voltage stabilizers increase or decreases the power supply to rectify the deviation and brings the power supply to normal level. Automatic voltage stabilizer provides a continuous monitoring of output voltage by means of an electronic control circuit that compares the instantaneous output voltage with the set value. Voltage regulation is required for two distinct purposes; under-voltage and over-voltage conditions. Line voltage regulation is the process of maintaining constant output voltage to industrial and domestic users despite a wide variation in input voltage. Under-voltage might result into brownout, distortion or permanent damage while overvoltage in the form of spikes and surges could cause distortion, burn out, melt-down, fire, electro-pulsing and permanent damage. The two distinct reasons of voltage regulation afore mentioned could be caused by abnormal forces of nature, atmosphere conditions, generator power surge, power grid defects, power distribution imbalance etc[5]. With the wide

spread use of switched mode power supplies, color television sets today have eliminated the need for a voltage stabilizer. But it is preferable to employ one even for them, to safeguard against momentary voltages over 250V and 120V on the mains.

2. SERVO SYSTEM VOLTAGE STABILIZER

In this journal, automatic voltage stabilizer consists of regulating unit and measuring unit. Fig 1 shown below are the block diagram and circuit diagram of the voltage stabilizer connected to an appliance or load. The stabilizers sizes generally with its rating, which is given in kVA.

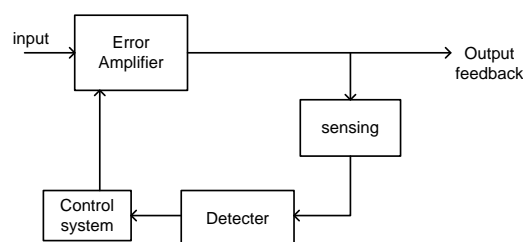


Figure 1. Block diagram of servo controlled voltage stabilizer

The regulating unit consists of toroidal type variable autotransformer. The purpose of the regulating unit is that of acting under the signal from the measuring unit in such a manner as to correct the output voltage of the stabilizer, as near as possible, a constant or predetermined value. Measuring unit includes control circuit. The function of the measuring unit is that of detection a change in the input or output voltage of automatic voltage stabilizer and producing a signal to operate the regulating unit.

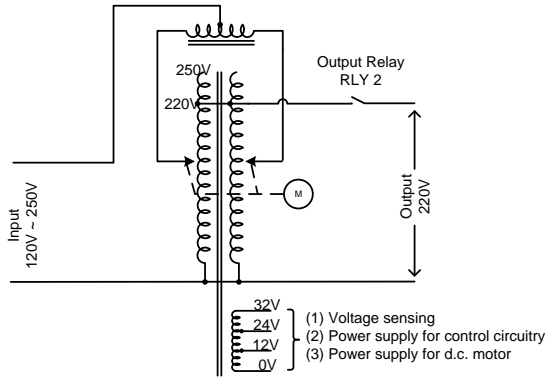


Figure 2. Schematic diagram of automatic voltage stabilizer

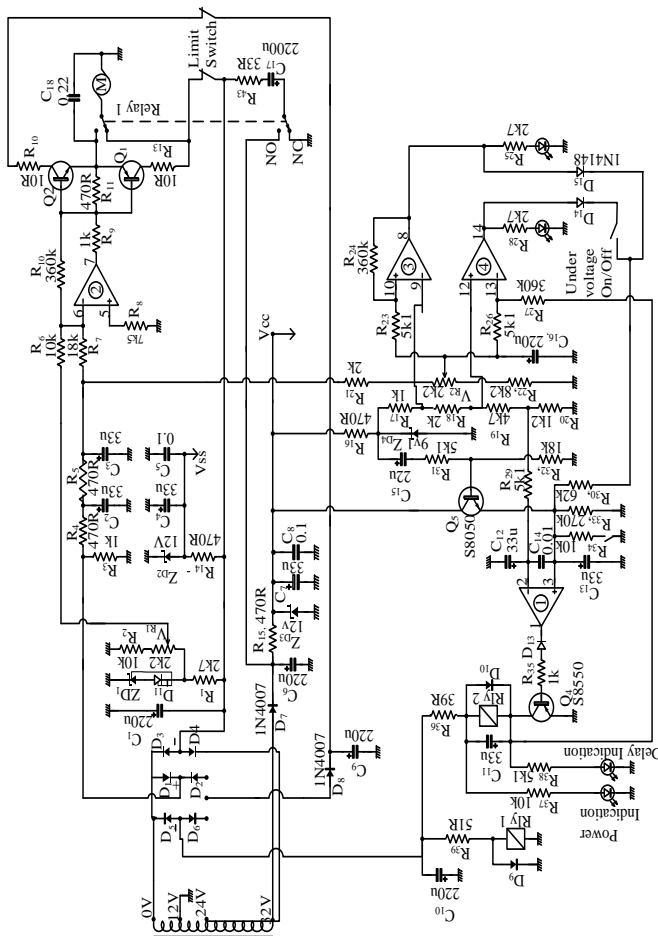


Figure 3 . Overall Circuit Diagram of AVS

Overall circuit diagram of control circuit for AVS is shown in fig:2. Transformer steps down the AC source voltage to 12V. Then, the transformer output is rectified by bridge rectifier. The rectifier output voltage is filtered by capacitor. In this circuit, LM324 is used as comparator and indicator. The non-inverting input ($-V_{in}$) the op-amp is greater than the inverting input ($-V_{in}$) the op-amp is ON-state. At normal condition, positive voltage sensing only. If V_{R1} is adjusted so that when output AC voltage is 220V, the op-amp output is zero. Op-amp (3) is used for over-voltage condition. It is connected as voltage comparator. When transistor Q_2 base receives forward bias and Q_2 goes ‘ON’ motor runs in the direction to raise voltage. When transistor Q_1 base is forward biased and Q_1

goes ‘ON’ motor runs in the other direction to lower voltage. After the preset time, op-amp output swings positive and release the relay. The control system is automatically shut down when the voltage fluctuation is lower than 120V and higher than 250V.

3. DESIGN CONSIDERATION

Power supply system is an essential part of each electronic system from simplest to the most complex. Input voltage supply is 220V AC supply. Automatic voltage stabilizer control system is based on mainly control circuit.

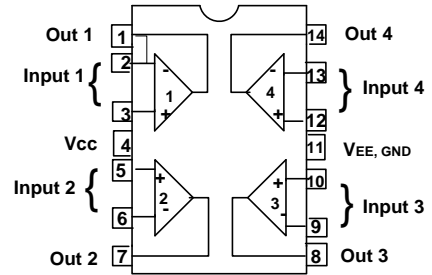


Figure 4. Diagram of Pin Function of LM324

In figure 3 , LM324 is a 14 pin IC consisting of four independent operational amplifiers (op-amp) compensated in a single package. Op-amp are high gain electronic voltage amplifier with differential input and usually, a single-ended output. The output voltage is many times higher than the voltage difference between input terminals of an op-amp.

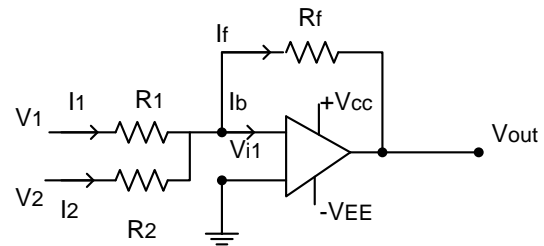


Figure 5. Summing amplifier of op-amp

Applying Kirchoff’s Current Law (KCL),

$$I_1 + I_2 = I_f + I_b$$

$$I_1 + I_2 \approx I_f$$

$$\frac{V_1 - V_2}{R_1} + \frac{V_2 - V_{i1}}{R_2} = \frac{V_{i1} - V_0}{R_f}$$

$$\text{The open loop gain, } A = \frac{V_0}{V_{id}} = \frac{V_0}{V_{i2} - V_{i1}}$$

$$\therefore V_0 = -R_f \left[\frac{V_1}{R_1} + \frac{V_2}{R_2} \right]$$

4. RESULTS AND DISCUSSION

In this section the results obtained from the design calculation of stabilizer controller. There are three conditions by the unstable input supply.

4.1 Normal Condition

The parameter of Op-amp 2,

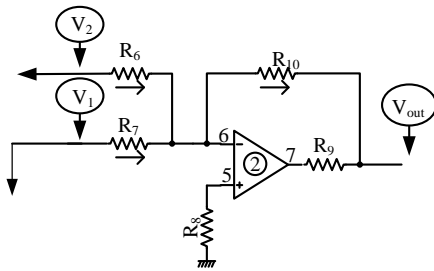


Figure 6. Circuit Diagram of Op-amp 2 of LM324N

Op-amp (2) is connected as a summing amplifier.

Applying KCL,

At pin 6 and virtual ground concept.

$$\frac{V_{out}}{R_{10}} = - \left(\frac{V_1}{R_7} + \frac{V_2}{R_6} \right)$$

V_1 is positive and represents the sample of output a.c voltage.

V_2 is fixed negative voltage: it acts as reference voltage.

Assume, $V_1=9.87V$, $V_2=-5.48V$

Apply the KCL,

$$\frac{V_1}{R_7} + \frac{V_2}{R_6} = 0 \quad (Q \text{ In normal condition, } V_{out} = 0)$$

$$5.48R_7 = 9.87R_6$$

If $R_6=10k\Omega$, $R_7=18k\Omega$

\therefore The standard of $R_6=10k\Omega$ and $R_7=18k\Omega$

$$\text{And then, } I_6 = \frac{V_2}{R_6} = - \frac{5.42}{10k} = -0.55 \text{ mA}$$

$$I_7 = \frac{V_1}{R_7} = \frac{9.87}{18k} = 0.55 \text{ mA}$$

If AC output voltage is 1% change,

$$V_1 = 0.99 \times 9.87 = 9.77V$$

$$\frac{V_{out}}{R_{10}} = - \left(\frac{V_1}{R_7} + \frac{V_2}{R_6} \right)$$

$$V_{out} = \left(- \frac{9.77}{18k} + \frac{5.48}{10k} \right) R_{10}$$

$$V_{out} = 5.22 \times 10^{-6} R_{10}$$

Assume motor pick-up voltage =2V

$$R_{10} = 382k\Omega$$

\therefore The standard value of $R_{10}=382k\Omega$

In this research, $R_8=7.5k\Omega$ and $R_9=1k\Omega$ are chosen.

When V_1 falls below normal, inverting input becomes negative and op-amp output swings positive and drives the motor in the direction to increase output voltage. If V_1 increase above normal, the process is reverse order.

time delay is calculated by the equation, $V_c = V.e^{-\frac{t}{\tau}}$

$$R=9.642k\Omega, C=33\mu F, V=12V, V_c=1.23V$$

$$-\frac{t}{\tau} = \ln\left(\frac{1.23}{13}\right)$$

$$\therefore t = 0.7\text{sec}$$

4.2 Over-Voltage Condition

The parameter of Op-amp 3,

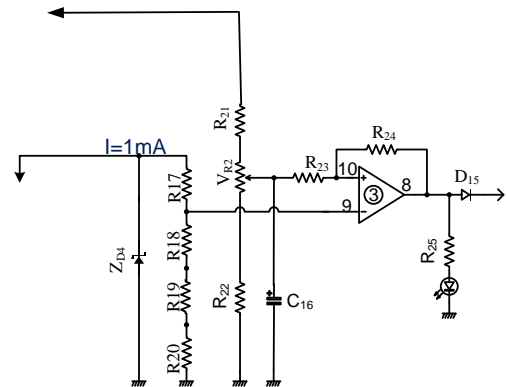


Figure 7. Circuit Diagram of Op-amp 3 of LM324N

From normal condition, node voltage $V=9.87V$

Assume, the non-inverting input (pin 9) = 8.08V (fixed voltage)

Assume, $I=0.8\text{mA}$

Non-inverting input (pin 10) is fed from voltage sensing supply through voltage divider R_{21} , VR_2 , R_{22}

Apply by KVL,

$$IR_{21} + IV_{R2} + IR_{22} = 9.87V$$

$$R_{21} + V_{R2} + R_{22} = 12.34k\Omega$$

By Ohm's Law,

$$V = IR$$

$$R_{21} = \frac{9.87 - 8.3}{0.8\text{m}} = 1.96k\Omega$$

$$V_{R2} = \frac{8.3 - 6.5}{0.8\text{m}} = 2.2k\Omega$$

$$R_{21} + V_{R2} + R_{22} = 12.34k\Omega$$

$$R_{22} = 8.2\Omega$$

\therefore The standard value of $R_{21}=2k\Omega$, $V_{R2}=2.2k\Omega$ and

$$R_{22}=8.2k\Omega$$

V_{R2} is adjusted so that at normal condition there is about +7.35 at pin 10.

At normal condition, op-amp output is negative because $8.08 > 7.35V$

When output voltage increase to 242V,

$$\text{Pin 10 voltage} = 8.085V$$

Since $8.085V > 8.08V$, op-amp output goes positive and drives the relay.

Assume $I=1\text{mA}$ through voltage divider R_{17} , R_{18} , R_{19} , R_{20} .

$$R_{17} = 1.02 \text{ k}\Omega$$

Apply by KVL,

$$IR_{18} + IR_{19} + IR_{20} = 8.08V$$

$$R_{18} + R_{19} + R_{20} = \frac{8.08}{1\text{m}} = 8.08 \text{ k}\Omega$$

$$R_{18} = \frac{8.3 - 6.5}{1\text{m}} = 1.8 \text{ k}\Omega$$

By Ohm's Law,

$$R_{20} = \frac{1.23}{1\text{m}} = 1.2\text{ k}\Omega$$

$$R_{18} + R_{19} + R_{20} = 8.08\text{ k}\Omega$$

$$R_{19} = 5.08\text{ k}\Omega$$

∴ The standard value of $R_{17}=1\text{ k}\Omega$, $R_{18}=2\text{ k}\Omega$, $R_{19}=4.7\text{ k}\Omega$ and $R_{20}=1.2\text{ k}\Omega$.

In this circuit, $R_{23}=5.1\text{ k}\Omega$, and $R_{24}=360\text{ k}\Omega$ is used for prevent short circuit.

Assume, $I=5\text{ mA}$ for LED lamp

$$R_{25} = \frac{12}{5\text{m}} = 2.4\text{ k}\Omega$$

∴ The standard value of $R_{25}= 2.7\text{ k}\Omega$

4.3 Under-Voltage Condition

The parameter of Op-amp 4,

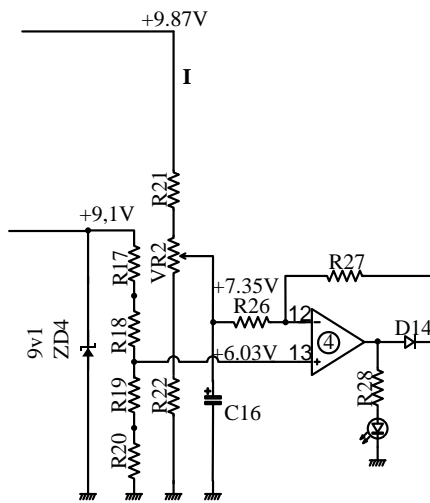


Figure 8. Circuit Diagram of Op-amp 4 of LM324N

Under-voltage condition circuit is almost same as over-voltage condition except that op-amp inputs are interchanged.

Reference voltage at non-inverting input is 6.03V

Assume, fixed voltage $V=6.03\text{ V}$ and $I=1\text{ mA}$

$$R_{17} = \frac{9.1-8.08}{1\text{m}} = 1.02\text{ k}\Omega$$

$$R_{17} + R_{18} = 3.07\text{ k}\Omega$$

$$R_{18} = 2.07\text{ k}\Omega$$

Apply by KVL,

$$IR_{18} + IR_{19} + IR_{20} = 8.08\text{ V}$$

$$R_{18} + R_{19} + R_{20} = 8.08\text{ k}\Omega$$

$$R_{19} + R_{20} = 6.03\text{ k}\Omega$$

Assume time delay voltage = 1.23V

By Ohm's Law,

$$V = IR$$

$$R_{20} = \frac{1.23}{1\text{m}} = 1.23\text{ k}\Omega$$

$$\therefore R_{18} + R_{19} + R_{20} = 8.08\text{ k}\Omega$$

$$R_{19} = 4.78\text{ k}\Omega$$

∴ The standard value of $R_{17}=1\text{ k}\Omega$, $R_{18}=2\text{ k}\Omega$, $R_{19}=4.7\text{ k}\Omega$ and $R_{20} = 1.2\text{ k}\Omega$.

In this circuit, $R_{26}=5.1\text{ k}\Omega$ and $R_{27}=360\text{ k}\Omega$ is used for prevent short circuit.

Assume, $I=5\text{ mA}$ for LED lamp

$$R_{28} = \frac{12}{5\text{m}} = 2.4\text{ k}\Omega$$

∴ The standard value of $R_{25}=2.7\text{ k}\Omega$

If a.c output voltage falls below 180V, pin 13 voltage falls below +6.03 V and op-amp output goes positive.

When output voltage decreases to 180.4V,

$$\text{pin 12 voltage} = \frac{7.35}{220} \times 180.4 = 6.02\text{ V}$$

Since $6.02 < 6.03$, op-amp output goes positive and drives the relay.

A variable resistor V_{R2} is used so that the user can adjust the voltages settings at the desired position. In this case, over-voltage setting $\approx 240\text{ V}$ and under-voltage setting $\approx 180\text{ V}$.

time delay is calculated by the equation, $V_c = V_e \cdot e^{-\frac{t}{\tau}}$

$$R=9.642\text{ k}\Omega, C=33\mu\text{F}, V=12\text{ V}, V_c=1.23\text{ V}$$

$$-\frac{t}{\tau} = \ln\left(\frac{1.23}{13}\right)$$

$$\therefore t = 0.7\text{ sec}$$

Table 1. Summary of Detailed Data for Normal Condition

Condition	Symbol	Units	Design Values
Normal Voltage	R_6	$\text{k}\Omega$	10
	R_7	$\text{k}\Omega$	18
	R_8	$\text{k}\Omega$	7.5
	R_9	$\text{k}\Omega$	1
	R_{10}	$\text{k}\Omega$	382

Table 2. Summary of Detailed Data for Over-voltage Condition

Condition	Symbol	Units	Design Values
Over- Voltage	R_{17}	$\text{k}\Omega$	1
	R_{18}	$\text{k}\Omega$	2
	R_{19}	$\text{k}\Omega$	4.7
	R_{20}	$\text{k}\Omega$	1.2
	R_{21}	$\text{k}\Omega$	2
	R_{22}	$\text{k}\Omega$	8.2
	R_{23}	$\text{k}\Omega$	5.1
	R_{24}	$\text{k}\Omega$	360
	5. R_{25}	$\text{k}\Omega$	2.7
	V_{R2}	$\text{k}\Omega$	2.2

Table 3. Summary Design Detailed for Under-voltage Condition

Condition	Symbol	Units	Design Values
Under- Voltage	R ₁₇	kΩ	1
	R ₁₈	kΩ	2
	R ₁₉	kΩ	4.7
	R ₂₀	kΩ	1.2
	R ₂₅	kΩ	2.7
	R ₂₆	kΩ	5.1
	R ₂₇	kΩ	360
	R ₂₈	kΩ	2.7

If the supply voltage is lower than 120V and more than 250V, the supply of the motor will be cut out. After that the relay will cut out the supply. So, automatic voltage stabilizer will not produce the power supply without being 220 stable voltage. If the input voltage of the stabilizer is lower than output voltage, the sensing circuit is unbalanced that and the op-amp output is positive. The motor rotates clockwise direction as to increase the stabilizer output voltage to 220V. If the input voltage of the stabilizer is higher than output voltage, the sensing circuit is unbalanced that and the op-amp output is positive. The motor rotates anti-clockwise direction as to decrease the stabilizer output voltage to 220V.

6. CONCLUSION

1. In this circuit when the input voltage is lower than 220V, the relay starts energized and the motor rotates the clockwise direction.
2. The input voltage is higher than 220V, the motor rotates the anticlockwise direction.
3. The control circuit components are available in local market. So, the circuit component can be replaced easily when they are damaged. This automatic voltage stabilizer is very suitable and economical for all electrical equipments.
4. This automatic voltage stabilizer is very convenience and economic for domestics and industries. So, automatic voltage stabilizer having with these conditions will offer the stable output voltage or stable output voltage for all electrical equipments and will improve productivities and reduce downtime.

Considering all the above on design of control system. Automatic voltage control system works between the voltage range of 120V and 250V efficiently. The control circuit is to drive the motor and adjust the stable output voltage. The output voltage accuracy is $\pm 1\%$ and efficiency is above the 98 %.

7. ACKNOWLEDGMENTS

The author is deeply grateful to her dissertation superior and co-supervisor. The author also thanks to all teachers at Technological University (Thanlyin) and all who provided her with necessary assistance for this paper. The author wishes to express her guidance to all persons who helped directly or indirectly towards the successful completion of paper. Finally, the author wishes to express her special thanks to her parents for their support and encouragement to attain her destination without any trouble.

8. REFERENCES

- [1] G NAVEEN KUMAR. "DESIGN OF A LOW COST SERVO CONTROLLED VOLTAGE STABILIZER." International Journal of Research in Engineering & Technology (IMPACT: IJRET) Vol.4, Issue 3, Mar 2016, 43-46.
- [2] Servo controlled voltage stabilizer introduction, amjadeeseminars.blogspot, 1st December 2012.
- [3] P. Eswaran, "Design of fuzzy logic controller for customized servo voltage stabilizer", 2nd International Conference on Electronic and Communication Systems, 26-27 February 2015, pages 103-106.
- [4] Instruction manual for servo-controlled stabilizer, Servel Electronics Private Limited.
- [5] McGranaGhan M. F., Mueller D. R. and Samotyi m. J. (1993), "Voltage Sag in Industrial Systems," IEEE Transactions on Industry Applications, Vol.29, pp.397-403.
- [6] M. Htay and K. San Win, "Design and Construction of an Automatic Voltage Regulator for Diesel Engine Type Stand-alone Synchronous Generator," PP.652-658
- [7] Instruction manual for servo voltage stabilizer with isolation transformer, Suvik electronic PVT.LTD.
- [8] A text book of power electronic P.S. Bhimra.

Design of Single-Sided Linear Induction Motor Used in Elevator

Aye Mya Mhway
Department of Electrical Power
Engineering
Technological University
(Thanlyin),
Myanmar

Nan Win Aung
Department of Electrical Power
Engineering
Technological University
(Thanlyin),
Myanmar

May Nwe Yee Tun
Department of Electrical Power
Engineering
Technological University
(Thanlyin),
Myanmar

Abstract: Linear induction motor (LIM), is basically an advanced types of motor that is use to obtain rectilinear motion instead of rotational motion as in ordinary conventional three phase induction motors. The LIM has been used in many different applications starting from moving sliding door to high speed trains around the world, due to easy maintenance, high acceleration/deceleration and no need of transformation system from rotary to translational motion. There are different types of linear induction motors (LIMs), among them, single-sided linear induction motors (SLIMs) are widely used in transportation system. In this paper, the methodology for the design of a single-sided linear induction motor which will accelerate the secondary (Aluminum sheet) with a specified mass with the required acceleration to the target distance are suggested and described. The SLIM design and performance equations and design procedure are developed and its predicted by using equivalent circuit model. Longitudinal end effect and other effects account (transverse edge, saturation ,etc.) are ignored in this study.

Keywords: Single-Sided Linear Induction Motor (SLIM),Equivalent Circuit Model, Linear Machine Design

1. INTRODUCTION

Linear induction motors (LIMs), are counterparts of rotary induction motors. LIM operates on the same principle as the conventional rotary induction motor. They may be obtained by “cutting” and “unrolling” the rotary induction machines to yield flat, single-sided topologies, where the cage secondary may be used as such or replaced by an Aluminium sheet placed between two primaries to make the double-sided LIM. Linear motor potentially have unlimited applications. Linear induction motors (LIMs) alone have found application in the following general areas: conveyor systems, material handling and storage, people mover (Elevators), liquid metal pumping, machine tool operation, operation of sliding doors and low and high speed trains. The single-sided linear induction motor (SLIM) is by far the most widely used in linear induction motor. In this paper, single-sided linear induction motor (SLIM) with short primary has been studied for the vertical conveying application because its main characteristic is the linear motion, which takes place without transformation mechanisms, increasing efficiency and the reliability of the system and also eliminating the need for large machine room on the roof. The SLIM has the following advantages comparing with the rotary induction motor (RIM): simple construction, direct electromagnetic thrust propulsion, safety and reliability, precise linear positioning, separate cooling, all electro-mechanical controlled systems used for an induction motors can be adopted for a SLIM without any bigger changes, economical and cheap maintenance.

2. STRUCTURE OF THE SINGLE-SIDED LINEAR INDUCTION MOTOR

The structure diagram of a single-sided linear induction motor (SLIM) is shown in figure 1. The primary or stator of a SLIM consists of a rectangular slotted structure formed by a stack of steel laminations. Within the slots of the primary stack are laid the polyphase windings to produce the linearly traveling magnetic field, just like the rotating magnetic field in a rotary induction motor, produced by the polyphase stator windings. The secondary, similar with the rotary induction motor (RIM) rotor, often consists of a sheet conductor, such as copper or aluminum, with or without a solid back iron plates, completes the magnetic circuit and creates the magnetic flux linkage across the air gap. This in turn induces a voltage on the conductive wall, which generates an eddy current in the conducting outer layer of the secondary. The interaction between the eddy current and the changing electromagnetic thrust on the plate in the longitudinal direction of the motor.

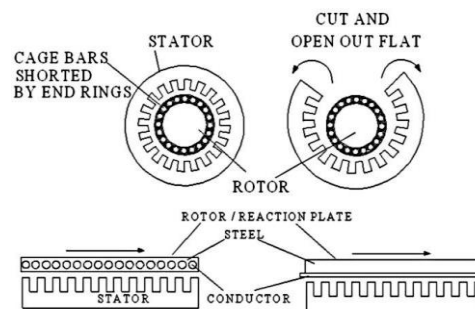


Figure 1. Structure of the single-sided linear induction motor (SLIM)

3. DESIGN PROCEDURE OF SINGLE-SIDED LINEAR INDUCTION MOTOR

The specifications of SLIM
 Targe thrust, F_s : 16000 N
 Rated velocity, v_r : 10 m/s
 Rated Slip, s : 10%
 Rated line voltage, V_1 : 400 V
 Number of phase, m : 3phase
 Number of poles, p : 4poles
 Frequency, f : 50 Hz
 Types of winding: Single Layer Winding

And, this machine is supposed to be applied in the elevator, achieving vertical transportation with ascending/rising speed v_r and acceleration a up to 10m/s and 2m/s² upwards, respectively. Therefore, the size of the cabin, total weight of cabin and necessary mechanical connection to it, and maximum allowable passenger and the average weight of each passenger are needed to know. All the necessary information are mentioned below

Size of cabin, (height \times length \times width)_{cabin} = 2.5 \times 2 \times 1m³
 Total weight of cabin and bearing, m_{cabin} : 500kg
 Number of passenger in one cabin, n_p : 5
 Average weight of each passenger, $m_{passenger}$: 75kg

3.1 Design of Primary (Stator)

Stator unit is designed according to the following procedure. First, assign the constant values

Permeability of free space, $\mu_0 = 4\pi \times 10^{-7}$ H/m
 Volume resistivity of Copper, $\rho_w = 19.27 \times 10^{-9}$ Ω m
 Volume resistivity of Aluminum $\rho_r = 28.85 \times 10^{-9}$ Ω m
 Stator current density, $J_1 = 6$ A/mm²
 Maximum tooth flux density, $B_{tmax} = 1.6$ Tesla
 Maximum yoke flux density, $B_{ymax} = 1.3$ Tesla
 Coil span in electrical radians, $\theta_p = \pi$
 Number of slot per pole per phase, $q_1 = 1$
 Aluminum thickness, $d = 3$ mm
 Width of stator, $W_{st} = 1000$ mm
 Mechanical air gap, $g_m = 5$ mm

Continuously, to obtain the target thrust in a Single-Sided Linear Induction Motor, the following equations are used.

$$\text{Synchronous velocity, } v_s = \frac{v_r}{1-s} \quad (1)$$

$$\text{Pole pitch, } \tau = \frac{v_s}{2f} \quad (2)$$

$$\text{Slot pitch, } \lambda = \frac{\tau}{mq_1} \quad (3)$$

$$\text{Length of primary (Stator), } L_s = \tau p \quad (4)$$

$$\tau = 3W_s + 3W_t \quad (5)$$

In this design, the number of slot is 12 and single-layer winding

$$W_t = 1.5W_s \quad (6)$$

And then, get the value tooth width and slot width shown in figure 2.

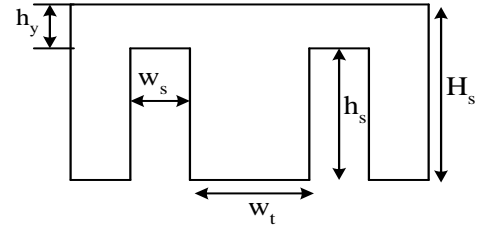


Figure. 2 Dimension of Stator Slot

$$\text{Number of turn per phase, } N_1 = N_c p q_1 \quad (7)$$

Where N_1 is the number of turn per phase and set the number of turn per slot N_c to one and increment it by one until the target thrust is obtained.

Now, let assume the product of $\eta \cos \phi$ between 0 and 1 arbitrary.

And find, the value of stator current,

$$I_1' = \frac{F_s' v_r}{3V_{ph} \eta \cos \phi} \quad (8)$$

$$\text{Area of copper wire, } A_w' = \frac{I_1'}{J_1} \quad (9)$$

Total cross-sectional area of copper wire,

$$A_{wt} = N_c A_w' \quad (10)$$

$$\text{Cross-sectional area of slot, } A_s = \frac{10}{7} N_c A_w' \quad (11)$$

$$\text{Stator slot height, } h_s = \frac{A_s}{W_s} \quad (12)$$

$$\text{Length of end connection, } L_{ce} = \frac{\theta_p}{180} \tau \quad (13)$$

$$\text{Effective stator width, } W_{est} = W_{st} + L_{ce} \quad (14)$$

Mean length of one turn of the stator winding per phase,

$$L_{w1} = 2W_{est} \quad (15)$$

$$\text{Length of copper wire per phase, } L_w = N_1 L_{w1} \quad (16)$$

$$\text{Total length of copper wire, } T_{Lw} = m L_w \quad (17)$$

After assuming the value of Aluminum thickness of conducting layer, d , the magnetic air gap, g_0 is calculated

$$g_0 = g_m + d \quad (18)$$

And also find the equivalent stator width,

$$W_{seq} = W_{st} + g_0 \quad (19)$$

Gamma for calculating carter's coefficient,

$$\gamma = \frac{4}{\pi} \left[\frac{W_s}{2g_0} \arctan \left(\frac{W_s}{2g_0} \right) - \ln \sqrt{1 + \left(\frac{W_s}{2g_0} \right)^2} \right] \quad (20)$$

$$\text{Carter's coefficient, } k_c = \frac{\lambda}{\lambda - \gamma g_0} \quad (21)$$

$$\text{Effective air gap, } g_e = k_c g_0 \quad (22)$$

$$\text{The goodness factor, } G = \frac{2\mu_0 f \tau^2}{\pi \frac{\rho_r}{d} g_e} \quad (23)$$

$$\text{Pitch factor, } k_p = \sin \frac{\theta_p}{2} \quad (24)$$

$$\text{Slot angle, } \alpha = \frac{\pi}{mq_1} \quad (25)$$

$$\text{Distribution factor, } k_d = \frac{\sin q_1 \frac{\alpha}{2}}{q_1 \sin \frac{\alpha}{2}} \quad (26)$$

$$\text{Winding factor, } k_w = k_p \times k_d \quad (27)$$

3.2 Equivalent Circuit Model

The equivalent parameters of SLIM can be determined using the per-phase equivalent circuit as shown in figure 3.

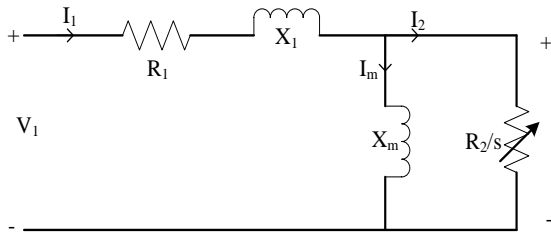


Figure. 3 Equivalent Circuit of Linear Induction Motor

$$\text{Per-phase stator resistance, } R_1 = \frac{\rho_w L_w}{A_{wt}} \quad (28)$$

Per-phase slot leakage reactance,

$$X_1 = \frac{2\mu_0 \pi f \left\{ \left[\lambda_s \left(1 + \frac{3}{p} \right) + \lambda_d \right] \frac{W_{st}}{q_1} + \lambda_e L_{cc} \right\} N_1^2}{p} \quad (29)$$

Slot, differential and end connection permeance are

$$\lambda_s = \frac{h_s (1 + 3k_p)}{12W_s}$$

$$\lambda_d = \frac{5 \left(\frac{g_e}{W_s} \right)}{5 + 4 \left(\frac{g_e}{W_s} \right)} \quad (30)$$

$$\lambda_e = 0.3(3k_p - 1)$$

Magnetizing reactance per phase,

$$X_m = \frac{24\mu_0 \pi f W_{seq} k_w N_1^2 \tau}{\pi^2 p g_e} \quad (31)$$

$$\text{Per-phase rotor resistance, } R_2 = \frac{X_m}{G} \quad (32)$$

Using the equivalent circuit parameters from the above equations (28), (29), (31) and (32), and the circuit diagram

shown in figure 3, the rated value of impedance can be calculated by

$$Z = R_1 + jX_1 + \frac{j \left(\frac{R_2}{s} X_m \right)}{\frac{R_2}{s} + jX_m} \quad (33)$$

$$\text{Power factor the design motor, } \cos \phi = \frac{\text{Re}(Z)}{|Z|} \quad (34)$$

$$\text{The rated primary RMS phase current, } I_1 = \frac{V_1}{|Z|} \quad (35)$$

Then magnitude of magnetizing current,

$$I_m = \frac{\frac{R_2}{s}}{\sqrt{\left(\frac{R_2}{s} \right)^2 + X_m^2}} \times I_1 \quad (36)$$

Also the magnitude of secondary phase current I_2 can be calculated from

$$I_2 = \frac{X_m}{\sqrt{\left(\frac{R_2}{s} \right)^2 + X_m^2}} \times I_1 \quad (37)$$

$$\text{The SLIM input active power, } P_i = mV_1 I_1 \cos \phi \quad (38)$$

$$\text{The output power, } P_0 = P_i - mI_1^2 R_1 - mI_2^2 R_2 \quad (39)$$

And then efficiency is calculated by following equation

$$\eta = \frac{P_0}{P_i} \times 100\% \quad (40)$$

The electromagnetic force F_s produced by a machine is given by

$$F_s = \frac{P_0}{v_r} \quad (41)$$

3.3 Required Force Calculation

Resulting magnetomotive force (MMF),

$$\theta_m = \frac{4\sqrt{2}mk_w N_1 I_m}{\pi p} \quad (42)$$

By mean of MMF, the peak value of the normal component of the magnetic flux density is given by

$$B_{gmax} = \frac{\mu_0 \theta_m}{2g_0} \quad (43)$$

Theoretically, the flux in the air gap is sinusoidal because of the sinusoidal voltage source. Thus, the average flux density

B_{gavg} can be gained, based on the relation with the peak value of that, i.e

$$B_{gavg} = \frac{2}{\pi} B_{gmax} \quad (44)$$

The yoke of the primary core refer to the section at the top of the core showed in figure 2.

$$h_y = \frac{B_{gavg} \tau}{2B_{gmax}} \quad (45)$$

Making use of L_s , W_{st} and h_y , the volume of the yoke is

$$V_{yoke} = L_s W_{st} h_y \quad (46)$$

In addition, the volume of one tooth of the primary core is

$$V_{tooth} = W_{st} W_t h_s \quad (47)$$

Since the teeth have uniform size, the volume of the total teeth is derived as

$$V_{teeth} = (mpq_1) V_{tooth} \quad (48)$$

Where mpq_1 is the number of slot in a primary core. So, the volume of the iron core of the primary V_{iron} is

$$V_{iron} = V_{yoke} + V_{teeth} \quad (49)$$

The weight of the entire iron core, $W_{iron} = \rho_i V_{iron}$ (50)

The weight of copper wire, $W_c = \rho_c A_w T_{1w}$ (51)

The weight of one primary unit W_{stator} , consisting of iron core and copper wire, is easily obtained as

$$W_{stator} = W_{iron} + W_c \quad (52)$$

Number of primary unit, $n_{stator} = \frac{h_{cabin}}{1.2L_s}$ (53)

And then, the **total output thrust** can be calculated as

$$F_t = n_{stator} F_s \quad (54)$$

Now checking the require force by **Newton's Second Law**,

The mass of the whole rising system,

$$m_t = n_p m_{passenger} + n_{stator} W_{stator} + m_{cabin} \quad (55)$$

The moving resistance of the system D , consists of two components in this specific case, which are

Rolling resistance, $D_r = m_t (c_1 + c_2 v_r)$ (56)

Where c_1 and c_2 are coefficient of correlation, normally defined as 0.01-0.02 N/kg and 0.00015-0.0003 N/kg.

and aerodynamic resistance, $D_a = \frac{1}{2} \rho v_r^2 A$ (57)

Where ρ is the air density 1.205kg/m^3 and A is the top or bottom area of cabin 2m^2 .

Total moving resistance is given by

$$D = D_r + D_a \quad (58)$$

Now, making use of Newton's Second Law of Motion, the force required to be produced by the propulsion system

$$F'_s = m_t (a+g) + D \quad (59)$$

Where g is acceleration of gravity, 9.8m/s^2 .

Finally, $F_t \geq F'_s$ becomes a greatly important criterion to decide whether this machine design is satisfied or not.

3.4 Design of Secondary

The single-sided linear induction motor secondary (rotor) design contains conduction layer design and reaction plate design, it is illustrated in figure 4.

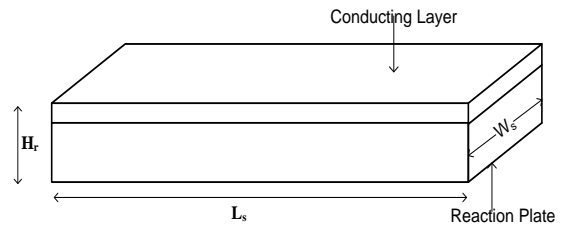


Figure.4 Dimension of Secondary (Rotor)

The secondary reaction plate design which can consist of either solid or laminated design. To improve performance, the reaction plate is coated with conduction sheet of either aluminium or copper. For standard operating, the reaction plate should not be any less than 6mm thick and the attached conducting sheet should not be any less than 3mm thick. The best thrust per size ratio is obtained.

$$W_{se} = W_{st} + \frac{2\tau}{\pi} \quad (60)$$

Where W_{se} is width of secondary and W_{st} is width of primary.

4. RESULT AND DISCUSSION

According to the design procedure in section 3, design calculation result of single-sided linear induction motor are mentioned with the following tables.

Table 1. Design of Primary

	Parameters	Symbol	Values	Unit
Stator winding design	Copper wire size	-	1	SWG
	Diameter of wire	-	7.62	mm
Stator core design	Length of stator	L_s	450	mm
	Width of stator	W_{st}	1000	mm
	Slot width	W_s	14.7	mm
	Tooth width	W_t	22	mm
	Slot height	h_s	32.73	mm
	Yoke height	h_y	12.51	mm

Table 2. Design of Secondary

Parameters	Symbol	Values	Unit
Length of secondary	L_{se}		
Width of secondary	W_{se}	1100	mm
Thick of conducting layer	d	3	mm
Thick of reaction plate		6	mm

The length of the secondary will be as long as the motion length. So, the length of secondary is not illustrated in table 2. The design data sheet of electrical parameters of SLIM is presented in table 3. In the electrical parameters design, neglect the core losses.

Table 3. Design Output of Electrical Parameters

Parameters	Symbol	Values	Unit
Per-phase stator resistance	R_1	0.00356	Ω
Per-phase stator slot leakage reactance	X_1	0.1371	Ω
Per-phase magnetizing reactance	X_m	1.1795	Ω
Per-phase rotor resistance	R_2	0.2055	Ω
Supply current	I_1	201.605	A
Input active power	P_i	62.854	KW
Output power	P_o	56.211	KW
Efficiency	η	0.89	%
Power factor	$\cos\phi$	0.45	-

This motor is designed to move the total mass of 1643.5kg. It is needed 19.54KN output thrust with the rated velocity 10m/s. The outputs for the design motor are tabulated below table 4.

Table 4. Design Output of SLIM

Parameters	Symbol	Values	Unit
Total output thrust	F_t	22.5	KN
Velocity	v_r	10	m/s

5. CONCLUSION

In this paper, the main features of a single-sided linear induction motor with short primary designed for vertical transportation application are described. The design procedure was first done analytically considering the parameters required like velocity, output thrust, efficiency, size of elevator cabin, etc. The motor design was thus carried out systematically and desired characteristics and performance was obtained. In this study, the study of elevator system was not performed because the goal of this study was the designing the model for a single-sided linear induction motor based on the elevator system. The single-sided linear induction motor was chosen only as an application case study to show how the technology can be used and optimized. Finally, it can be concluded a single-sided linear induction motor with short primary is a suitable electric motor to fulfill all the demands of modern elevator system.

6. ACKNOWLEDGMENTS

The author is deeply grateful to Dr. Nan Win Aung, my dissertation supervisor and Daw May Nwe Ye Tun, my co-supervisor. The author also thanks to all teachers at Technological University (Thanlyin) and all who provided her with necessary assistance for this paper. The author wishes to express her guidance to all persons who helped directly or indirectly towards the successful completion of paper. Finally, the author wishes to express her special thanks to her parents

for their support and encouragement to attain her destination without any trouble.

7. REFERENCES

- [1] Hoang, Viet Nam: "Design of A Single-Sided Linear Induction Motor", University of Queensland, (2003).
- [2] IN. ., Degree Project Electrical Power Engineering 120 Credits. Second Cycle. ., Stockholm Sweden 2015. "Linear Induction Motor Investigation and Design for Articulated Funiculator". YIFEI HU
- [3] Sarveswara Prasad Bhamidi: "Design of a Single-Sided Linear Induction Motor (SLIM) Using a User Interactive Computer Program", M.sc. Thesis, University of Missouri- Columbia, May (2005).
- [4] Boldea, I., and Syed N. A: "The Induction Machine Handbook", Electric Power Engineering Series, (2002)
- [5] Yamamura: "Theory of Linear Induction Motors", 2nd Edition, John Wiley & Sons, Inc. New York, (1979).
- [6] <http://www.electricalpowerenergy.com/Linear-induction-motor/>
- [7] <https://en.m.wikipedia.org/wiki/Linear-induction-motor>
- [8] Nahid Ahmadi. "The linear Induction Motor(LIM) & Single Linear Induction Motor (SLIM)". American Journal of Electrical Power and Energy Systems. Vol. 3, NO. 4, 2014.
- [9] "Design & Performance Analysis of Single Sided Linear Induction Motor", K.S.Lingamurthy, P.Mallikarjuna Rao, T.Sandhya, K.Sri chandan/International Journal of Engineering Reserch and Applications(IJERA), www.ijera.com
- [10] Nasar, S.A. and Boldea, I.: "Linear Electric Motors", Prentice-Hall, Inc., Englewood Cliffs, New Jersey, (1987).
- [11] Kaye, R.J and Prof. Eisuke Masada: "Comparison of Linear Synchronous and Induction Motors," Sandia National Laboratories, Science University of Tokyo, Japan, June (2004).

Optimization and Modeling of Electrical Discharge Machining Using Response Surface Methodology Part-I

Rania Ahmad Elrifai
Benghazi University, Industrial and Manufacturing System Engineering
Benghazi, Libya

Abstract: To improve and optimize the response of Electrical Discharge Machining process, the various input machining control parameters are to be set at an optimal value. As FW4 is a newly developed hot die material widely used in Forging Dies manufacturing. The optimal selection of the machining conditions is one of the most important aspects to be taken into consideration in the Electrical Discharge Machining (EDM) of FW4. In this paper, an attempt has been to develop and optimize mathematical model of relating Material Removal Rate (MRR) and the machining parameters (current, pulse -on time, voltage). Experiments are designed and the correlating the desired response and the control parameters are established using Response Surface Methodology (RSM), finally (RSM) is applied to search the optimal parametric values for the optimal response. Using RSM, maximum Material Removal Rate obtained is 30.5541mm³/min which is 0.3641 less in magnitude than experimentally measured value, Thus, the result proves RSM to be optimization technique which can be used to optimize Electrical Discharge Machining Processes.

key words: Electrical Discharge Machining (EDM); Response Surface Methodology (RSM); ANOVA; Material Removal Rate.

1. INTRODUCTION

EDM is a common technique used in industry for high-precision machining of all types of conductive materials such as: metals, metallic alloys, graphite, some ceramic materials, and any hardness[2]. FW4 is a welded steel, that is the most important and applicable welded material on the basis of chromium . Using welded material increases the lifetime of forging moulds more than 150% and periodical replacement time of moulds up 200% as compared to moulds made of ordinary steel tool . Also it causes a decrease in materials and mould`s expenses to 62% the hardness of the weld metal will be controlled in the scale of 30-50 HRC, the weld metal will be resistant in hot strength, high temperature , wear and thermal fatigue crack [1]. At present , EDM is a widespread technique used in industry for high-precision machining of all types of conductive materials such as : metals, metallic alloys ,graphite ,or even some ceramic materials,of any hardness[2]. EDM is nontraditional machining process based on removing material from part by means of successive electrical discharges occurring between an electrode and a work piece immersed in a dielectric fluid[2]. The photographic view of the Schematic diagram of machine and machining has been shown in figure.1 (a) and (b) respectively. The other details of the experimentation and design of experiment have been shown in Table 1.

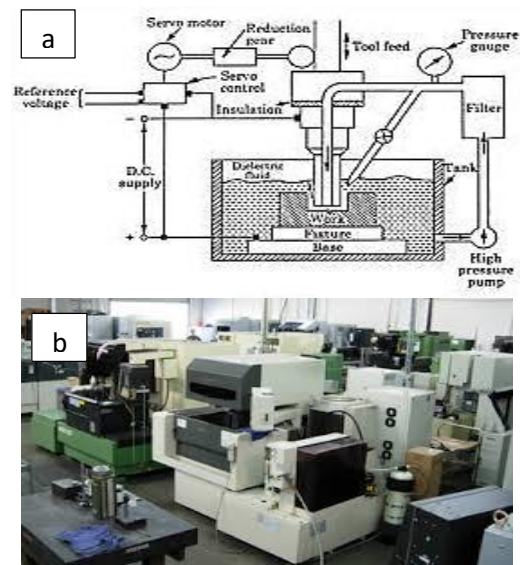


Figure 1: (a) Schematic diagram of Electrical Discharge Machining process; (b) Machining

Optimization of machining process first requires a mathematical model to be established to correlate the desired response and the process control parameters. Thereafter an optimization technique is applied to find optimal setting of control parameters to drive the desired response, since EDM is complex machining process , in order to achieve the economic objective of this process , optimal conditions have to be determined and so mathematical models need to be established ; therefore, Statistical - Mathematical models are always used by scientists to describe the correlation between characteristics and machining output results, and setting of input parameters . Regression Analysis are the most

important and major modeling methods, employed in the EDM process modeling [4]. Regression analysis is regarded as powerful tool for representing the relation between input parameters and process response [5]. Mathematical model for electrical discharge machining of WC-Co, SiC and conductive ceramic on the basis of experiments designing techniques. They introduced the obtained - mathematical model, using regression analysis [5-8]. The effects of electrode tool material and electrical discharge machining were studied input parameters such as: current, pulse-on time, on AISI D3 EDM characteristic, by the use of variance analysis and experiments designing techniques [9]. They reported that the graphite electrode, having highest material removal rate and precise dimension and low tool wear ratio, is the most appropriate material for steel machining [9]. Estimated Regression Coefficients for MRR are been used data in uncoded units that they used for make relation between input parameters and EDM process such as peak current, pulse-on time and voltage and the process output has been modeled, using the techniques of Design Of Experiment (DOE) method, multi linear regression techniques and Response Surface Methodology (RSM) [10]. Also effect of input parameters on characteristic of machining FW4 steel has been analyzed. The result of this research, leads to desirable process output, finally optimization of input parameters and output of process.

2. MATERIALS AND METHODS

2.1 Material

The material used for work piece was FW4 welded tool steel. To prepare FW4 samples, first a sheet of common steel was used as a base, and the welding process was done using a forge weld semi-automatic MIG welding station. Welding process occurs by the systematic deposition of weld layers achieving a build-up of 3-5 mm per layer with "covered welding wires of FW4", in several pulses, separating welding dust from the basic sheet, raw block of FW4 steel are prepared. Raw blocks were cut to circular tables 20 mm height by wire EDM and then ground to parallel faces, EC-16 graphite tool electrode material has particle size from 3 to 5 micron. Graphite tools were cut from 20mm dia. Rod and machined by using a very accurate CNC lathe. Table 1 shows the samples and tools physical and mechanical properties [11].

Table 1: Workpiece and electrodes physical properties

Properties of FW4 (work piece)		Properties of EC-16 (Tool)	
Density	7.7623(1000kg/m ³)	Bulk density	1018(g/cm ²)
Melting Point	2670°C	Specific resistance	1650(μohm-cm)
Poisson Ratio	0.34	Flexural strength	750 (kg/cm ²)
Hardness	4505 HRC	Shore hardness	70
Elastic Modulus	210(Gpa)		
Thermal Conductivity	27.2(W/m.k)		

In this study, an attempt is made to establish the input-output relationship of Material Removal Rate (MMR) of the transportation processes parameters by pipeline. It is important to note that selection of the range of the operating parameters is an important consideration. There are a large number of factors to consider within the EDM process, put in this work peak current (I), pulse - on time (T_{on}) and voltage (v) have only been taken into account as design factors. The reason why these three factors have been selected as design factors is that they are the most widespread and used amongst EDM researchers.

Table 2: Factors and selected for the experiments

No	Factors	Units	Levels		
			-1	0	+1
1	Current	A	8	16	24
2	Pulse - on time	μs	12.8	25	50
3	Voltage	V	160	180	200

2.2. Method

The choice and the implementation of an experimental design type is an important decision. A single integrated package performs the ED and RSM in Minitab16 software. A response variable (Material Removal Rate (MMR)). The experimental design is implemented using RSM in two steps:

1. Full Factorial Design (FFD)
2. Central Composite Design (CCD)

In order to study the effect of EDM process parameters of FW4 material on the volumetric metal removal rate, second-order polynomial response can be fitting into the following equation (1):

$$Y = \beta_0 + \beta_1 X + \beta_2 \Phi + \beta_3 \Psi + \beta_{12} X\Phi + \beta_{13} X\Psi + \beta_{23} \Phi\Psi + \beta_{11} X^2 + \beta_{22} \Phi^2 + \beta_{33} \Psi^2 \quad (1)$$

Where Y is the response and X, Φ, ψ are the quantitative variables. β₁, β₂ and β₃ represent the linear effect of X, Φ and ψ respectively, β₁₁, β₂₂ and β₃₃ represent the quadratic effects of X, Φ and ψ, β₁₂, β₁₃ and β₂₃ represent linear - by- linear interaction between "X and Φ", "X and ψ", "Φ and ψ", respectively. These quadratic models work quite well over the entire factor space and the regression coefficients were computed according to least -square procedure. For the three variables the design required with eight star points (cube points), six axial points to form central composite design with five center points for replication to estimate the experimental error. The design was generated and analyzed using MINITAB16 statistical package. The levels of each factor were chosen as -1, 0, + 1 in coded form to have a central composite design as shown in Table 3.

Table 3: Randomized design table for three parameters (uncoded) and outputs

No	Current (A)	Pulse-on time(μs)	Voltage(v)	MRR(mm ³ /min)
1	16	12.8	180	12.5013
2	16	31.4	180	19.6183
3	8	12.8	200	7.4420
4	8	50	200	9.5043
5	16	31.4	180	19.6183
6	24	12.8	200	15.8079
7	16	31.4	180	19.6183
8	8	50	160	4.6120
9	24	50	200	30.9180
10	16	31.4	180	19.6183
11	16	12.8	160	12.1110
12	24	50	160	24.322
13	24	31.4	180	19.6183
14	16	31.4	180	19.6183
15	16	31.4	160	23.3422
16	24	31.4	180	22.4833
17	16	31.4	200	9.3188
18	8	50	180	20.2945
19	16	31.4	180	19.6183
20	16	12.8	160	3.7549

3. Mathematical modeling and statistical analysis by using response surface methodology

Table 4: shows the p-values that determine whether the effects are significant or insignificant.

Source	Df	Seq SS	Adjss	AdjMS	F	P
Regression	9	953.25	953.25	105.92	470.18	0.00
Linear	3	708.43	708.43	236.13	1048.3	0.00
Current	1	516.52	516.52	516.52	2292.9	0.00
Pulse	1	6144.6	6144.6	6144.6	642.16	0.00
Voltage	1	47.250	47.250	47.250	209.75	0.00
Square	3	167.91	167.91	55.971	248.46	0.00
Current*current	1	132.48	36.546	36.546	162.23	0.00
Pulse*pulse	1	32.258	35.207	35.207	156.29	0.00
Voltage*voltage	1	3.177	3.177	3.177	14.10	0.00
Interaction	3	76.904	76.904	25.635	113.80	0.00
Current*pulse	1	74.432	74.432	74.432	330.41	0.23
Current*voltage	1	0.367	0.367	0.367	9.35	0.01
Pulse*voltage	1	2.105	2.105	2.105	*	*
Residual Error	10	2.253	2.253	.225		
Lack- of-fit	5	2.253	2.253	0.451		
Pure Error	5	0.000	0.000	0.000	1048.3	
Total	19	955.49			2292.9	

Table 5: Estimated Regression Coefficients for MRRmm³/min)

Term	Coef
Constant	63.6345
Current	1.83650
Plus	0.277772
Voltage	-0.923390
current*current	-0.0569603
plus*plus	-0.0103424
voltage*voltage	0.00268710
current*plus	0.0204989
current*voltage	0.00133852
plus*voltage	0.00137907

After identifying the significant effects (main and two-way interactions) in the analysis of variance table, a look at the estimated effects and coefficients table. Table 3 shows that all the p-values associated with each individual model term are all significant and < 0.05. The p-values indicate that quadratic effect are significant. The p-values indicate that just one two-way interaction are significant. Equation(2) shows the model for predictions and calculating MRR:

$$MRR = 63.6345 + 1.8366 I + 0.2778 T_{on} - 0.9234V - 0.0570I^2 - 0.0103T_{on}^2 + 0.002710 V^2 + 0.0205 I * T_{on} + 0.0013 I * V \quad (2)$$

Where:

I = current,

T_{on} = pulse -on time and

V = voltage.

To check on the obtained results, probability plot is also used to identify the appropriate distribution. The Normal probability plot. Various fits, histograms and order distributions are shown in Figure3. It can be seen from the probability plots, that the normal distribution is the best one, since all data fall within the 95% confidence interval.

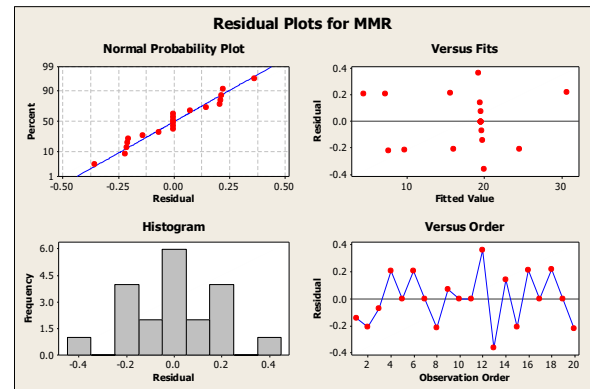


Figure 3: Probability plots for MRR(mm³/min)

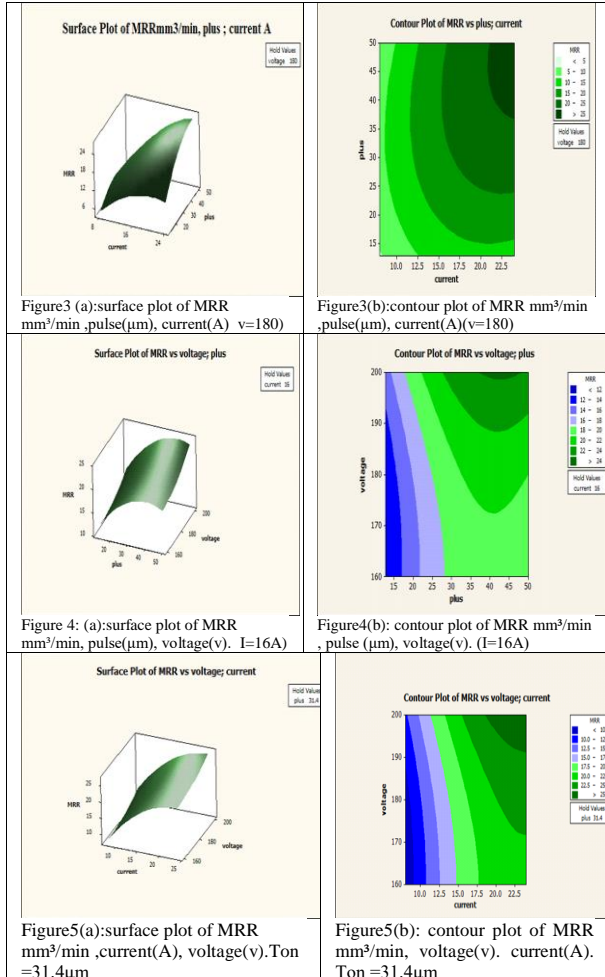
4. Results and discussion for the effects of process variables on Material Removal Rate (MRR), based on RSM.

Since the model have enough characteristics for changing data we can study the effect of input parameters on the machining characteristics by graphs on the basis of models and predict response change`s value on middle surface of input changes.

4.1 Effect the input parameters on MRR

Material Removal Rate in EDM process is an important factor because of its vital effect on the industrial economy. Figures3,4 and 5 show the response surface and contour of MRR versus current, pulse-on time and voltage. Increasing the current, pulse-on time and voltage values lead to an increase in the amount of Material Removal Rate. But the most influential factors are peak current and pulse-on time, also the MRR increase gradually with the voltage. In this process, the spark energy affects the material removal speed and energetic sparks increases the material removal rate Energy of each spark, according to its electrical concepts, is a function of spark current, pulse-on time and voltage.

The Figures 3(a) and 5(a) show that in all the currents, the MRR decreases after a particular T_{on} . The major reason for the decrease in MRR is high gap pollution and low energy density during pulse-on time. In the view point of industrial economy it is desirable to obtain higher values of MRR, should be identified (Figures3,4,5).



Figures 3,4,5: show surface and contour plots

5. Optimization Using RSM (Response Surfaces Methodology)

Many designed experiment involve determining optimal conditions that will produce the "best" value for the response. Depending on the design type (factorial, response surface, or mixture), the operating conditions that you can control may include one or more of the following design variables: factors, components, process variables, or amount variables.

For example, in product development, we may need to determine the input variable settings that result in a product with desirable properties (responses). Since each property is important in determining the quality of the product, you need to consider these properties simultaneously. For example, we may want to increase the yield and decrease the cost of a chemical production process.

Optimal settings of the design variables for one response may be far from optimal or even physically impossible

for another response. Response optimization is a method that allows for compromise among the various responses.

Minitab provides two commands to help we identify the combination of input variable settings that jointly optimize a set of responses. These commands can be used after we have created and analyzed factorial designs, response surface designs, and mixture designs.

Response Optimizer Provides we with an optimal solution for the input variable combinations and an optimization plot. The optimization plot is interactive; we can adjust input variable settings on the plot to search for more desirable solutions.

Overlaid contour shows how each response considered relates to two design variables (factorial and response surface designs) or three continuous design variables (mixture designs), while holding the other variables in the model at specified levels. The contour plot allows we to visualize an area of compromise among the various responses.

6. Optimization Of EDM Process Using RSM

The present research work optimize the desired response and control parameters using Minitab software Figure (6) shows the RSM output of the best measured response of maximum MRR as 30.5541 mm³/min. Response optimization by RSM has been obtained by two values the lower and the upper from the table of experiments were run , then the optimization parameters are current as 24A, pulse as 50 µs ,voltage 200v with desirability 98.65%.

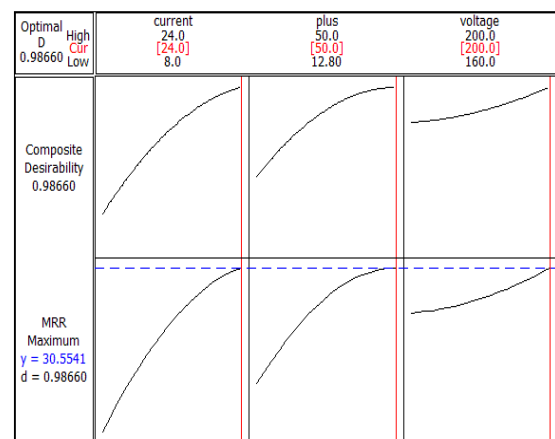


Figure 6: shows the optimal values of input parameters and the response (MMR)

7. Conclusion

In this paper, an experimental investigation was performed to consider the machining in EDM process of FW4 welded steel and the following results were concluded :

1. RSM provides a cost effective soft computing technique for optimizing machining operations.

2. Results show that the central composite design (CCD) is a powerful tool for providing experimental diagrams and statistical-mathematical models, to perform the experiments appropriately and economically.
3. In this paper, an attempt was made to consider the effect of voltage, pulse-on time, and current on material removal rate in EDM process . According to the ANOVA results, voltage, pulse-on time, and current are the not significant parameters on Material Removal Rate whereas interaction voltage and current are the most significant.
4. Based on the optimization results, it has been found that 200V as voltage, 50µs as pulse-on time, 24 A as current .
5. The optimization value of material removal rate found very close to the experimental value of experimental value at optimum level of input process parameters.
6. Based on the test results predicated using RSM ,this technique can be accommodated within an intelligent manufacturing system for automated process planning .

[10] George, P.M., Raghunath, B.K., Manocha, L.M., Warriar, A.M., 2007, EDM machining of carbon–carbon composite—a Taguchi approach, *J. Mater. Process. Technol.*, 153-154: 920–924.

[11] www.MVI.com

[12] Montgomery, D.C., 1997, *Design and Analysis of Experiments*, Wiley, NewYork. *World Academy of Science, Engineering and Technology Vol:28 2009-04-29.*

★ ★ ★ ★ ★ ★

REFEENCES

- [1] www.corewire.com
- [2] Fonda, P., Wang, Z., Yamazaki, K, Akutsu, Y., 2007, A fundamental study on Ti–6Al–4V’s thermal and electrical properties and their relation to EDM productivity, *J. Mater. Process. Technol.*,
- [3] Mukherjee, I., Ray, P.K., 2006, A review of optimization technique in metal cutting process, *Computer & Industrial Engineering*, 50: 15-34.
- [4] Hewidy, M.S., El-Taweel, T.A., El-Safty, M.F., 2005, Modelling the machining parameters of wire electrical discharge machining of Inconel 601 using RSM, *J. Mater. Process. Technol.*, 169: 328–336.
- [5] Puertas, I., Luis, C.J., Álvarez, A., 2004, Analysis of the influence of EDM parameters on surface quality, MRR and EW of WC–Co, *J. Mater. Process. Technol.*, 153–154: 1026–1032.
- [6] Puertas, I., Luis, C.J., 2004, A study on the electrical discharge machining of conductive ceramics, *J. Mater. Process. Technol.*, 153–154: 1033–1038.
- [7] Puertas, I., Luis, C.J., Villa, G., 2005, Spacing roughness parameters study on the EDM of silicon carbide, *J. Mater. Process. Technol.*, 164–65:1590–1596.
- [8] Luis, C.J., Puertas, I., 2007, Methodology for developing technological tables used in EDM processes of conductive ceramics, *J. Mater. Process. Technol.*, 189: 301–309.
- [9] Khoshkish, Ashtiani, Goreyshi, Effects of Tool electrode material on electrical discharging machining process of hardened tool AISI D3, *Iran Conference of Manufacturing Engineering.*

Performance Analysis of LTE Downlink Transmission

Thida
 Department of Electronic
 Engineering,
 Technological University
 (Thanlyin), Myanmar

Dr. Ei Ei Khin
 Department of Electronic
 Engineering,
 Technological University
 (Thanlyin), Myanmar

Thinzar Kyaw
 Department of Electronic
 Engineering,
 Technological University
 (Thanlyin), Myanmar

Abstract: Mobile networks have triggered advances and changes in telecommunications world over the last two decades. In addition to the voice communication, the data usage has grown day by day. The recent increase of the data usage in mobile networks and appearance of new applications such as online gaming, mobile TV, streaming contents have greatly motivated the 3rd Generation Partnership Project (3GPP) to work on the Long Term Evolution (LTE). 3GPP LTE is the evolution of the Universal Mobile Telecommunications System (UMTS) which will make possible to deliver high quality multimedia services according to the users' expectations. LTE offers many significant improvements over previous technologies such as UMTS and High-speed packet access (HSPA). Higher downlink and uplink speeds, lower latency and simpler network architecture are among the new and important features that are provided in LTE. In this paper, the simulations for the performance analysis of LTE are presented. The effects of different parameters and other factors are investigated. The performance analysis results are shown in terms of Block Error Ratio (BLER) and Throughput versus Signal-to-Noise Ratio (SNR).

Keywords: LTE, BLER, SNR, downlink, throughput

1. INTRODUCTION

The LTE base stations are called Evolved NodeBs (eNodeBs) which is the main component of the LTE radio access network (RAN) architecture. The mobile terminals are commonly referred to as user equipments (UEs). The functionalities of eNodeB and UEs are divided into different protocol layers. The IP packets enter the protocol stack at Packet Data Convergence Protocol (PDCP) layer and flows through the protocol stack down to the Physical layer before entering the radio interface.

In cellular communication systems, the quality of the signal received by a UE depends on the channel quality from the serving cell, the level of interference from other cells, and the noise level. To optimize system capacity and coverage for a given transmission power, the transmitter should try to match the information data rate for each user to the variations in the received signal [3]. This is commonly referred to as link adaptation and is typically based on Adaptive Modulation and Coding (AMC).

For the downlink data transmissions in LTE, the eNodeB typically selects the Modulation and Coding Scheme (MCS) depending on the Channel Quality Indicator (CQI) feedback transmitted by the UE in the uplink.

2. BACKGROUND KNOWLEDGE

In LTE, MIMO technologies have been widely used to improve downlink peak rate, cell coverage, as well as average cell throughput. To achieve this diverse set of objectives, LTE adopted various MIMO technologies including transmit diversity, single user (SU)-MIMO, multiuser (MU)-MIMO, closed-loop rank-1 precoding, and dedicated beamforming. The transmit diversity scheme is specified for the configuration with two or four transmit antennas in the downlink, and with two transmit antennas in the uplink.

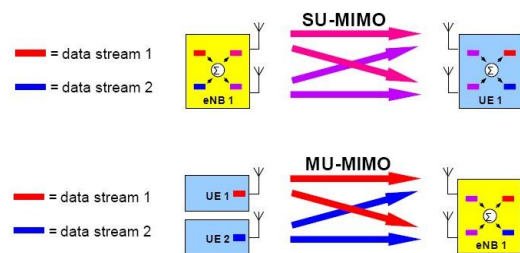


Figure. 1 SU-MIMO and MU-MIMO

The closed-loop rank-1 precoding scheme is used to improve data coverage utilizing SU-MIMO technology based on the cell-specific common reference signal while introducing a control signal message that has lower overhead. The dedicated beamforming scheme is used for data coverage extension when the data demodulation based on dedicated reference signal is supported by the UE [4].

2.1 Transmit Diversity

SFBC with two transmit antennas on downlink:

$$\begin{matrix} \text{Antenna}_0 \\ \text{Antenna}_1 \end{matrix} \begin{matrix} \xrightarrow{\text{Subcarrier}} \\ \left[\begin{array}{cc} S_0 & S_1 \\ -S_1^* & S_0^* \end{array} \right] \end{matrix}$$

SFBC + FSTD with 4 transmit antennas on downlink:

$$\begin{matrix} \text{Antenna}_0 \\ \text{Antenna}_1 \\ \text{Antenna}_2 \\ \text{Antenna}_3 \end{matrix} \begin{matrix} \xrightarrow{\text{Subcarrier}} \\ \left[\begin{array}{cccc} S_0 & S_1 & 0 & 0 \\ 0 & 0 & S_2 & S_3 \\ -S_1^* & S_0^* & 0 & 0 \\ 0 & 0 & -S_3^* & S_2^* \end{array} \right] \end{matrix}$$

Modified SFBC + FSTD for PHICH with four transmit antennas on downlink:

$$\begin{array}{l}
 \text{Type}_1: \begin{array}{l} \text{Antenna}_0 \\ \text{Antenna}_1 \\ \text{Antenna}_2 \\ \text{Antenna}_3 \end{array} \begin{array}{c} \xrightarrow{\text{Subcarrier}} \\ \left[\begin{array}{cccc} S_0 & S_1 & S_2 & S_3 \\ 0 & 0 & 0 & 0 \\ -S_1^* & S_0^* & -S_3^* & -S_2^* \\ 0 & 0 & 0 & 0 \end{array} \right] \begin{array}{c} \left[\begin{array}{cccc} 0 & 0 & 0 & 0 \\ S_0 & S_1 & S_2 & S_3 \\ 0 & 0 & 0 & 0 \\ -S_1^* & S_0^* & -S_3^* & -S_2^* \end{array} \right] \begin{array}{c} \left[\begin{array}{cccc} S_0 & S_1 & S_2 & S_3 \\ 0 & 0 & 0 & 0 \\ -S_1^* & S_0^* & -S_3^* & -S_2^* \\ 0 & 0 & 0 & 0 \end{array} \right] \end{array} \\
 \xrightarrow{1^{\text{st}} \text{ repetition}} \quad \xrightarrow{2^{\text{nd}} \text{ repetition}} \quad \xrightarrow{3^{\text{rd}} \text{ repetition}}
 \end{array} \\
 \text{Type}_2: \begin{array}{l} \text{Antenna}_0 \\ \text{Antenna}_1 \\ \text{Antenna}_2 \\ \text{Antenna}_3 \end{array} \begin{array}{c} \xrightarrow{\text{Subcarrier}} \\ \left[\begin{array}{cccc} 0 & 0 & 0 & 0 \\ S_0 & S_1 & S_2 & S_3 \\ 0 & 0 & 0 & 0 \\ -S_1^* & S_0^* & -S_3^* & -S_2^* \end{array} \right] \begin{array}{c} \left[\begin{array}{cccc} 0 & 0 & 0 & 0 \\ S_0 & S_1 & S_2 & S_3 \\ 0 & 0 & 0 & 0 \\ -S_1^* & S_0^* & -S_3^* & -S_2^* \end{array} \right] \begin{array}{c} \left[\begin{array}{cccc} 0 & 0 & 0 & 0 \\ S_0 & S_1 & S_2 & S_3 \\ 0 & 0 & 0 & 0 \\ -S_1^* & S_0^* & -S_3^* & -S_2^* \end{array} \right] \end{array} \\
 \xrightarrow{1^{\text{st}} \text{ repetition}} \quad \xrightarrow{2^{\text{nd}} \text{ repetition}} \quad \xrightarrow{3^{\text{rd}} \text{ repetition}}
 \end{array}
 \end{array}$$

Once the number of transmit antennas at eNodeB is detected, a specific transmit diversity scheme applicable to the other physical downlink channels is determined. Transmit diversity schemes defined for LTE downlinks. The space-frequency block code (SFBC) as indicated in the first equation is used if the eNodeB has two transmit antennas. For the eNodeB with four transmit antennas, a combination of the SFBC and the frequency switched transmit diversity (FSTD) as in the second equation is used to provide robustness against the correlation between channels from different transmit antennas and for easier UE receiver implementation. The transmit diversity scheme shown in second equation can be used for all downlink channels other than PHICH. The transmit diversity scheme used for PHICH is in the third equation. When there are multiple PHICHs transmitted, using type 1 or type 2 alternatively for different PHICHs would be helpful to keep uniform power distribution over eNodeB transmit antennas [4].

2.2 Open Loop Spatial Multiplexing

The eNodeB sends the scheduled UE the information about what precoding matrix is used as a part of downlink control information, using a three-bit information field for two transmit antennas and a six-bit information field for four transmit antennas. This information field is denoted transmit precoding matrix indication (TPMI). To support frequency-selective precoding without excessive downlink signaling overhead, the TPMI can also indicate that the precoding matrices reported in the most recent PMI report from the scheduled UE are used for their corresponding frequency resources. Use of the transmit diversity is indicated by TPMI.

The open-loop spatial multiplexing may be operated when reliable PMI feedback is not available at the eNodeB, for example, when the UE speed is not slow enough or when the feedback overhead on uplink is too high. The feedback consists of the RI and the CQI in open-loop spatial multiplexing. In contrast to the closed-loop spatial multiplexing, the eNodeB only determines the transmission rank and a fixed set of precoding matrices are applied cyclically across all the scheduled subcarriers in the frequency domain [4].

2.3 Channel Quality

In LTE downlink, the quality of channel is measured in the UE and sent to the eNodeB in the form of so-called CQIs (Channel Quality Indicator). The quality of the measured signal depends not only on the channel, the noise and the interference level but also on the quality of the receiver, e.g. on the noise figure of the analog front end and performance of the digital signal processing modules. That means a receiver with better front end or more powerful signal processing algorithms delivers a higher CQI. The signal quality measurements are done using reference symbols.

In the LTE physical layer, resources are managed with the so-called RM Modules (Resource Management), which assign

incoming data blocks to resource blocks. One resource block consists of 12 sub-carriers and one time slot. The resource management in LTE can be seen in Fig. 2 CQI values are used also to select the optimum resource block i.e. the optimum sub-carrier and the optimum time slot.

There are two kinds of CQI reporting: periodic and aperiodic, where the PUCCH (Physical Uplink Control Channel) is used for periodic CQI reporting only and PUSCH (Physical Uplink Shared Channel) for aperiodic CQI reporting.

Periodic CQIs are reported by the UE in periodic time intervals. If the eNodeB wishes channel quality information at a specific time, aperiodic CQIs are triggered. In order to define the frequency granularity of the CQI, the whole system bandwidth is divided into N sub-bands, each consisting of k contiguous Physical Resource Blocks (PRBs). The number of sub-bands is given by $N = N_{RB}^{DL} / k$ and determines the frequency granularity of the CQI reporting, where N_{RB}^{DL} is the number of resource blocks (RB) in the whole system bandwidth (DL stands for Downlink).

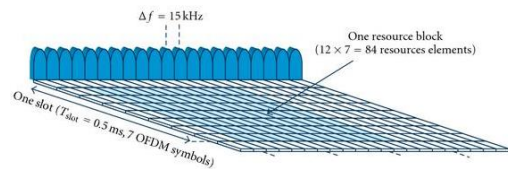


Figure. 2 Two Dimensional Resource Management in LTE

2.4 Periodic CQI Reporting

The periodic reporting of the CQIs is done over the PUCCH. Periodic CQI can be either wideband or UE-selected sub-band feedback for all downlink transmission modes. The type of CQI is decided by the eNodeB. In the wideband mode, one CQI value is measured in the whole system bandwidth and sent to the eNodeB. In the UE-selected sub-band feedback the total number of subbands N in the whole system bandwidth is divided into j fractions called bandwidth parts. In each bandwidth part a particular sub-band is selected and the measured channel quality in this sub-band with its position in the bandwidth part is sent to eNodeB. In Table 1 sub-band size (k) and bandwidth parts (J) versus downlink system bandwidth N_{RB}^{DL} can be seen.

Normally periodic CQIs are used but if eNodeB needs channel quality information at times rather than time raster of the periodic CQI, it can also wish aperiodic transmission of the CQIs by the UE. Losses of synchronization or handover situations are also cases, where aperiodic CQIs are used. Aperiodic CQI reporting is done over the PUSCH and requested by the eNodeB by setting a CQI request bit on the Physical Downlink Control Channel (PDCCH).

The type of CQI is set by the eNodeB and can be one of the following modes:

1. Wideband feedback: in this mode as in the periodic reporting, the UE reports one CQI value for the whole system bandwidth.
2. eNodeB-configured sub-band feedback: there are two kinds of CQI reported in this mode, one for the whole system bandwidth and one for the sub-bands. In the calculation of sub-band CQIs, it is assumed that transmission takes place only in the relevant sub-band.

3. UE-selected sub-band feedback: as in the eNodeB-configured mode, two types of CQIs are used, one wideband CQI value for the whole system bandwidth and one for reporting the average measured CQI in M selected sub-bands each of the size k. The UE decides which sub-bands are selected. The UE sends also the position of the M selected sub-bands.

The throughput results are compared to the system capacity C of an AWGN channel calculated according to Shannon capacity:

$$C = FB \log_2(1 + SNR)$$

Here, SNR is the Signal to Noise Ratio, B the bandwidth occupied by the data subcarriers as shown below, and F a correction factor. The bandwidth B is calculated as

$$B = \frac{N_{SC} \cdot N_S \cdot N_{rb}}{T_{sub}}$$

where $N_{SC} = 12$ is the number of subcarriers in one RB, S N is the number of OFDM symbols in one sub-frame (usually equal to fourteen when the normal Cyclic Prefix (CP) is set), N_{rb} is the number of RBs that fit into the selected system bandwidth (for example 6 RBs within a 1.4MHz system bandwidth), and T_{sub} is the duration of one sub-frame equal to 1ms. The transmission of an OFDM signal requires also the transmission of a CP to avoid intersymbol interference and the reference symbols for channel estimation. Therefore, the well-known Shannon formula is adjusted in $C = FB \log_2(1 + SNR)$ by factor F. This factor F as shown below, accounts thus for the inherent system losses and is calculated as

$$F = \frac{T_{frame} - T_{CP}}{T_{frame}} \cdot \frac{N_{SC} \cdot N_S / 2 - 4}{N_{SC} \cdot N_S / 2}$$

$\underbrace{\hspace{10em}}_{CP_{loss}} \quad \underbrace{\hspace{10em}}_{reference\ symbol\ loss}$

where T_{frame} is the fixed frame duration equal to 10 ms and T_{CP} is the total CP time of all OFDM symbols within one frame [5].

3. PERFORMANCE ANALYSIS AND SIMULATION RESULTS

In LTE, one of the main features that provide transmission robustness is hybrid-ARQ (HARQ), which in LTE provides physical layer retransmission using incremental redundancy and soft combining. A transmission scheme based on H-ARQ combines detection and Forward Error Correction (FEC) plus a retransmission of the erroneous packet. LTE additionally uses soft combining, in which a given received packet is combined with the previously received packets and the resulting more powerful FEC code is then decoded. Hence, for each H-ARQ retransmission that the LTE system can employ, an improvement of the Block Error Rate (BLER) or throughput is expected.

From Figure 3 and Figure 4, the LTE simulations for the HARQ evaluation process were performed for a single-user scenario corresponding to the simulation parameters shown on figures' titles in 5MHz BW and when there is no HARQ, while Figure 5 and Figure 6 with the same parameters when there are 3 retransmissions. Even there is no much difference on high SNR values, the difference on the throughput and BLER can easily be observed that in lower SNR values such as -5 to 5 dB, there is significant improvement thanks to HARQ.

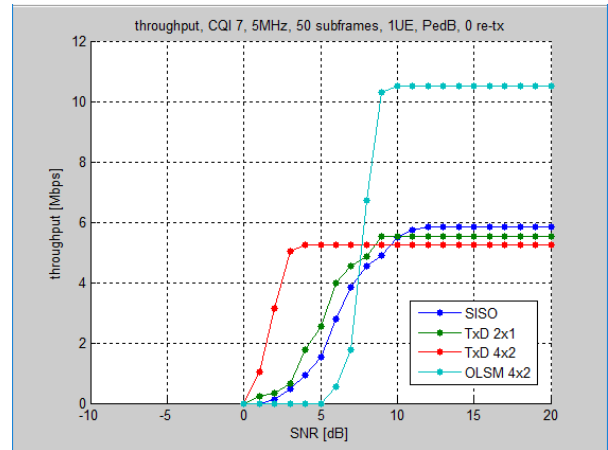


Figure. 3 Throughput Performance of the SISO, MIMO and OLSM in 5MHz with No HARQ

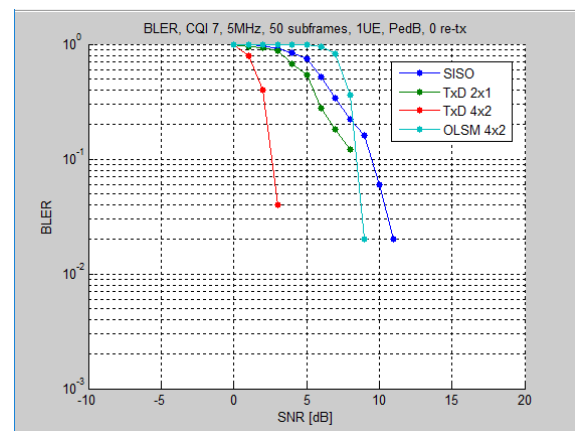


Figure. 4 BLER Performance of SISO, MIMO and OLSM in 5MHz with No HARQ

In addition to HARQ, the effects of MIMO are also investigated in figures from 3 to 6. In these four figures, the throughput of SISO, 2x1 (MISO) transmit diversity (TxD), 4x2 transmit diversity (MIMO), and 4x2 Open Loop Spatial Multiplexing (OLSM) is compared when transmitting over Pedestrian B (PedB) channel type over 5MHz channel BW. Again in these simulations the CQI value is set to 7.

The maximum throughput values achieved by the different MIMO schemes in Figures depends on the number of transmit antennas and on the number of data streams. If more transmit antennas are utilized for the transmission, more pilot symbols are inserted in the OFDM frame and thus lower maximum throughput can be achieved.

In the case of Open-Loop Spatial Multiplexing (OLSM), spatial multiplexing forms multiple independent links (on same channel) between transmitter and receiver to communicate at higher total data rates (Increases data rates by transmitting parallel data streams). Two spatially separated data streams are transmitted, thus leading to twice the maximum throughput of the 4x2 TxD systems.

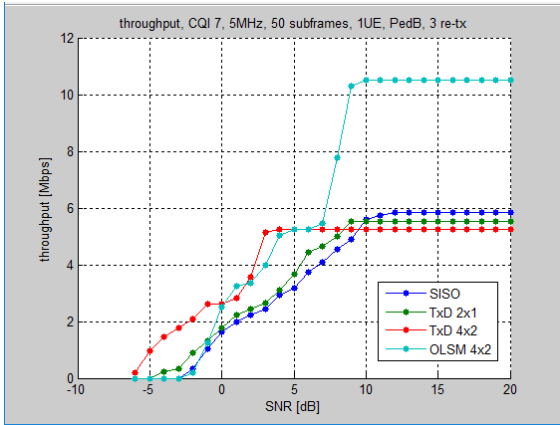


Figure. 5 Throughput Performance of the SISO, MIMO and OLSM in 5MHz with Retransmissions

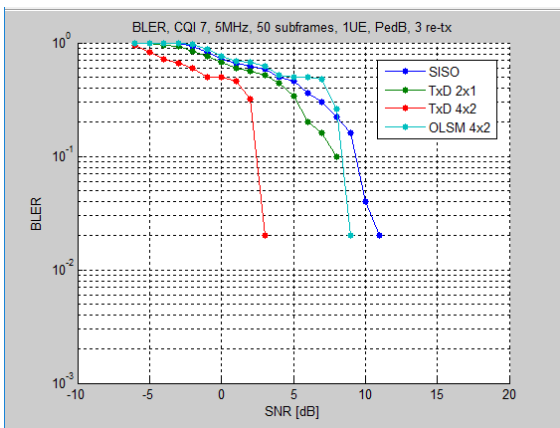


Figure. 6 BLER Performance of the SISO, MIMO and OLSM in 5MHz with Retransmissions

In Figure 7 and Figure 8, under the same simulation settings and parameters of Figure 3 and Figure 4 (No-HARQ), the performance of LTE is investigated for 10MHz BW. As expected, both BLER and throughput results are improved with respect to (w.r.t.) 5MHz. Throughput value is about 22 Mbps for 10 MHz while the throughput results are about 11 Mbps for 5MHz respectively. It shows that there is a linear improvement in the throughput results with respect to BW. But there is no big improvement with respect to the BLER results.

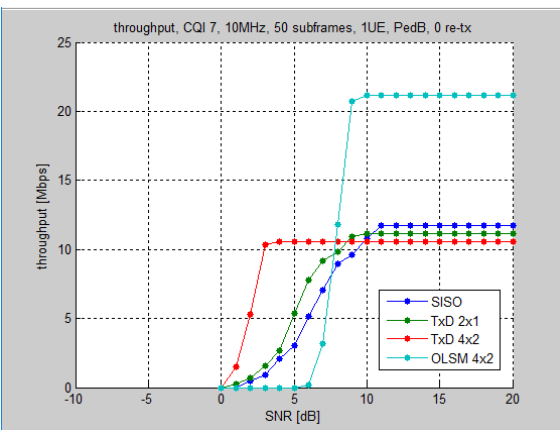


Figure. 7 Throughput Performance of the SISO, MIMO and OLSM in 10MHz with No HARQ

Maximum throughput is achieved with OLSM since spatial multiplexing works by creating separate data streams on multiple antennas. In spatial multiplexing, the eNodeB divides the data to be sent to a given UE on a given sub-channel into data streams, called layers. The number of layers is the same as the rank of the transmission. Transmission rank is determined according to channel conditions at the UE, as well as other considerations such as available resources at the eNodeB. Each layer reaches each Rx along a different path. The UE then reconstructs the layers using information from all antennas.

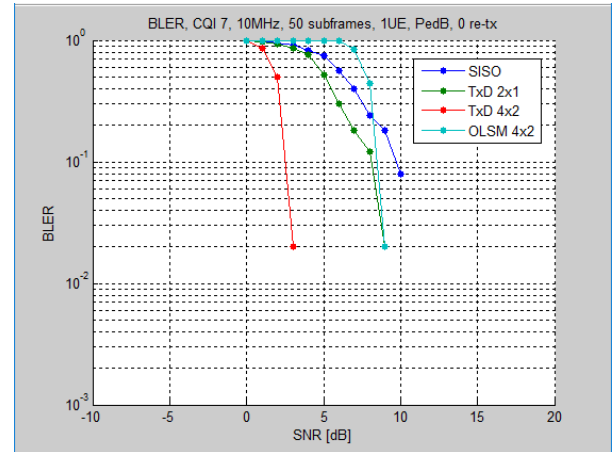


Figure. 8 BLER Performance of the SISO, MIMO and OLSM in 10MHz with No HARQ

In Figure 9 and Figure 10, the throughput and BLER results for different channel BWs are shown such as 1.4, 5 and 10MHz, again for PedB channel type and SISO system implementation. In 1.4MHz the saturated throughput is about 0.8Mbps, and 3.5Mbps and 7Mbps for 5MHz and 10MHz, respectively. Figure 9 shows that there is about 2x improvements in 10MHz w.r.t. 5MHz and more than 7x gain w.r.t. 1.4MHz channel BWs. These improvements show that there is a linear improvement in the throughput as the channel BW increases.

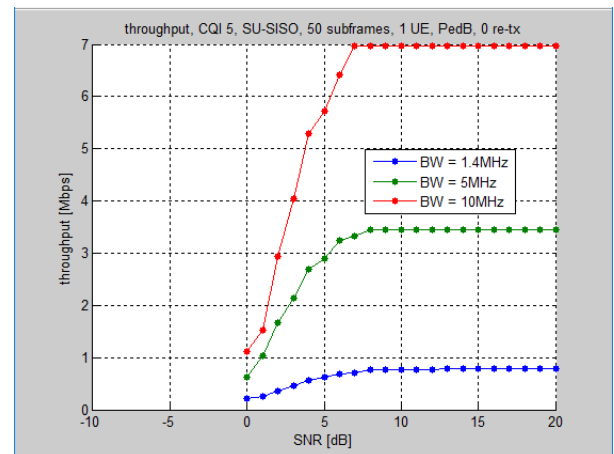


Figure. 9 Throughput Results for Different Channel Bandwidths

The effect of different channel types is shown in Figure 11 and Figure 12 including non-fading environment (AWGN). One can see that for the high and low SNR values all the channel types are reaches the same value (3.5Mbps at high SNR). However, for the medium SNR values there are some throughput differences for different channel models as shown.

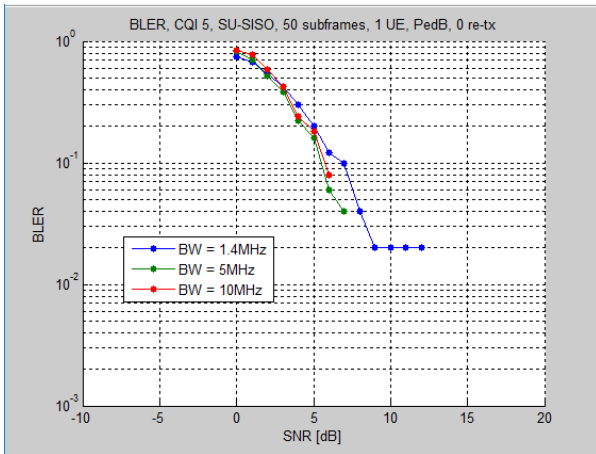


Figure. 10 BLER Results for Different Channel Bandwidths

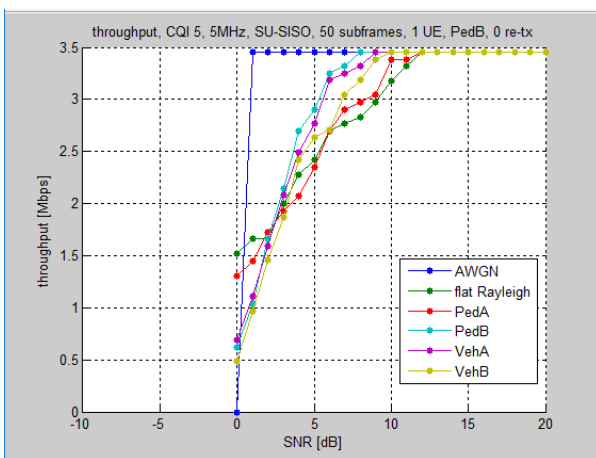


Figure. 11 Throughput Results for Different Channel Types

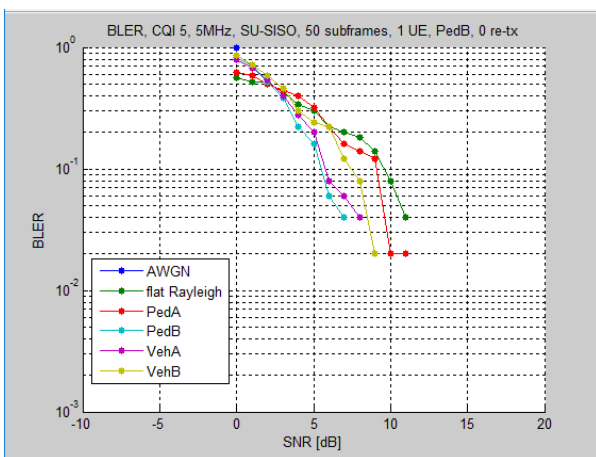


Figure. 12 BLER Results for Different Channel Types

4. CONCLUSION

In the light of the simulation results, it is observed that when the HARQ is used, even there is no much difference on high SNR values, the difference on the throughput and BLER can easily be observed that in lower SNR values such as -5 to 5 dB, there is significant improvement thanks to HARQ.

The maximum throughput values achieved by the different MIMO schemes depends on the number of transmit antennas and on the number of data streams. If more transmit antennas are utilized for the transmission, more pilot symbols are inserted in the OFDM frame and thus lower maximum throughput can be achieved.

The effect of different channel types has been investigated including non-fading environment (AWGN). One can see that for the high and low SNR values all the channel types reach the same value. However, for the medium SNR values there are some throughput differences for different channel models.

5. ACKNOWLEDGMENTS

The author would like to express her profound gratitude to Dr. Theingi, Rector, Technological University (Thanlyin), for her encouragement and managements and the author would like to express her thanks to thesis supervisor, Dr. Ei Ei Khin, Professor of Electronic Engineering, for her motivation and encouragement to complete this research in time. After all, the author would like to express her thanks to all her teachers and her parents, for their supports and encouragements.

6. REFERENCES

- [1] Rohde & Schwarz, (2010), "UMTS Long Term Evolution (LTE). Technologies Introduction", available at: http://pwrk.cachefly.net/rs/fileadmin/customer/downloads/PDF/UMTS_Eng.pdf (Accessed March, 25, 2014).
- [2] Dahlman, E., Parkvall, S., Sköld, J., and Beming, P., (2008), 3G Evolution: HSPA and LTE for Mobile Broadband, 2nd ed., Elsevier, Oxford, UK.
- [3] Sesia, Stefania, Toufik, Issam, and Baker, Matthew, (2011), LTE – The UMTS Long Term Evolution: From Theory to Practice, John Wiley and Sons, The Atrium, Southern Gate, Chichester, West Sussex, UK.
- [4] Lee, Juho, Han, Jin-Kyu, and Zhang, Jianzhong (Charlie), (2009), "MIMO Technologies in 3GPP LTE and LTE-Advanced", EURASIP Journal on Wireless Communications and Networking, Volume 2009.
- [5] Mehlführer, C., Caban, S., Wrulich, M., and Rupp, M., (2008), "Joint throughput optimized CQI and precoding weight calculation for MIMO HSDPA", 2008 42nd Asilomar Conference on Signals, Systems and Computers, Pacific Grove, CA, 26-29 Oct., 2008.

Evaluate and Improve High School Students for Some Skills using Quality Function Deployment

Rania Ahmad Elrifai
Benghazi University, Engineering Faculty,
Industrial and Manufacturing System Engineering Department
Benghazi, Libya

Abstract: The current study, which deals with the quality of education, is an identification of the necessary needs from the point of view of faculty members regarding the skills required for secondary students. These are the necessary requirements that must be met in the course of secondary education before the student joins scientific faculties to proceed to a higher academic stage. The Department of Industrial Engineering and Manufacturing Systems at the College of Engineering at the University of Benghazi proposed the teaching of some of the skills already included in the existing curriculum in order to prepare the students for the next stage (undergraduate) through the quality function of publishing technology. The key stakeholders in this audit were identified as the faculty members of all departments (Industrial Engineering and Information Systems, Electrical, Civil, Mechanical, Petroleum and General Department) and secondary teachers. Customer expectations that were immediately identified through the survey of all faculty members were summarized and prioritized. The requirements of the two shareholders differed only in their order of priority. The requirements were then converted to quality characteristics.

Keywords: Quality Function Deployment; Total Quality Management (TQM); School Curriculum; High School; Relationship matrix; House of quality

1. INTRODUCTION

Secondary education in Libya changed over a course of three stages, beginning in the fifties with the contract system that lasted until 1991 and consisted of general high school and three years of studying general topics. When it began, it was what is known as specialised secondary education, which was then a solution that helped the student adapt initially in the university these were opinion since. However, there was a shortage of qualified teachers for each specialisation, which led to the teachers' study topics not being related to their fields. In this, the paper focuses on to evaluate and Improve high school students for some skills using Quality Function Deployment which skills in the form of requirements took their importance depending on the customers who are faculty members, who are from the point of view of professional and found that the skills were one of the first to be before they enter college , and that was one of the shortcomings of the high school students the scientific, the author found that a quality function deployment is an effective tool for overcoming this difficulty QFD is the management technique for comprehending the "voice of the customer" and enables a translation of the customer requirements into the appropriate quality characteristics. Its use facilitates the process of concurrent engineering and encourages teamwork while working towards a common goal of ensuring customer satisfaction. QFD also provides the means for inter-functional planning and communications. based on the previous study that has been reviewed by QFD[1]. In this paper, evaluate and improve some skills of high school students in Schools of Higher Education for adapting for studying in

University Education as well as next steps have been reviewed and evaluated by the QFD technique.

2. QFD review of the skills of high school students in Schools of Higher Education

Quality Function Deployment (QFD) is one of the Total Quality Management (TQM) techniques which can be applied for process and design improvement. QFD was used as a tool for quality improvement and benchmarking in higher education institutions of Pakistan. The study is based on primary data have been collected from five hundred students which were considered as customers and five hundred teachers, considered as technical describer from six Pakistani national degree awarding universities, QFD assessment showed the comparison of different universities in certain areas of their quality teaching was first applied to education at the beginning of the 1990s [2]. The Quality Function Deployment was applied at two stages:

Stage1, where each course's goals and outcomes were related to the program goals and institutional learning outcomes.

Stage 2, where actual end-of-the-semester data from student assessments and faculty evaluations were collected and fed to the Quality Function Deployment system, the results of the exercise can be used to evaluate the effectiveness of the program's yearly cycle and to devise appropriate interventions for improving the program and course design and delivery strategies[3].

The curriculum of the tire technology department at the Kocaeli university, vocational school of higher education (KU-KVSHE) has been reviewed by using the quality

function deployment (QFD) technique, the university senate has approved the new curriculum proposed in this study and the school management has decided to apply the new curriculum as of the fall term of the 2002–2003 school year [1]. Application of QFD, in a higher education curriculum redesign, has been made at the Rain Star University, in Scottsdale, Arizona. This curriculum was for a master's degree program in acupuncture and oriental medicine[4]. The QFD allowed to assess the learning needs of students in an accounting course and translate them into educational strategies (specific techniques) able to satisfy such needs, the results allowed to define "the right things to do for the first time", a significant support for the improvement of university courses [5]. Quality Function Deployment (QFD) has been applied for process and design improvement. The research developed a framework for quality in an educational institute on the basis of literature review. A relationship matrix was developed between the set of identified groups of 'Dimensions of Quality' and sets of 'Enablers' in an educational institute[6]. One of the earliest uses of QFD in studies in education was done, the requirements of customers-students, academic staff and industry were analysed separately [7]. Evaluation of E-learning service is to insist that in spite of the importance of having standards to maintain the quality, and to commit to the aim of quality by achieving customer satisfaction, it reveals the importance of Quality Function Deployment (QFD), to ensure that the voice of customer derives all actions concerned with quality. It can help keep high standards of benchmarking[8]. A matrix Quality Function Deployment (QFD) has been used. It allowed transforming-requirements of clients/students of nursing to easily measurable parameters of service process – process of tutoring, providing their desired values. Due to benefits of introducing QFD, the method can be used on different stages of the quality management process, so you should be exploited in the process or improving the quality of practical training of future nurses [9]. The authors did not consider the students as stakeholders by reasoning that students use the curriculum but often lack information regarding the university needed in their comprehensive and are unable to assess the curriculum from a customer's point of view. However, the high school should have the competency to evaluate the skills to be taken by the students. The risk here occurs if the lecturer-faculty lacks industrial experience, in which case their priorities and ranking would differ from real-life.

3. Voice of the Stakeholders/Customers

Seven local departments of engineering faculty were selected for the survey. The total number of lecturers varied 43 which done in the survey, lecturers Where lecturers involved in the study of both doctors and Master Professor and professors assistant of sections of the whole college. One-on-one interviewing was used for collecting the voice of the stakeholders. A special questionnaire form having 7 questions was prepared. The

lectures from an industrial engineering department, mechanical engineering department, electrical engineering department, the civil engineering department and general engineering department. The skill and qualification expectations of the stakeholders from all departments were collected in their own words. The priority of each customer need was also asked during the interview. The stakeholders ranked these needs from 1 to 9 (higher number means higher importance). These interview forms were then analysed by the QFD team. 301 requirements were be identified. These stakeholder requirements were then categorized, shortened, sorted and prioritized taking into consideration the customer's evaluation. A total of 7 ranked requirements were acquired to become the inputs of the "House of Quality" as given in Table 1. After the determination of the requirements and their relative importance, the QFD team underwent successive meetings. Each acquired requirement was transformed into a quality characteristic, namely into courses. The QFD team has then determined the quality characteristics that are likely to affect one or more stakeholder requirements. The desired requirements were investigated step by step, looking at the current curriculum courses and their content, so as to decide whether the requirement could be met with the skills of the current curriculum or not. Whenever the team concluded the impossibility of meeting the requirements of an existing course, the necessary modification was done. All the requirements were transferred into quality characteristics following an extensive analysis of all the courses. The relationship between requirements and quality characteristics were established and indicated in the relationship matrix. There are different weighting methodologies in the discussion, the most widely preferred categories of 'strong, medium, weak and no relationship' with the values of 9,3,1and 0, respectively, were applied. The 1–9 scale represents a geometric progression discriminating heavily against the weak relationship as opposed to the strong relationship. These weightings are subjective [10]. Since all the quality characteristics were affected positively by each other, the house of quality roof matrix was not considered. The customer evaluation of the competitive products, i.e., the benchmarking of graduates from different schools was not done due to a lack of sufficient data. Next, the necessary analysis for the technical difficulties, the necessity of qualified teachers, and the additional cost of financing the improvement of quality characteristics were done. In our study, the school management and faculty ranked the technical difficulties. The degree of technical difficulty relates to how hard or easy it is to carry out the quality characteristics. Therefore, it is common to use a scale from 1 to 5 with 1 denoting the easiest. In order to determine the ranking of the relative importance of customer requirements, the QFD team decided to use a method that would weigh the customer's view based on the number of employees it had. Therefore, the importance weight each customer had assigned to every quality characteristic was multiplied by a coefficient.

This coefficient was determined on a scale from 1 to 5 with 1 denoting the least populated company. These weighted figures were then summarized and normalized to rank the relative importance of the customer requirements as seen in Figure 1.

Relationship matrices symbols
 Strong Relationship : ● - 9
 Medium Relationship : ○ - 3
 Weak Relationship : △ - 1

Quality characteristics (COURSES)	Stakeholders/ Customer Needs	Relative importance	Human development courses for teachers, including a mechanism for how to give these skills	Activating the laboratory coursework in English (listen – Conversation)	The provision of a private computer labs to provide practical training for students	The allocation of a science project for collective action at the school level to raise the teamwork and time management	Electronic network linking schools to search	How to allocate a portion of the research work and the work of the project subject of the study (search through the electronic network)	Educational institutions keen on activating share during the week to improve the skill of <i>auditions and Conversation</i>	Application software practically rather than theoretical
English language skills (writing – reading – listening)	5.284		●					●		
Computer skills for the purpose of solving problems related to the area of study	4.354			●	○	●	●		●	
Skills of contact with faculty members	4.348	●	○	●	△	△	○	○	○	
Skills of teamwork	4.14	●		○	●	●	○	○	△	
Skill of interactive education	4.033	●	△	○	○	●	●	○	●	
Computer skill for the purpose of writing reports	3.926			●	●	●	●		●	
Time management skills	13.912	●	○		●	△			△	
Scores		507.89	236.36	468.17	477.31	536.33	466.28	265.11	451.91	
Relative Importance (%)		14.896	6.932	13.731	13.999	15.731	13.676	7.776	13.254	
Ranking		2	8	4	3	1	5	7	6	
Degree Of Technical difficulties										
New Lecturer Necessity ? (Yes/ No)		N	N	N	N	N	N	N	N	
Additional Cost Increase ? (Yes/ No)		Y	Y	Y	N	Y	Y	N	Y	

Figure 1: HOUSE OF QUALITY for the curriculum

4. Decision and Analysis :

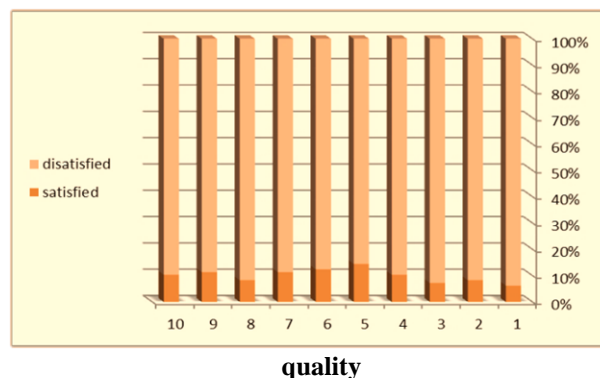
In order above the house quality deployment, QFD can be used to improve high school education level through enabling some skills that have been found in the curriculum, but they have needed simple mechanisms for application by insurance about improvement level of high school student before going head to faculty. In this study some skills must be activated for raising the level

of student especially in writing, conversation, listen in English language and programming, writing by computer ..etc., all these according to an expectation of customers (stakeholders) from undergraduates of all local departments were determined by survey with the questioner. From constructed " House Quality Deployment" in figure (1), it has shown from the point of view of customers (Stakeholders/Customer Needs) that the most relative importance is the internet

linking of the schools to search, improve these the skills which related to the curriculum, such reviewing the student the topics with developing the skills therein for each subject then human development courses for teachers, including a mechanism for how to give these skills, through this characteristic can enable the teachers how to activate these skills can be activated through the tutorials, then the allocation of a science project for collective action at the school level to raise the teamwork and time management , the provision of a private computer labs to provide practical training for students which is integrated with the first quality characteristic which can't be applied without it , How to allocate a portion of the research work and the work of the project subject of the study (search through the electronic network) so that quality character depended on the first quality character that emphasizes the importance of this characteristic . Application software practically rather than theoretical that because the programs must be shown and run practically that enabling correctly understanding process, other words in almost educational institutions do not have computer labs and basically curriculum mostly programming languages necessary to be applied on the computer in the event enable this will overcome the weaknesses and strengthen the idea of thinking and perception (carried out practical image and earn the right idea and the ability of the development). Educational institutions keen on activating share during the week to improve the skill of auditory and Conversation, also Activating the room coursework in English (listen – Conversation) because both will contribute in improvement of level of student , then The allocation of a science project for collective action at the school level to raise the teamwork and time management as same importance nearly as How to allocate a portion of the research work and the work of the project subject of the study (search through the topics for supporting an ability of student for aware and more understanding through the internet linking). Application of the software practically rather than theoretically as tackling above of ways. After that, internet linking schools to search such as this very important characteristic by it can be enabled some skills are integrated as research in internet, time management and contact with faculty members. These seven Customer Needs are the most important from opinion of customer than other Customer Needs that the least importance, based on previous study about a simple way to measure customer satisfaction, so that must be considered satisfaction of customer such as made another survey about rating satisfied of customer about the recent customer requirements such can be found both the high

importance and the least satisfaction [11]. The results were the following that relative rating dissatisfied is higher than relative rating satisfied, so that was necessary focused on this region for improvement the recent situation for level of high school education, also form all these conclusions can be summaries some the recommendations in below. This Figure (2) is approximately data and not actual data, they have been put here just to give manifestation to the written comment.

Figure 2: shows the presented data from house of



5. RECOMMENDATIONS

Due to the needing for the inevitable to raise the level of academic must attention means that enable to improve the level of education , which has become the other nations advanced dramatically despite the fact that these methods do not cost a lot of money, time and effort g spite of the results that will return us over time, which will advance our Islamic nation, especially the Arab world General, and therefore we recommend in our study that the characteristics we have learned to be starting out in the early stages, even before the beginning of the school stage(kindergarten), for example, enable the child to display a simple subject and talk about it in front of his colleagues earned many skills, including the courageous confrontation, connect with others and instil confidence that makes a strong base for the personal leadership of the children, and do not forget that the child is affected by the environment around them, so take care of this opportunity to improve our future generations, through our study, there are some of the things want to be displayed and recommend as the following:

2. Use laptops instead of bags that weigh weights strain our children as well as the ease to download the curriculum according to each level
3. The use of laptop computers to facilitate the process of Internet connectivity and to keep pace with scientific development.
4. Focus on the internet linking and connection with as consideration a part of topics of courses inside the

curriculum for raising the education quality level of each level.

5. Concern on these skills from the beginning of the school at first stage as consider the basic level is the base for future a generation.
6. Mainstreaming the introduction of these skills in the early stages of the study as consider there are available applications but need funder and support from the government.
7. Support the confidence of children through the presentation in front of his colleagues and his parents are present.

6. ACKNOWLEDGMENT

In this study, I would like to thank Dr Galal Abdella. Assistant Professor of the faculty of the Faculty of Engineering, Benghazi University, Department of Industrial and Manufacturing Engineering, who taught us this scientific material in the master degree in 2014 AD, which he has provided us with a lot of information and which has always been a race for creative ideas. By equipping students to the level of international universities. All thanks and appreciation

7. REFERENCES:

1. AYS, E AYTAC and VELI DENIZ,2005, Quality Function Deployment in Education: A Curriculum Review, *Quality & Quantity*,39,pp. 507–514.
2. Muhammad, Khalid, 2012, Quality Function Deployment in Higher Education Institutes of Pakistan, 12 (8), pp.1111-1118.
3. Khalid, Abdelkader, 2011, Using Quality Function Deployment as a higher education management and governance tool, 6(1),pp. 31–52.
4. Bier, I. D & Cornesky, R. (2001). Using QFD to construct a higher education curriculum, *Quality Progress* 64–68.
5. Ida Verna,2014, The Quality Function Deployment and The Customer Satisfaction. The Case of Universities, *European Scientific Journal*, Issn 1857- 7431.
6. Abhishek , sanjay,2015, study of parameters for improving quality of higher education with customer satisfaction via quality function deployment, *journal of social sciences and humanities research* 17(1), www.advancesjournals.org.
7. Ermer, D. S. (1995). Using QFD becomes an educational experience for students and faculty. *Quality Progress* 28(5): 131–36.Chen, J. & Chen, C. J. (2001). QFD-based technical textbook evaluation-procedure and a case study. *Journal of Industrial Technology* 18(1): 1–8. Ola Ibrahim, 2013.
8. E-learning benchmark and quality function deployment role, *Comprehensive Research Journal of Management and Business Studies (CRJMBS)* Vol. 1(1) pp. 0013-017.
9. Danuta, 2016, Quality Function Deployment as A Method Used in The Development of The Quality Of Education for The Nursing Practice, Pp. 42-5.
10. Owlia, M. S. & Aspinwal, E. M. (1998). Application of QFD for the improvement of quality in an engineering department. *European Journal of Engineering Education* 23: 105–115.
11. staceybarr ,A simple way to measure customer satisfactionwww.staceybarr.com, staceybarr@staceybarr.com

Experimental Investigation on Effect of Bamboo Leaf Ash Replacing Cement on Compressive Strength

Thu Thu Hnin
Department of Civil
Engineering
Technological University
(Thanlyin)
Republic of the Union of
Myanmar

Kyaw Lin Htet
Department of Civil
Engineering
Technological University
(Thanlyin)
Republic of the Union of
Myanmar

Ni Ni Moe Kyaw
Department of Civil
Engineering
Technological University
(Thanlyin)
Republic of the Union of
Myanmar

Abstract: Due to the emission of harmful gas that pollute the atmosphere and rising cost of Ordinary Portland Cement (OPC), the use of waste material is considering as a replacement for cement. In this research, the use of agricultural waste on experimental investigation on the use of Bamboo Leaf Ash (BLA) as a partial replacement for cement. The content of percentage replacement of OPC with BLA from 0%, 5%, 10% and 15% by weight with 0.4 and 0.5 water-cement ratios. The compressive strengths were tested with a total of 72 (150 x 150 x 150) mm concrete cubes according to American Concrete Institute (ACI) provisions at 7 days, 14 days and 28 days respectively. In this study, local product of ‘Apache’ brand Portland cement, ‘wanet’ bamboo leaves, crushed stones and river sand were used. The chemical composition of BLA are tested by Energy Dispersive X-ray Fluorescence Spectroscopy (EDXRF) method. Research findings have carried out that the workability and strength of the concrete depend on the percentage of the ash, water-cement ratio, mixing time and age of the curing days. In this research, 5% and 10% BLA was optimum for medium grade concrete. As a conclusion, BLA have a high silica content and good supplementary cementitious properties and so it can be used for partial replacement of concrete for reducing environmental wastes and emission of carbon dioxide (CO₂) in production of cement and reducing costs.

Keywords: Bamboo Leaf Ash (BLA), Ordinary Portland Cement (OPC), Energy Dispersive X-ray Fluorescence Spectroscopy (EDXRF), water-cement ratio, agricultural waste, carbon dioxide (CO₂), compressive strength

1. INTRODUCTION

Cement is an essential part of binding material to become concrete in the construction industry. To produce the cement, not only consume a lot of energy and high temperature (about 1500 °C) but also emits harmful gas such as CO₂, NO₃ and CH₄ to the atmosphere. By solving this problem, researchers are considered for a partial replacement for cement using waste materials.

There are two types of waste materials for replacing of cement ; (i) industrial waste and (ii) agricultural waste. And then these wastes are subdivided into natural and recycled. Some agricultural waste by-products like peanut shell ash, sawdust ash, sugarcane bagasse ash and bamboo leaf ash and so on are now considered for a partial replacement of cement mixed with OPC. Utilization of bamboo leaf ash provided as an effective way for reducing environmental wastes, saving energy and impact of greenhouse gas emission to the environment. Reusing agro-wastes for producing panels, plaster, blocks suitable for passive houses. Thus, it should be considered for the solving problem of the disposal of agro-wastes.

Bamboo is used as scaffolding for construction, paper production and household products. In Myanmar, bamboo is abundantly growing and used for variety of purposes so generating high volumes of solid waste.

There are 1250 bamboo species in the world and 102 species in bamboo diversity in Myanmar. But 18 species are commercial used in the country. Depending on the bamboo species, the chemical and physical compositions may be

different. Among them, “wanet” bamboo leaves are used in this research. Because of these bamboo species are growing abundantly in research area.

Bamboo leaf ash is made up of inorganic minerals, Silica, Calcium, Potassium and Magnesium. Silica content is the highest among the minerals. When calcium hydroxide (Ca(OH)₂) is react with silica to form calcium silicate hydrate (C-S-H), the main secondary cementitious compound is obtained.

Thus, both economical and environmental point of view, BLA should be used for a partial replacement of cement with the optimum percentage for mortar and concrete.

2. AIM

The objective of this research is to investigate the effect of bamboo leaf ash and to save the environment from disposing waste.

3. METERIALS AND METHODS

The materials used in this research were cement, aggregates (fine and coarse), water and bamboo leaf ash (BLA). Both physical and chemical properties were tested for cement and bamboo leaf ash. And only physical properties was tested for both aggregates and water.

3.1 Materials

In this research, the used of local materials are Ordinary Portland Cement, River Sand, Crushed Stone, Water and ‘Wanet’ bamboo leaves.

Bamboo leaves have been collected from household productions in Pindaya township, Shan State. The collected bamboo leaves were sun dried and burnt in a closed metallic drum. After that these ashes spread on the surface and allowed to cool for 24 hours and finally got the bamboo leaves ash of gray colour.

The cement used was Type I, Ordinary Portland Cement ‘Apache’ brand and the fine aggregates were of sharp sand and coarse aggregates were of nominal maximum size of 19 mm respectively. The water from tube well of High-Tech Concrete Company Limited. The bamboo leaf and bamboo leaf ash were shown in Figure 1.



Figure 1. Bamboo Leaf and Bamboo Leaf Ash

3.2 Methods

Expect from chemical analysis of bamboo leaf ash the physical properties of BLA and OPC and strength tests were tested according to American Society of Testing and Materials (ASTM) standards.

3.2.1. Chemical Analysis of Bamboo Leaf Ash (BLA)

The chemical composition on the samples were analyzed by Energy Dispersive X-Ray Fluorescence Spectroscopy (EDXRF) test in West Yangon University.

3.2.2. Physical Properties of BLA and OPC

Specific gravity were tested with BLA only and consistency and setting time tests were tested with OPC mixed with a varied percentage of BLA.

3.2.3. Workability Test

The OPC was mixed with a varied percentage of BLA with the water-cement ratios of 0.4 and 0.5 and to determine the workability of concrete and consequently the compressive strength for 7 days, 14 days, 28 days and 56 days respectively.

3.2.4. Density Test

The density test was carried out with a varied percentage of BLA mixed with OPC of a fresh concrete.

3.2.5. Compressive Strength Test

The compressive strength tests, a total of 36 cubes (150 x 150 x 150) mm for each water-cement ratio were tested in High-Tech Concrete Company Limited. Three cubes were tested for each percent and then took the average.

4. RESULTS AND DISCUSSION

The research materials of the physical properties of cement, sand, aggregate, water and bamboo leaf ash were shown below.

4.1. Chemical Analysis of Bamboo Leaf Ash (BLA)

The chemical analysis of OPC and BLA were tested and compare the main chemical composition test results were shown in Table.1.

Table 1. The chemical composition of OPC and BLA

Constituent	Ordinary Portland Cement(OPC)	Bamboo Leaf Ash(BLA)
Silicon dioxide (SiO ₂)	21.47 %	67.78 %
Aluminum oxide (Al ₂ O ₃)	4.61%	-
Ferric oxide (Fe ₂ O ₃)	3.32 %	0.156 %
Calcium Oxide (CaO)	64.61 %	6.138 %

4.2. Standard Consistency Test

The consistency test was carried out according to ASTM C 187. In this test, the higher the BLA %, the more water is added and the results were shown in Table 2.

Table 2. The standard consistency test result of OPC mixed with BLA

Test	BLA 0%	BLA 5%	BLA 10%	BLA 15%
Standard consistency	28 %	33.15 %	36.5 %	43 %

4.3. Setting Time Test

The initial and final setting time is performed according to ASTM C 191. The results show the initial and final setting time of OPC mixed with BLA is more than the OPC. The test results were shown in Table 3.

Table 3. The setting time test result of OPC mixed with BLA

Test	BLA 0%	BLA 5%	BLA 10%	BLA 15%
Initial Setting time	2 hr 30 min	3 hr 20 min	4 hr 05 min	4 hr 25 min
Final Setting time	3 hr 40 min	5 hr 00 min	5 hr 45 min	6 hr 15 min

4.4. Workability Test

The workability is determined by slump test. In this research, the increase in percentage of BLA, the decrease in workability of concrete. The greater percentage of BLA tend to be fall down in slump. The test results of the water cement ratios (w/c) and percentage of BLA were shown in Table 4. And a higher

temperature reduces the workability and increases the slump loss.

Table 4. The slump Test Result of OPC mixed with BLA

W/C	0% BLA	5% BLA	10% BLA	15% BLA
0.4	170	60	35	10
0.5	225	175	130	65

4.5. Density

The density of control concrete (0%) is greater than the BLA (5, 10, 15) %. The density is decreased when the BLA added to OPC. The test results were shown in Figure 2.

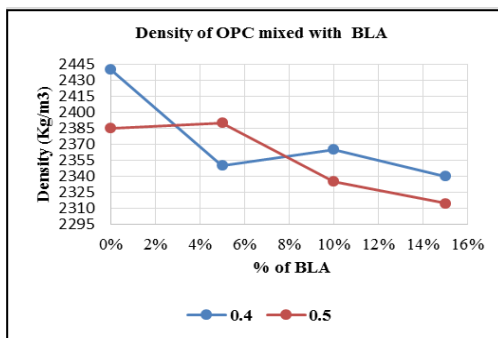


Figure 2. Fresh density with % of ash and water-cement ratio

4.6. Compressive Strength of Cement

The compressive strength of the cement is the determining the strength of cement only and mixed with BLA with their percentage within the curing periods of 3, 7 and 28 days respectively. In this paper, the compressive strength of BLA 5% replacement is higher than the OPC (0% replacement) at the standard age of 28 days period. And then the compressive strength of the replacement of 10% BLA is nearly the same as OPC and 15% replacement is slightly decreased. Figure 3 shows the compressive strength of BLA with cement with a standard mortar of the water-cement ratio of 0.485.

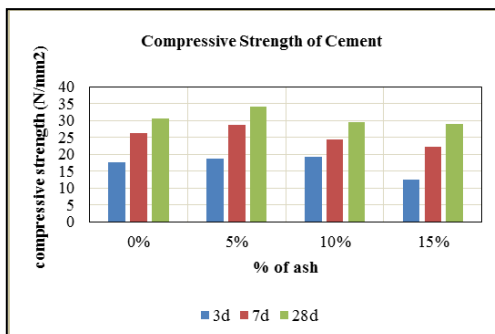


Figure 3. Compressive strength of cement

4.7. Compressive Strength of Concrete

The compressive strength of the concrete within the curing period of 7, 14, 28 and 56 days respectively. According to the

strength activity index, at the standard age of 28 days period, the value of compressive strength is above 75% in 5% and 10% BLA respectively and 15% BLA is below 75%.

This show that the increase percentage of BLA reduces the decrease in strength. Based on these data, the optimum percentage level of BLA 5% and 10% for the production of medium grade concrete. Table 4 shows the compressive strength at various curing ages of BLA. Table 5 and 6 show the compressive strength of BLA mixed with cement varied water-cement ratios at 28 days curing age.

Table 4. Compressive strength at various curing ages of BLA with 0.4 water-cement ratio

% of BLA	Curing age	Compressive Strength (N/mm ²)
0%	7 days	42.8
5%	7 days	36.21
10%	7 days	36.95
15%	7 days	35.45
0%	14 days	47.8
5%	14 days	42.7
10%	14 days	40.1
15%	14 days	38.6
0%	28 days	48.7
5%	28 days	40.5
10%	28 days	39.7
15%	28 days	37.6

Table 5. Compressive strength at various curing ages of BLA with 0.5 water-cement ratio

% of BLA	Curing age	Compressive Strength (N/mm ²)
0%	7 days	25.6
5%	7 days	25.6
10%	7 days	24.9
15%	7 days	24.5
0%	14 days	32.95
5%	14 days	30.9
10%	14 days	29.7
15%	14 days	28.5
0%	28 days	41.8

5%	28 days	35.7
10%	28 days	32
15%	28 days	31.2

Table 5. Strength activity index of the bamboo leaf ash with 0.4 water-cement ratio at 28 days curing age

% of BLA	Compressive strength (N/mm ²)	Strength activity index (%)
0%	47.6	100
5%	42.07	88.38
10%	35.63	74.85
15%	31.33	65.81

Table 6. Strength activity index of the bamboo leaf ash with 0.5 water-cement ratio at 28 days curing age

% of BLA	Compressive strength (N/mm ²)	Strength activity index (%)
0%	41.77	100
5%	35.73	85.54
10%	32	76.61
15%	31.17	74.62

5. CONCLUSION

From the results, it can be concluded that ;

- The percentage of silicon dioxide in BLA is over three times more than OPC, so the calcium silicate hydrate (C-S-H) the secondary hydration is formed at later day strength.
- The more added the BLA, the more water is needed in the standard consistency test.
- The setting time of concrete increased when percentage of BLA increased.
- The workability is inversely proportional to the percentage of BLA.
- The density of OPC mixed with BLA is lighter than OPC only because the specific gravity value of BLA is smaller.

- The compressive strength of concrete decreased when the content of BLA increased.
- The strength activity index of BLA 5% and 10% is optimum because its value is above 75%.
- Finally, the replacement of BLA is convenient for Grade 30 to G 40 but not compare to the strength of OPC only.

6. ACKNOWLEDGMENTS

Firstly, the author would like to acknowledge Dr. Thein Gi, Rector of Technological University (Thanlyin), for her kind permission to carry out this research work. The author particularly wishes to acknowledge Dr. Kyaw Linn Htet (Supervisor) and Dr. Ni Ni Moe Kyaw (Co-Supervisor) for their support, encouragement and invaluable guidance in preparation of this research. Finally, the author deeply thanks to High-Tech Concrete Company Limited for giving a permission of using Quality Control Laboratory.

7. REFERENCES

- [1] John Newman. Ban Seng Choo, “Advanced Concrete Technology”
- [2] S.K Duggal, “BUILDING MATERIALS”
- [3] North Carolina Division of Highways Materials and Tests Unit, “Materials and Tests Unit”, CONCRETE MIX DESIGN TECHNICIAN STUDY GUIDE, Revised July 2016.
- [4] Olutoge F.A., Oladunmoye O.M. “Bamboo Leaf Ash as Supplementary Cementitious Material”, American Journal of Engineering Research, 2017.
- [5] G. Dhinakaran and Gangava Hari Chanadana, “Compressive Strength and Durability of Bamboo Leaf Ash Concrete”, Jordan Journal of Civil Engineering, 2016.
- [6] H.M.A. Mahzuz, “Performance Evaluation of Bamboo with Mortar and Concrete”, Journal of Engineering and Technology Research Vol. 3 (12), November 2011.
- [7] Nur Aqilah Bt. Abd Karim, “Strength Performance Of Banana Fiber Ash As Cementitious Material With Different Temperature”, Faculty Of Engineering And Earth Resources, University Malaysia Pahang, July 2014.
- [8] Utodio N.F., “Investigation of the Effect of Bamboo Leaf Ash Blended Cement on Engineering Properties of Lateritic Blocks”, University of Uyo, Journal of Sustainable Development Studies, Volume 8, Number 1, 2015.
- [9] Stefania Liuzzi, Sara Sanarica, Pietro Stefanizzi, “ Use of Agro-Wastes in Building Materials in the Mediterranean Area: a review”, 72nd Conference of the Italian Thermal Machines Engineering Association, ATI2017.
- [10] ACI 318: Building Code Requirements for Reinforced Concrete.
- [11] ACI C 204-00: Standard Test Method for Fineness of Hydraulic Cement by Air-Permeability Apparatus.

- [12] ACI C 187-04: Standard Test Method for Normal Consistency of Hydraulic Cement.
- [13] ACI C91-04b: Standard Test Method for Time of Setting of Hydraulic Cement by Vicat Needle.
- [14] ACI C188-95: Standard Test Method for Density of Hydraulic Cement.
- [15] ACI C109/C 109M-02: Standard Test Method for Compressive Strength of Hydraulic Cement Mortars (Using 2-in, or (50-mm) Cube Specimens).
- [16] Aye Aye Mar, “Experimental Study on Variations of Concrete Properties Using Local Raw Materials in Northern-Shan State”, M.E thesis, Department of Civil Engineering, Yangon Technological University, Yangon, Myanmar, 2015.